

Generalized Semiclassical Ehrenfest Method: A Route to Wave Function-Free Photochemistry and Nonadiabatic Dynamics with Only Potential Energies and Gradients

Yinan Shu and Donald G. Truhlar*



Cite This: *J. Chem. Theory Comput.* 2024, 20, 4396–4426



Read Online

ACCESS |

Metrics & More

Article Recommendations

ABSTRACT: We reconsider recent methods by which direct dynamics calculations of electronically nonadiabatic processes can be carried out while requiring only adiabatic potential energies and their gradients. We show that these methods can be understood in terms of a new generalization of the well-known semiclassical Ehrenfest method. This is convenient because it eliminates the need to evaluate electronic wave functions and their matrix elements along the mixed quantum-classical trajectories. The new approximations and procedures enabling this advance are the curvature-driven approximation to the time-derivative coupling, the generalized semiclassical Ehrenfest method, and a new gradient correction scheme called the time-derivative matrix (TDM) scheme. When spin–orbit coupling is present, one can carry out dynamics calculations in the fully adiabatic basis using potential energies and gradients calculated without spin–orbit coupling plus the spin–orbit coupling matrix elements. Even when spin–orbit coupling is neglected, the method is useful because it allows calculations by electronic structure methods for which nonadiabatic coupling vectors are unavailable. In order to place the new considerations in context, the article starts out with a review of background material on trajectory surface hopping, the semiclassical Ehrenfest scheme, and methods for incorporating decoherence. We consider both internal conversion and intersystem crossing. We also review several examples from our group of successful applications of the curvature-driven approximation.



1. INTRODUCTION

Born and Oppenheimer¹ showed that the eigenvalues of the electronic Hamiltonian (defined as the total Hamiltonian without the nuclear kinetic energy, i.e., the Hamiltonian for stationary nuclei) play the role of potential energy functions for nuclear motion. The associated eigenfunctions are now usually called the Born–Oppenheimer states. In the present article, we use this term to denote fixed-nuclei electronic states calculated without spin–orbit coupling (SOC). Born and Oppenheimer’s treatment used an expansion in powers of the small parameter $(m/M)^{1/4}$ (where m is electronic mass and M is an average nuclear mass) and the differences $\mathbf{R} - \mathbf{R}_0$ (where \mathbf{R} denote a set of nuclear coordinates, and \mathbf{R}_0 is the center of the expansion); they showed that the electronic states are not coupled by low-order terms. In fact, in their notation, the leading coupling between electronic states² is of order $[(m/M)^{1/4}]^6$. Later work provided an improved treatment of the expansion.³

The Born–Oppenheimer expansion is concerned with molecular energies, not dynamics. A few years later, Mott⁴ attempted to calculate the probability of collision-induced electronic nonadiabaticity by what is now often called the classical path method, but which may also be considered an early example of a mixed quantum-classical method. (A nonadiabatic process is one where the quantum numbers are not conserved, and an electronically nonadiabatic process is

one where the electronic state changes.) Mott simplified the problem to nuclear motion along a single coordinate Z and found (his eq (7)) that the coupling was caused by a term $-i\hbar v \frac{\partial \psi}{\partial Z}$, where v is velocity and ψ is the Born–Oppenheimer electronic wave function. Generalizing this to multidimensional nuclear motion gives $-i\hbar \mathbf{v} \cdot \nabla \psi$, where \mathbf{v} is the velocity vector, and ∇ is the gradient with respect to nuclear coordinates (i.e., ∇ is $\frac{\partial}{\partial \mathbf{R}}$, where \mathbf{R} is a $3N_{\text{atoms}}$ -dimensional vector of Cartesian nuclear coordinates for the N_{atoms} atoms). The corresponding matrix element coupling electronic states I and J is $-i\hbar \mathbf{v} \cdot \mathbf{d}_{IJ}$, where \mathbf{d}_{IJ} is $\langle \psi_I | \nabla | \psi_J \rangle$. In the current literature, \mathbf{d}_{IJ} is called the nonadiabatic coupling (NAC), and it plays the key role in treatments^{5–11} of electronically nonadiabatic processes in terms of Born–Oppenheimer states.

An early example of the peak in the nonadiabatic coupling between two electronically adiabatic surfaces potentials in

Received: March 30, 2024

Revised: May 13, 2024

Accepted: May 16, 2024

Published: May 31, 2024



terms of a derivative of basis functions with respect to a nuclear coordinate is given in a 1932 paper of London.^{12,13}

In a paper presented at the 1937 Faraday Discussion on Reaction Kinetics,¹⁴ Wigner discussed the criterion of electronic adiabaticity as being a question of whether “the electronic motion will be able to follow the motion of the nuclei.” He said this would occur “if that latter motion is not too rapid and if the electronic wave function does not change too radically for a small change in the nuclear positions.” This statement is a direct invocation of small \mathbf{v} and small \mathbf{d}_{Jl} , as introduced in the paragraph about Mott’s paper. However, Wigner continued, “In all cases in which a nonadiabatic reaction is assumed, the rapid change of the wave function in the neighborhood of an approximate crossing of energy levels is made responsible for it. I think that for an energy surface which does not show singularities in abnormal curvatures, etc., the adiabatic condition cannot cause serious discrepancies.” This reformulates the condition of small \mathbf{d}_{Jl} as a condition of smooth potential energy surfaces, and the quantification of this connection is a main subject of the present perspective article.

Another notable aspect of Wigner’s reformulation is that he said the rapid change of the wave function would occur in the neighborhood of an approximate crossing of energy levels. Also in 1937, Teller¹⁵ showed that in a system with F internal coordinates (F is $3N_{\text{atoms}} - 6$ for a general molecule, where N_{atoms} is the number of atoms in the molecule), that intersections generally occur along $(F - 2)$ -dimensional conical intersection seams. In a later paper¹⁶ he gave a clear discussion of why electronically nonadiabatic transitions usually occur near such conical intersection seams. More recently, it has been shown that when gaps between potential energy surfaces go through a local minimum along some path, one is inevitably on the shoulder of a conical intersection.¹⁷ That is, a local minimum of adiabatic potential energy gap along a path (along a trajectory) is not an actually avoided crossing but rather an indication of a real crossing of adiabatic surfaces to the side of the path. Therefore, we label local minima in the adiabatic energy gap along a path as locally avoided crossings to avoid the implication that the potential energy surfaces avoid crossing when viewed globally. Since a trajectory of a multidimensional system is unlikely to go precisely through a conical intersection, we conclude that a semiclassical picture of electronically nonadiabatic processes should be dominated by paths through locally avoided crossings.

In 1951, Born¹⁸ pointed out that the expansion of Born and Oppenheimer is only valid if \mathbf{R} is near a structure \mathbf{R}_0 where the gradient vanishes. In order to make a treatment valid at any \mathbf{R} , he made an expansion

$$\Psi(\mathbf{r}, \mathbf{R}) = \sum_J \phi_J^{\text{elec}}(\mathbf{r}; \mathbf{R}) X_J^{\text{nuc}}(\mathbf{R}) \quad (1)$$

where \mathbf{r} denotes the set of electronic coordinates, $\phi_J^{\text{elec}}(\mathbf{r}; \mathbf{R})$ is a member of a complete set of Born–Oppenheimer electronic states, and $X_J^{\text{nuc}}(\mathbf{R})$ is a time-independent nuclear wave function. (We changed the notation to be more consistent with the present paper. Note that the derivation based on eq 1 was recapitulated in a monograph, and this book section in English is often cited¹⁹ rather than the original report,¹⁸ which is in German.) He then derived

$$\left(\frac{1}{2} \sum_a^{N_{\text{atoms}}} \frac{1}{M_a} \mathbf{P}_a^2 + V_J(\mathbf{R}) - E \right) X_J^{\text{nuc}} + \sum_{I \neq J} C_{JI}(\mathbf{R}, \mathbf{P}) X_I^{\text{nuc}} = 0 \quad (2)$$

where M_a and \mathbf{P}_a are the mass and momentum of nucleus a , V_J is the adiabatic potential energy surface of state J , E is the total energy, and \mathbf{P} denotes the collection of the \mathbf{P}_a . To keep the presentation simple, we give C_{JI} only for the cases where all $M_a = M$. Then¹⁸

$$C_{JI} = \frac{\hbar}{i} \mathbf{d}_{Jl} \cdot \mathbf{P} - \frac{\hbar^2}{2M} \langle \psi_J | \nabla^2 | \psi_I \rangle \quad (3)$$

where $i = \sqrt{-1}$, \hbar is Planck’s constant divided by 2π , and we corrected a missing factor of $1/2$ in Born’s derivation. This is the first paper where adiabatic electronic wave functions were used to derive the coupled equations for nuclear motion in electronically nonadiabatic processes, and eq 3 is the first occurrence of the NAC in the time-independent Schrödinger equation for coupled motion in multiple electronic states. Equation 2 agrees with the modern time-independent quantum mechanical equations for electronically nonadiabatic dynamics in an electronically adiabatic basis (see, for example, eq (9) in the review of Hirschfelder and Meath²⁰ for a particularly clear treatment or eq (5) in a later paper²¹), and it can be used for converged quantum mechanical calculations of electronically nonadiabatic atom–diatom reactions,²² but it becomes too expensive for practical use on larger systems. The present article focuses instead on the time-dependent mixed quantum-classical methods that are more practical.

The connection between the NAC and the character of the potential energy surfaces near a conical intersection seam can be made quantitative by a power series in terms of displacements from the conical intersection seam.^{21,23–25}

Following a presentation of background theory in Section 2, further work making useful approximations for the NAC without using wave functions to calculate \mathbf{d}_{Jl} is presented in Sections 3 and 4, leading up to the curvature-driven approximation that is the key feature of this article. Section 5 then reviews the incorporation of the curvature-driven approximation in practical mixed quantum-classical methods for electronically nonadiabatic simulations, and Section 6 reviews successful applications, which are very encouraging. Section 7 has concluding remarks.

The present article is a perspective article containing both new work and selected background; the discussion of previous work focuses on the background of the new work that attempts to understand recent wave function-free dynamics methods in the context of a new generalization of the well-known semiclassical Ehrenfest method. Readers seeking a discussion of other current work on electronically nonadiabatic dynamics are referred to reviews.^{26–33}

For the convenience of the reader, Appendix A explains all acronyms and abbreviations used in this article.

2. BACKGROUND: MIXED QUANTUM-CLASSICAL NONADIABATIC DYNAMICS METHODS

We distinguish two categories of mixed quantum-classical nonadiabatic dynamics methods, namely, trajectory surface hopping (TSH), in which the trajectory is propagated on a single potential energy surface for each segment of time,^{34–37} and self-consistent potential (SCP) methods, in which the trajectory is propagated on a mean-field potential.^{38–42} The

classic form of TSH methods is Tully's fewest switches trajectory-surface-hopping method (FS-TSH),³⁴ and the classic SCP method is the semiclassical Ehrenfest (SE) method.^{38,41}

The nonadiabatic dynamics calculations—by either a TSH method or an SCP method—can be performed in two ways: (i) direct dynamics, in which all the required electronic structure information is computed on-the-fly from electronic structure software as needed during the propagation of trajectories; or (ii) dynamics with analytic surfaces, in which all the required electronic structure information is incorporated via prefitted analytic potential energy surfaces and their couplings. Such a fit is often carried out in a diabatic representation.⁴³ A diabatic basis is one where all electronic-state couplings arising from the nuclear momentum operator are negligible, i.e. C_{JI} in eq 3 is negligible. (This is sometimes called quasidiabatic, but we call it diabatic because strictly diabatic bases, where C_{JI} in eq 3 is identically zero, do not exist⁴⁴ except for the trivial, nonphysical basis where all basis functions are independent of nuclear coordinates.) Most of the discussion presented in the current perspective is applicable to both direct dynamics and dynamics with analytic surfaces although we focus more on direct dynamics because constructing global diabatic representations can be arduous.⁴³

Early developments of nonadiabatic dynamics methods were primarily concerned with internal conversion processes (processes in which the electronic spin state does not change), without SOC. In recent years, practical methods^{45–51} have been developed for performing nonadiabatic dynamics for simulations including SOC, which allows intersystem crossing (processes involving a change in electronic spin state) to be treated. The reason that new methods are required for practical calculations involving SOC is that analytic gradients for direct dynamics calculations are usually available in the Born–Oppenheimer basis (which diagonalizes the spin-free electronic Hamiltonian) but not in the fully adiabatic basis (which diagonalizes the electronic Hamiltonian including SOC).

In Section 2.1, we review generalized SE (GSE). This was first defined in ref 52 but has not previously been fully discussed; here we show how we obtain the equations of motion (EOMs) for GSE. As will be explained below, the GSE differs from the conventional SE in that we use a more general definition of the nonadiabatic force on the trajectory. As should be clear from the names of the methods, SE can be considered as a special case of GSE, and our treatment here is in terms of the more comprehensive GSE. In Section 2.2, we review FS-TSH.

Both Sections 2.1 and 2.2 will be presented in a general electronic basis, which may be either adiabatic or diabatic, or spin-adiabatic or spin-diabatic when SOC presents. In Section 2.3, we will discuss the popular choices of basis. Section 2.4 summarizes the EOMs for GSE, SE, and FS-TSH in specific bases.

Section 2.5 provides a quick discussion of the inclusion of decoherence^{53,54} in mixed quantum-classical nonadiabatic dynamics.

2.1. Generalized Semiclassical Ehrenfest Method. In the mean-field approximation, the wave function of the system is written as a product,

$$\Psi(\mathbf{r}, \mathbf{R}, t) = \Phi^{\text{elec}}(\mathbf{r}, t)\chi^{\text{nuc}}(\mathbf{R}, t) \quad (4)$$

where Φ^{elec} and χ^{nuc} are the electronic wave function and nuclear wave packet, \mathbf{r} and \mathbf{R} denote the electronic and nuclear

coordinates respectively, and t is time. This is often called time-dependent self-consistent field approximation.^{39,55} The wave function is propagated according to the time-dependent Schrödinger equation,

$$i\hbar \frac{d}{dt} \Psi(\mathbf{r}, \mathbf{R}, t) = H \Psi(\mathbf{r}, \mathbf{R}, t) \quad (5)$$

where H is molecular Hamiltonian given by

$$H = T^{\text{nuc}} + H^{\text{elec}} \quad (6)$$

where T^{nuc} is the nuclear kinetic energy operator, and H^{elec} is the electronic Hamiltonian, which includes electronic kinetic energy, all Coulomb interactions of electrons and nuclei, and possibly SOCs. A time-dependent Hartree treatment of this product wave function leads to an electronic mean-field equation,

$$i\hbar \frac{\partial}{\partial t} \Phi^{\text{elec}} = \langle \chi^{\text{nuc}} | H | \chi^{\text{nuc}} \rangle_{\mathbf{R}} \Phi^{\text{elec}} \quad (7)$$

and a nuclear mean-field equation,

$$i\hbar \frac{\partial}{\partial t} \chi^{\text{nuc}} = \langle \Phi^{\text{elec}} | H | \Phi^{\text{elec}} \rangle_{\mathbf{r}} \chi^{\text{nuc}} \quad (8)$$

Using a phase–amplitude representation of the nuclear wave function,^{11,56–62}

$$\chi^{\text{nuc}} = W(\mathbf{R}, t) \exp[iS(\mathbf{R}, t)/\hbar] \quad (9)$$

where W and S are a real-valued amplitude and a real-valued phase, respectively, and taking a classical limit ($\hbar \rightarrow 0$), one can obtain⁵⁸

$$\frac{dS}{dt} + \sum_a^{N_{\text{atoms}}} \frac{1}{2} M_a^{-1} \left(\frac{\partial S}{\partial \mathbf{R}_a} \right)^2 + \langle \Phi^{\text{elec}} | H^{\text{elec}} | \Phi^{\text{elec}} \rangle_{\mathbf{r}} = 0 \quad (10)$$

$$\frac{dW}{dt} + \sum_a^{N_{\text{atoms}}} M_a^{-1} \left(\frac{\partial W}{\partial \mathbf{R}_a} \right) \left(\frac{\partial S}{\partial \mathbf{R}_a} \right) + \sum_a^{N_{\text{atoms}}} \frac{1}{2} M_a^{-1} W \left(\frac{\partial S}{\partial \mathbf{R}_a} \right)^2 = 0 \quad (11)$$

where M_a is the mass of nucleus a , \mathbf{R}_a is the position vector of nucleus a , N_{atoms} is the number of atoms in the molecule. The first of the above two equations is the Hamilton–Jacobi equation, which is equivalent to Newton's equation,^{11,58–60}

$$\dot{\mathbf{P}} = -\frac{\partial}{\partial \mathbf{R}} \langle \Phi^{\text{elec}} | H^{\text{elec}} | \Phi^{\text{elec}} \rangle_{\mathbf{r}} \quad (12)$$

where $\dot{\mathbf{P}}$ is the total time-derivative of nuclear momentum. (In general, we use an overdot to denote a time derivative.) See for example, the footnote of ref 60. by Curchod et al. for a more detailed derivation. In interpreting this result, note that the classical limit of quantum mechanics is an ensemble of classical trajectories—not a single trajectory.⁶¹ The simplifications and subtleties in the classical limit and the difficulty of using this argument for a consistent trajectory-based classical limit are discussed elsewhere.^{61,62}

Equations 4–12 are presented here as a framework for mixed quantum-classical trajectory approximations; other workers have discussed the factorization of eq 4 and its consequences and use more rigorously,^{55,63,64} but that is not needed for the present work.

The electronic mean-field equation involves an electronic wave function propagating on a potential determined by the nuclear wave packet. We make the semiclassical approximation

of replacing the wave packet by an ensemble of independent trajectories, and then we make the independent-trajectory approximation for the ensemble and denote a given trajectory by $\mathbf{R}(t)$; this procedure yields

$$i\hbar \frac{d}{dt} \Phi^{\text{elec}}(\mathbf{r}; \mathbf{R}(t)) = H^{\text{elec}}(\mathbf{r}; \mathbf{R}(t)) \Phi^{\text{elec}}(\mathbf{r}; \mathbf{R}(t)) \quad (13)$$

i.e., for each trajectory the instantaneous electronic Hamiltonian depends parametrically on a single nuclear configuration, the time-dependent nuclear configuration of the mixed quantum-classical trajectory. The independent-trajectory approximation does not give a good approximation to an actual quantal wave packet,⁶⁵ but it is a commonly used approximation in mixed quantum-classical trajectory methods.⁶⁶

In either the original semiclassical Ehrenfest method or the generalized semiclassical Ehrenfest method, the electronic wave function can be expanded in a general basis (GB), and we will use that expansion in the present Perspective:

$$\Phi^{\text{elec}}(\mathbf{r}; \mathbf{R}(t)) = \sum_{j=1}^{N_{\text{states}}} c_j^{\text{GB}}(t) \phi_j^{\text{GB}}(\mathbf{r}; \mathbf{R}(t)) \quad (14)$$

where $c_j^{\text{GB}}(t)$ is the time-dependent coefficient of basis state J , whose wave function is $\phi_j^{\text{GB}}(\mathbf{r}; \mathbf{R}(t))$. For practical direct dynamics calculations, the basis states are usually the Born–Oppenheimer states, and when SOC is neglected, this is called the adiabatic representation. When SOC is included, one needs more nuanced notation. In the literature, the Born–Oppenheimer states (defined above as being calculated without SOC) are called the molecular-Coulomb-Hamiltonian (MCH) representation, the spin–orbit-free basis, the spin-adiabatic basis, or the spin-free adiabatic basis; and the electronic states obtained by a diagonalization of a spin–orbit-inclusive Hamiltonian are called the diagonal basis, the fully adiabatic basis, or the spin-adiabatic basis. When SOC is neglected, the spin-free adiabatic basis and the fully adiabatic basis are the same. The MCH and diagonal bases are not the same when SOC is included in the electronic Hamiltonian, but they are identical when there is no SOC, i.e., both diagonalize the electronic Hamiltonian that does not have SOC. In Section 2.3, we use the language used in the SHARC program,^{45,48} namely MCH and diagonal. Notice that we have used representation and basis as synonyms.

Substituting eq 14 into eq 13 and projecting with $\langle \phi_I^{\text{GB}} |$ gives the EOM for the time-dependent coefficients

$$\frac{d}{dt} c_I^{\text{GB}}(t) = - \sum_J^{N_{\text{states}}} \left(\frac{i}{\hbar} H_{IJ}^{\text{elec[GB]}} + T_{IJ}^{\text{GB}} \right) c_J^{\text{GB}}(t) \quad (15)$$

where $H_{IJ}^{\text{elec[GB]}}$ is a matrix element of the electronic Hamiltonian in the GB basis (notice that in the following equations, the bra-ket integral involves integration over electronic coordinate \mathbf{r} , and the subscript \mathbf{r} will be dropped for simplicity),

$$H_{IJ}^{\text{elec[GB]}} = \langle \phi_I^{\text{GB}} | H^{\text{elec}} | \phi_J^{\text{GB}} \rangle \quad (16)$$

and T_{IJ}^{GB} is called time derivative coupling (TDC) in the GB basis,

$$T_{IJ}^{\text{GB}} = \left\langle \phi_I^{\text{GB}} \left| \frac{d}{dt} \right| \phi_J^{\text{GB}} \right\rangle \quad (17)$$

Eq 15 is called the GSE electronic EOM. By using the chain rule, the TDC can be written as,

$$T_{IJ}^{\text{GB}} = \dot{\mathbf{R}} \cdot \mathbf{d}_{IJ}^{\text{GB}} \quad (18)$$

where an overdot signifies a time derivative, and $\mathbf{d}_{IJ}^{\text{GB}}$ is the NAC in the general basis:

$$\mathbf{d}_{IJ}^{\text{GB}} = \langle \phi_I^{\text{GB}} | \nabla | \phi_J^{\text{GB}} \rangle \quad (19)$$

This is an $N_{\text{states}} \times N_{\text{states}} \times 3N_{\text{atoms}}$ tensor, but we treat it as an $N_{\text{states}} \times N_{\text{states}}$ matrix in which each IJ matrix element is a $(3N_{\text{atoms}})$ -dimensional vector. Because eq 18 shows that T_{IJ}^{GB} can be obtained as a projection of $\mathbf{d}_{IJ}^{\text{GB}}$ on the nuclear velocity direction, we sometimes call \mathbf{d} the full NAC to clearly distinguish it from T . Both TDCs and NACs are complex when SOC is included, but they may be taken as real when it is omitted. The TDCs and NACs are anti-Hermitian:

$$T_{IJ}^{\text{GB}} = -(T_{JI}^{\text{GB}})^* \quad (20)$$

$$\mathbf{d}_{IJ}^{\text{GB}} = -(\mathbf{d}_{JI}^{\text{GB}})^* \quad (21)$$

It is often convenient to write eq 15 in matrix form:

$$\dot{\mathbf{c}}^{\text{GB}}|_{\text{GSE}} = - \left(\frac{i}{\hbar} \mathbf{H}^{\text{elec[GB]}} + \mathbf{T}^{\text{GB}} \right) \mathbf{c}^{\text{GB}} \quad (22)$$

where the matrix elements of $\mathbf{H}^{\text{elec[GB]}}$ and \mathbf{T}^{GB} are shown in eqs 16 and 17 respectively, and $\mathbf{c}^{\text{GB}}|_{\text{GSE}}$ denotes that it is for GSE. It also is useful to define the electronic density matrix, whose matrix elements are

$$\rho_{IJ}^{\text{GB}} = c_I^{\text{GB}}(c_J^{\text{GB}})^* \quad (23)$$

Eqs 15 and 23 yield

$$\frac{d\rho_{IJ}^{\text{GB}}}{dt} = \sum_L^{N_{\text{states}}} \left(\left(-\frac{i}{\hbar} H_{IL}^{\text{elec[GB]}} - T_{IL}^{\text{GB}} \right) \rho_{LJ}^{\text{GB}} + \left(\frac{i}{\hbar} (H_{JL}^{\text{elec[GB]})^* - (T_{JL}^{\text{GB}})^* \right) \rho_{IL}^{\text{GB}} \right) \quad (24)$$

When $I = J$, this simplifies to

$$\frac{d\rho_{II}^{\text{GB}}}{dt} = 2 \sum_L^{N_{\text{states}}} \left(\frac{1}{\hbar} \text{Im}(H_{IL}^{\text{elec[GB]}} \rho_{LI}^{\text{GB}}) - \text{Re}(T_{IL}^{\text{GB}} \rho_{LI}^{\text{GB}}) \right) \quad (25)$$

Conservation of total energy requires that the time derivative of the molecular Hamiltonian function shown in eq 6 should be zero. (Notice that the Hamiltonian function in this context should be distinguished from the Hamiltonian operator in a quantum context.) Therefore,

$$\dot{H} = \dot{\mathbf{P}}^{\text{GB}} \cdot \dot{\mathbf{R}} + \frac{d}{dt} \text{tr}(\rho^{\text{GB}} \mathbf{H}^{\text{elec[GB]}}) = 0 \quad (26)$$

where $\text{tr}(\mathbf{M})$ denotes the trace of a matrix. This requires that,

$$\dot{\mathbf{P}}^{\text{GB}} \cdot \dot{\mathbf{R}} = - \frac{d}{dt} \text{tr}(\rho^{\text{GB}} \mathbf{H}^{\text{elec[GB]}}) = - \sum_{IJ}^{N_{\text{states}}} \rho_{IJ}^{\text{GB}} \frac{dH_{IJ}^{\text{elec[GB]}}}{dt} - \sum_{IJ}^{N_{\text{states}}} \frac{d\rho_{IJ}^{\text{GB}}}{dt} H_{IJ}^{\text{elec[GB]}} \quad (27)$$

We distinguish^{54,67} the two terms on the right-hand side of eq 27 as adiabatic force $\mathbf{F}^{\text{A[GB]}}$ and nonadiabatic force $\mathbf{F}^{\text{NA[GB]}}$:

$$\mathbf{F}^{\text{A[GB]}} \cdot \dot{\mathbf{R}} = - \sum_{IJ}^{N_{\text{states}}} \rho_{IJ}^{\text{GB}} \frac{dH_{JI}^{\text{elec[GB]}}}{dt} \quad (28)$$

$$\mathbf{F}^{\text{NA[GB]}} \cdot \dot{\mathbf{R}} = - \sum_{IJ}^{N_{\text{states}}} \frac{d\rho_{IJ}^{\text{GB}}}{dt} H_{JI}^{\text{elec[GB]}} \quad (29)$$

Therefore

$$\dot{\mathbf{P}}^{\text{GB}} = \mathbf{F}^{\text{A[GB]}} + \mathbf{F}^{\text{NA[GB]}} \quad (30)$$

We first consider the nonadiabatic force because this equation can be further simplified. Using eqs 24 and 29, we obtain

$$\begin{aligned} \mathbf{F}^{\text{NA[GB]}} \cdot \dot{\mathbf{R}} = & \frac{i}{\hbar} \sum_{IJL}^{N_{\text{states}}} [H_{IL}^{\text{elec[GB]}} \rho_{LJ}^{\text{GB}} - (H_{JL}^{\text{elec[GB]}})^* \rho_{IL}^{\text{GB}}] H_{JI}^{\text{elec[GB]}} \\ & + \sum_{IJL}^{N_{\text{states}}} [T_{IL}^{\text{GB}} \rho_{LJ}^{\text{GB}} + (T_{JL}^{\text{GB}})^* \rho_{IL}^{\text{GB}}] H_{JI}^{\text{elec[GB]}} \end{aligned} \quad (31)$$

The first term on the right-hand side of eq 31 is zero because

$$\begin{aligned} \sum_{IJL}^{N_{\text{states}}} [H_{IL}^{\text{elec[GB]}} \rho_{LJ}^{\text{GB}} - (H_{JL}^{\text{elec[GB]}})^* \rho_{IL}^{\text{GB}}] H_{JI}^{\text{elec[GB]}} = \\ \text{tr}(\mathbf{H}^{\text{elec[GB]}} \boldsymbol{\rho}^{\text{GB}} \mathbf{H}^{\text{elec[GB]}}) - \text{tr}(\mathbf{H}^{\text{elec[GB]}} \boldsymbol{\rho}^{\text{GB}} \mathbf{H}^{\text{elec[GB]}}) = 0 \end{aligned} \quad (32)$$

Therefore, the nonadiabatic force is reduced to

$$\mathbf{F}^{\text{NA[GB]}} \cdot \dot{\mathbf{R}} = \sum_{IJL}^{N_{\text{states}}} [T_{IL}^{\text{GB}} \rho_{LJ}^{\text{GB}} + (T_{JL}^{\text{GB}})^* \rho_{IL}^{\text{GB}}] H_{JI}^{\text{elec[GB]}} \quad (33)$$

Eq 33 can be written in a more compact matrix form,

$$\mathbf{F}^{\text{NA[GB]}} \cdot \dot{\mathbf{R}} = \text{tr}(\mathbf{T}^{\text{GB}} [\boldsymbol{\rho}^{\text{GB}}, \mathbf{H}^{\text{elec[GB]}}]) \quad (34)$$

where $[\mathbf{X}, \mathbf{Y}]$ denotes a commutator of matrices \mathbf{X} and \mathbf{Y} ,

$$[\mathbf{X}, \mathbf{Y}] = \mathbf{XY} - \mathbf{YX} \quad (35)$$

Note that both sides of eqs 28, 29, and 33 are scalars; this means that the scalar conservation-of-energy condition in eq 26 allows some flexibility in making physical choices of the directions of $\mathbf{F}^{\text{A[GB]}}$ and $\mathbf{F}^{\text{NA[GB]}}$. To take advantage of this, we introduce $N_{\text{states}} \times N_{\text{states}} \times 3N_{\text{atoms}}$ force direction tensors \mathbf{A}^{GB} , \mathbf{B}^{GB} , and \mathbf{C}^{GB} . We treat these tensors as matrices whose elements $\mathbf{A}_{JI}^{\text{GB}}$, $\mathbf{B}_{IL}^{\text{GB}}$, and $\mathbf{C}_{LJ}^{\text{GB}}$ are $(3N_{\text{atoms}})$ -dimensional vectors, where I, J, L are indices of electronic states. Then the most general expressions for $\mathbf{F}^{\text{A[GB]}}$ and $\mathbf{F}^{\text{NA[GB]}}$ that satisfy eqs 28 and 33 are

$$\mathbf{F}^{\text{A[GB]}} = - \sum_{IJ}^{N_{\text{states}}} \frac{\rho_{IJ}^{\text{GB}} \frac{dH_{JI}^{\text{elec[GB]}}}{dt} \mathbf{A}_{JI}^{\text{GB}}}{\mathbf{A}_{JI}^{\text{GB}} \cdot \dot{\mathbf{R}}} \quad (36)$$

and

$$\mathbf{F}^{\text{NA[GB]}} = \sum_{IJL}^{N_{\text{states}}} \left(\frac{T_{IL}^{\text{GB}} \rho_{LJ}^{\text{GB}} H_{JI}^{\text{elec[GB]}} \mathbf{B}_{IL}^{\text{GB}}}{\mathbf{B}_{IL}^{\text{GB}} \cdot \dot{\mathbf{R}}} - \frac{T_{LJ}^{\text{GB}} \rho_{IL}^{\text{GB}} H_{JI}^{\text{elec[GB]}} \mathbf{C}_{LJ}^{\text{GB}}}{\mathbf{C}_{LJ}^{\text{GB}} \cdot \dot{\mathbf{R}}} \right) \quad (37)$$

To prevent dividing by a zero in eqs 36 and 37, the $\mathbf{A}_{JI}^{\text{GB}}$, $\mathbf{B}_{IL}^{\text{GB}}$, and $\mathbf{C}_{LJ}^{\text{GB}}$ should not be normal to $\dot{\mathbf{R}}$. Because $\mathbf{F}^{\text{A[GB]}}$ and $\mathbf{F}^{\text{NA[GB]}}$ should be real, it is convenient to take matrix \mathbf{A}^{GB} to be Hermitian and matrices \mathbf{B}^{GB} and \mathbf{C}^{GB} to be anti-Hermitian; then the diagonal elements of matrices \mathbf{B}^{GB} and \mathbf{C}^{GB} are zero. We often require that force direction tensors to be real, although there are exceptions for which the complex parts are exactly canceled, which will be discussed below. Combining eqs 36 and 37, we see that the most general form of the GSE nuclear EOM that conserves the total energy is

$$\begin{aligned} \dot{\mathbf{P}}^{\text{GB}} = & - \sum_{IJ}^{N_{\text{states}}} \frac{\rho_{IJ}^{\text{GB}} \frac{dH_{JI}^{\text{elec[GB]}}}{dt} \mathbf{A}_{JI}^{\text{GB}}}{\mathbf{A}_{JI}^{\text{GB}} \cdot \dot{\mathbf{R}}} \\ & + \sum_{IJL}^{N_{\text{states}}} \left(\frac{T_{IL}^{\text{GB}} \rho_{LJ}^{\text{GB}} H_{JI}^{\text{elec[GB]}} \mathbf{B}_{IL}^{\text{GB}}}{\mathbf{B}_{IL}^{\text{GB}} \cdot \dot{\mathbf{R}}} - \frac{T_{LJ}^{\text{GB}} \rho_{IL}^{\text{GB}} H_{JI}^{\text{elec[GB]}} \mathbf{C}_{LJ}^{\text{GB}}}{\mathbf{C}_{LJ}^{\text{GB}} \cdot \dot{\mathbf{R}}} \right) \end{aligned} \quad (38)$$

Next, we discuss physical choices of \mathbf{A}^{GB} , \mathbf{B}^{GB} , and \mathbf{C}^{GB} tensors. We set them such that the adiabatic force reduces to that in the original SE method:

$$\mathbf{F}^{\text{A[GB]}} = - \sum_{IJ}^{N_{\text{states}}} \rho_{IJ}^{\text{GB}} \nabla H_{JI}^{\text{elec[GB]}} \quad (39)$$

This is accomplished by setting $\mathbf{A}_{JI}^{\text{GB}}$ equal to $\nabla H_{JI}^{\text{elec[GB]}}$; this is convenient because $\nabla H_{JI}^{\text{elec[GB]}}$ is readily available from electronic structure packages during the propagation of trajectories. Therefore, eq 28 is written as

$$\mathbf{F}^{\text{A[GB]}} \cdot \dot{\mathbf{R}} = - \sum_{IJ}^{N_{\text{states}}} \rho_{IJ}^{\text{GB}} \nabla H_{JI}^{\text{elec[GB]}} \cdot \dot{\mathbf{R}} \quad (40)$$

The choices of \mathbf{B}^{GB} and \mathbf{C}^{GB} are less straightforward. The symmetry of the two terms in eq 37 suggests setting \mathbf{B}^{GB} equal to \mathbf{C}^{GB} , and we shall only consider that case.

As shown in ref 69, assigning the direction of the nonadiabatic force tensors to the direction of a space-frame \mathbf{d}^{GB} of the kind produced by most electronic structure programs that can produce NACs fails to conserve angular momentum and center of mass momentum. The Ehrenfest method and surface hopping do conserve angular momentum and center-of-mass momentum if the NAC is in internal coordinates,⁶⁸ but, as discussed later in this section, SE EOMs with a space-frame \mathbf{d}^{GB} conserve total energy but fail to conserve angular momentum and center of mass momentum in direct dynamics. Hence, we want to choose a practical nonadiabatic force tensor that not only conserves total energy (as already accomplished in eq 38) but also conserves the total nuclear angular momentum and center of mass momentum. This imposes additional constraints on the choices of \mathbf{A}^{GB} , \mathbf{B}^{GB} , and \mathbf{C}^{GB} tensors:⁶⁹

$$\sum_a^{N_{\text{atoms}}} \mathbf{R}_a \times \dot{\mathbf{P}}_a^{\text{GB}} = \sum_a^{N_{\text{atoms}}} \mathbf{R}_a \times (\mathbf{F}_a^{\text{A[GB]}} + \mathbf{F}_a^{\text{NA[GB]}}) = 0 \quad (41)$$

$$\sum_a^{N_{\text{atoms}}} \dot{\mathbf{P}}_a^{\text{GB}} = \sum_a^{N_{\text{atoms}}} (\mathbf{F}_a^{\text{A[GB]}} + \mathbf{F}_a^{\text{NA[GB]}}) = 0 \quad (42)$$

where \mathbf{R}_a , $\dot{\mathbf{P}}_a^{\text{GB}}$, $\mathbf{F}_a^{\text{A[GB]}}$, and $\mathbf{F}_a^{\text{NA[GB]}}$ are 3-dimensional vectors denoting \mathbf{R} , $\dot{\mathbf{P}}^{\text{GB}}$, $\mathbf{F}^{\text{A[GB]}}$, and $\mathbf{F}^{\text{NA[GB]}}$ for nucleus a .

Our choice of the \mathbf{A}^{GB} tensor as $\nabla H_{JI}^{\text{elec[GB]}}$ readily conserves total nuclear angular momentum and center of mass momentum for the adiabatic force part,

$$\sum_a^{N_{\text{atoms}}} \mathbf{R}_a \times \mathbf{F}_a^{\text{A[GB]}} = \sum_a^{N_{\text{atoms}}} \mathbf{R}_a \times \left(- \sum_{IJ}^{N_{\text{states}}} \rho_{IJ}^{\text{GB}} \nabla_a H_{JI}^{\text{elec[GB]}} \right) = 0 \quad (43)$$

$$\sum_a^{N_{\text{atoms}}} \mathbf{F}_a^{\text{A[GB]}} = \sum_a^{N_{\text{atoms}}} \left(- \sum_{IJ}^{N_{\text{states}}} \rho_{IJ}^{\text{GB}} \nabla_a H_{JI}^{\text{elec[GB]}} \right) = 0 \quad (44)$$

where $\nabla_a = \frac{\partial}{\partial \mathbf{R}_a}$. The electronic structure of an isolated molecule is translationally and rotationally invariant, and therefore $\nabla H_{JI}^{\text{elec[GB]}}$ does not have nonzero components for overall translation and rotation.

However, the conservation of the total nuclear angular momentum and the center of mass momentum by the nonadiabatic force does lead to an additional restriction on the \mathbf{B}^{GB} tensor (and \mathbf{C}^{GB} because $\mathbf{C}^{\text{GB}} = \mathbf{B}^{\text{GB}}$) that it should not have nonzero overall translational and rotational components. To achieve this, we use a projection operator to remove the translational and rotational components of a preprojected \mathbf{B}^{GB} tensor,⁶⁹

$$\mathbf{B}_{IJ}^{\text{GB}} = (1 - \mathbf{Q}) \mathbf{B}_{IJ}^{\text{GB,preprojected}} \quad (45)$$

where $\mathbf{B}_{IJ}^{\text{GB,preprojected}}$ denotes a selected preprojected $\mathbf{B}_{IJ}^{\text{GB}}$ vector, and \mathbf{I} and \mathbf{Q} are the identity operator and the projection operator, respectively. Because $\mathbf{B}_{IJ}^{\text{GB}}$ is a $3N_{\text{atoms}}$ -dimensional vector, both \mathbf{I} and \mathbf{Q} are $3N_{\text{atoms}} \times 3N_{\text{atoms}}$ matrices. The projection operator is

$$\mathbf{Q}_{\alpha\gamma, \alpha'\gamma'} = \frac{1}{N_{\text{atoms}}} \delta_{\gamma\gamma'} + \sum_{\alpha}^{x,y,z} \sum_{\beta}^{x,y,z} \sum_{\alpha'}^{x,y,z} \sum_{\beta'}^{x,y,z} \varepsilon_{\alpha\beta\gamma} \Delta R_{\alpha\alpha'} [\tilde{\mathbf{I}}^{-1}]_{\beta\beta'} \varepsilon_{\alpha'\beta'\gamma'} \Delta R_{\alpha'\alpha'} \quad (46)$$

where a and a' are indices of nuclei, which vary from 1 to N_{atoms} ; $\alpha, \beta, \gamma, \alpha', \beta', \gamma'$ are indices of Cartesian directions, which take values of $x, y,$ or z ; $\tilde{\mathbf{I}}^{-1}$ is the inverse of matrix $\tilde{\mathbf{I}}$; matrix $\tilde{\mathbf{I}}$ is the same size as the moment of inertia matrix with all masses set to 1, and ε is a third-order unit pseudotensor whose elements are the Levi-Civita symbol. The first term of the projection operator corresponds to overall translation, and the second term corresponds to overall rotation. Therefore, eq 45 is our final suggested choice of a \mathbf{B}^{GB} tensor that conserves total nuclear angular momentum and center of mass momentum.

We make the above choice of \mathbf{A}^{GB} , \mathbf{B}^{GB} , and \mathbf{C}^{GB} tensors, and this gives the following nuclear EOM for GSE that we use:

$$\dot{\mathbf{P}}^{\text{GB}}|_{\text{GSE}} = - \sum_{IJ}^{N_{\text{states}}} \rho_{IJ}^{\text{GB}} \nabla H_{JI}^{\text{elec[GB]}} + \sum_{IJL}^{N_{\text{states}}} \left(\frac{T_{IL}^{\text{GB}} \rho_{LJ}^{\text{GB}} H_{JI}^{\text{elec[GB]}} \mathbf{B}_{IL}^{\text{GB}}}{\mathbf{B}_{IL}^{\text{GB}} \cdot \dot{\mathbf{R}}} - \frac{T_{LJ}^{\text{GB}} \rho_{IL}^{\text{GB}} H_{JI}^{\text{elec[GB]}} \mathbf{B}_{LJ}^{\text{GB}}}{\mathbf{B}_{LJ}^{\text{GB}} \cdot \dot{\mathbf{R}}} \right) \quad (47)$$

We have arrived at eqs 22 and 47 as the final electronic and nuclear EOMs for GSE. By using eq 45, GSE EOMs conserves

total energy, angular momentum, and center of mass momentum.

In SE, the electronic EOM is identical to that of GSE,

$$\dot{\mathbf{c}}^{\text{GB}}|_{\text{SE}} = - \left(\frac{i}{\hbar} \mathbf{H}^{\text{elec[GB]}} + \mathbf{T}^{\text{GB}} \right) \mathbf{c}^{\text{GB}} \quad (48)$$

The nuclear EOM of SE can be considered as a special case of GSE. In SE, the force direction tensors \mathbf{B}^{GB} and \mathbf{C}^{GB} are chosen as

$$\mathbf{B}^{\text{GB}}|_{\text{SE}} = \mathbf{C}^{\text{GB}}|_{\text{SE}} = \mathbf{d}^{\text{GB}} \quad (49)$$

where the elements of \mathbf{d}^{GB} is defined in eq 19. This gives the nuclear EOM of SE,

$$\dot{\mathbf{P}}^{\text{GB}}|_{\text{SE}} = - \sum_{IJ}^{N_{\text{states}}} \rho_{IJ}^{\text{GB}} \nabla H_{JI}^{\text{elec[GB]}} + \sum_{IJL}^{N_{\text{states}}} (\rho_{LJ}^{\text{GB}} H_{JI}^{\text{elec[GB]}} \mathbf{d}_{IL}^{\text{GB}} - \rho_{IL}^{\text{GB}} H_{JI}^{\text{elec[GB]}} \mathbf{d}_{LJ}^{\text{GB}}) \quad (50)$$

Because \mathbf{d}^{GB} could be complex, this can provide an exception already mentioned to the choice of the force direction tensors being real. Using \mathbf{d}^{GB} as the nonadiabatic force direction is physical choice because TDC \mathbf{T}^{GB} can be written as product of the NAC and the velocity vector, as shown in eq 18, and eq 34 can be written as

$$\mathbf{F}^{\text{NA[GB]}} \cdot \dot{\mathbf{R}}|_{\text{SE}} = \text{tr}(\mathbf{d}^{\text{GB}} \cdot \dot{\mathbf{R}} [\rho^{\text{GB}}, \mathbf{H}^{\text{elec[GB]}}]) \quad (51)$$

A NAC computed from a prefitted analytic representation of coupled diabatic surfaces does not suffer the angular-momentum-nonconservation problem if it is calculated in internal coordinates^{70–74} or in transformed Cartesian coordinates from which translation and rotation have been removed.^{75–78}

An important positive aspect of the GSE method is that it is directly derivable from the time-dependent Schrödinger equation, and SE is a special case of GSE. An advantage of GSE over SE is that one is not required to compute full NACs. By knowing TDCs and an appropriate choice of force tensor \mathbf{B}^{GB} , one can perform an SCP nonadiabatic dynamics calculation without full NACs. One has many choices of the force tensor \mathbf{B}^{GB} , for example in ref 52., we have used an effective NAC, which is defined as a combination of the difference gradient vector and the nuclear velocity vector:

$$\mathbf{B}_{IJ}^{\text{GB,preprojected}} = \mathbf{B}_{IJ}^{\text{GB,effNAC}} = \nabla H_{II}^{\text{elec[GB]}} - \nabla H_{JJ}^{\text{elec[GB]}} + \alpha_{IJ}^{\text{GB}} \dot{\mathbf{R}} \quad (52)$$

where α_{IJ}^{GB} is a parameter that is determined by requiring

$$\mathbf{B}_{IJ}^{\text{GB,effNAC}} \cdot \dot{\mathbf{R}} = T_{IJ}^{\text{GB}} \quad (53)$$

and this gives,

$$\alpha_{IJ}^{\text{GB}} = \frac{T_{IJ}^{\text{GB}} - (\nabla H_{II}^{\text{elec[GB]}} - \nabla H_{JJ}^{\text{elec[GB]}}) \cdot \dot{\mathbf{R}}}{\dot{\mathbf{R}} \cdot \dot{\mathbf{R}}} \quad (54)$$

Eqs 52–54 are an example of how $\mathbf{B}^{\text{GB,preprojected}}$ can be chosen.

In summary, eqs 22, 45, and 47 with user-supplied $\mathbf{B}_{IJ}^{\text{GB,preprojected}}$ define the electronic and nuclear EOMs for GSE, and eqs 48 and 50 define the special case of electronic and nuclear EOMs of SE, which is SE.

2.2. Fewest-Switches Trajectory Surface Hopping. A computational advantage of SE and GSE is that they are robust on the choice of representation, i.e., the simulated results are insensitive on the choice between adiabatic and diabatic representations; one obtains similar results if one propagates trajectories on MCH, diagonal, diabatic, or other representations. This is not true for TSH methods.^{79,80} Because TSH methods are often (not always) more accurate in fully adiabatic basis, one usually prefers to use the diagonal representation.^{11,53,81–87} This makes TSH methods more complicated when SOC is included.

The original FS-TSH method was developed for internal conversion processes.³⁴ Here, following the lead of Richter et al.,⁴⁵ we adopt a formalism that can be generalized to treat SOC in a practical way.

In FS-TSH and other TSH methods, the trajectories are propagated on one potential energy surface at a time, punctuated by surface hops to other surfaces. The active surface at any given time is labeled K . Therefore, between hops, the nuclear EOM for TSH is

$$\dot{\mathbf{P}}_{\text{TSH}}^{\text{GB}} = -\nabla H_{KK}^{\text{elec[GB]}} \quad (55)$$

The electronic EOM for TSH is identical to that of GSE or SE:

$$\dot{\mathbf{c}}_{\text{TSH}}^{\text{GB}} = -\left(\frac{i}{\hbar}\mathbf{H}^{\text{elec[GB]}} + \mathbf{T}^{\text{GB}}\right)\mathbf{c}^{\text{GB}} \quad (56)$$

In the fewest-switches method, the surface K is switched stochastically according to the following hopping probability:

$$P_{K \rightarrow I}^{\text{GB}}(t, t + \Delta t) = \max\left(\frac{b_{KI}^{\text{GB}}(t)\Delta t}{\rho_{KK}^{\text{GB}}(t)}, 0\right) \quad (57)$$

where b_{KI}^{GB} is the rate of population change from state K to state I in the GB basis during time interval t to $t + \Delta t$, where population is defined by eq 23 as $|\mathbf{c}^{\text{GB}}|^2$. The FS hopping probability minimizes the number of state switches required and to maintain the correct statistical distribution of electronic state populations in the case where the surfaces are degenerate; then eq 25 gives b_{KI}^{GB} as

$$b_{KI}^{\text{GB}}(t) = 2\left(\frac{1}{\hbar}\text{Im}(H_{KI}^{\text{elec[GB]}}\rho_{IK}^{\text{GB}}) - \text{Re}(T_{KI}^{\text{GB}}\rho_{IK}^{\text{GB}})\right) \quad (58)$$

The hop from one surface to another corresponds to a discontinuity in the active potential energy surface. To conserve energy, one adjusts the momentum discontinuously when a hop occurs. This adjustment is not random; it is adjusted along a certain direction called the momentum adjustment vector or the hopping direction. The velocity $\dot{\mathbf{R}}_a$ of atom a is adjusted after a $K \rightarrow I$ hop according to,

$$\dot{\mathbf{R}}_a(t)|_{\text{post}K \rightarrow I} = \dot{\mathbf{R}}_a(t)|_{\text{pre}K \rightarrow I} - f_{KI} \frac{\mathbf{h}_{KI,a}}{M_a} \quad (59)$$

where $\mathbf{h}_{KI,a}$ is the momentum adjustment vector of atom a , and f_{KI} is a factor determined by requiring energy conservation, which requires

$$\begin{aligned} & \sum_a^{N_{\text{atoms}}} \frac{1}{2} M_a (\dot{\mathbf{R}}_a(t)|_{\text{post}K \rightarrow I})^2 + H_{II}^{\text{elec[GB]}} \\ &= \sum_a^{N_{\text{atoms}}} \frac{1}{2} M_a (\dot{\mathbf{R}}_a(t)|_{\text{pre}K \rightarrow I})^2 + H_{KK}^{\text{elec[GB]}} \end{aligned} \quad (60)$$

Inserting eq 59 into 60 gives,

$$f_{KI} = \frac{E_h^{KI}(t) \pm \sqrt{(E_h^{KI}(t))^2 + 4E_{\text{kin},h}^{KI}(t)\Delta H_{KI}^{\text{GB}}(t)}}{2E_{\text{kin},h}^{KI}(t)} \quad (61)$$

where

$$\Delta H_{KI}^{\text{GB}}(t) = H_{KK}^{\text{elec[GB]}} - H_{II}^{\text{elec[GB]}} \quad (62)$$

$$E_h^{KI}(t) = \sum_a (\dot{\mathbf{R}}_A(t)|_{\text{pre}K \rightarrow I} \cdot \mathbf{h}_{KI,a}(t)) \quad (63)$$

$$E_{\text{kin},h}^{KI} = \sum_a \frac{1}{2} \frac{|\mathbf{h}_{KI,a}|^2}{M_a} \quad (64)$$

To have a real solution for f_{KI} , the following condition must be fulfilled:

$$\Delta E^{KI}(t) \equiv \frac{E_h^{KI}(t)^2}{4E_{\text{kin},h}^{KI}(t)} + \Delta H_{KI}^{\text{GB}}(t) \geq 0 \quad (65)$$

When eq 65 is not fulfilled, the called-for a hop is called frustrated, and no hop is made. Although there are arguments that frustrated hops are necessary to achieve detailed balance,^{88–92} frustrated hops are an intrinsic deficiency of TSH methods; they cause errors such as population leaking.^{93,94}

Downward hops are never frustrated. An upward hop may be frustrated because there is not enough energy to hop, but sometimes hops are frustrated even when there is enough energy to hop. The latter occurs if there is not enough momentum in the direction of the momentum adjustment vector. The literature has many choices of momentum adjustment vector, for examples, the nuclear velocity vector, the NAC, the difference gradient vector, or an effective NAC.⁵² The most convincing work shows that the NAC is probably the best choice,^{95–100} although in practice, as discussed next, one should use a projected NAC⁶⁹ if the NAC has been computed in the space frame.

The choice of momentum adjustment vector affects not only the possible success of a called-for hop but also the conservation of angular momentum and center of mass momentum.⁶⁹ As shown in ref 69, using a space-frame NAC (which is the kind of NAC produced by most electronic structure programs that can produce NACs) fails to conserve angular momentum and center of mass momentum. In that spirit, just as eq 60 requires the hopping process to conserve total energy, we require that the hopping process conserves total nuclear angular momentum and center of mass momentum:⁶⁹

$$\sum_a^{N_{\text{atoms}}} \mathbf{R}_a(t) \times M_a \dot{\mathbf{R}}_a(t)|_{\text{post}K \rightarrow I} = \sum_a^{N_{\text{atoms}}} \mathbf{R}_a(t) \times M_a \dot{\mathbf{R}}_a(t)|_{\text{pre}K \rightarrow I} \quad (66)$$

$$\sum_a^{N_{\text{atoms}}} M_a \dot{\mathbf{R}}_a(t)|_{\text{post}K \rightarrow I} = \sum_a^{N_{\text{atoms}}} M_a \dot{\mathbf{R}}_a(t)|_{\text{pre}K \rightarrow I} \quad (67)$$

Using eq 59 reduces eqs 66 and 67 to,

$$\sum_a^{N_{\text{atoms}}} \mathbf{R}_a(t) \times (-f_{KI} \mathbf{h}_{KI,a}) = 0 \quad (68)$$

$$\sum_a^{N_{\text{atoms}}} (-f_{KI} \mathbf{h}_{KI,a}) = 0 \quad (69)$$

Among popular choices of the momentum adjustment vector (which include the nuclear velocity vector, the difference gradient vector, and the space-frame NAC) only the difference gradient vector satisfies eqs 68 and 69. We do not want to restrict ourselves to this choice; therefore, for an arbitrary choice, $\mathbf{h}_{KI}^{\text{preprojected}}$, of momentum adjustment vector (which can be, for example, a NAC or nuclear velocity vector), we project

$$\mathbf{h}_{KI} = (\mathbf{1} - \mathbf{Q})\mathbf{h}_{KI}^{\text{preprojected}} \quad (70)$$

where $\mathbf{1}$ and \mathbf{Q} are the identity operator and projection operator⁶⁹ respectively (these are $3N_{\text{atoms}} \times 3N_{\text{atoms}}$ matrices). The projection operator is shown in eq 46. When $\mathbf{h}_{KI}^{\text{preprojected}}$ is the nuclear velocity vector, \mathbf{h}_{KI} becomes a vibrational velocity vector; when $\mathbf{h}_{KI}^{\text{preprojected}}$ is NAC, \mathbf{h}_{KI} corresponds to projected NAC.

With a computed factor f_{KI} from eq 61 and a choice of momentum adjustment vector or hopping direction according to eq 70, one obtains a hopping procedure that conserves total energy, angular momentum, and center of mass momentum.

Our recommended choice of momentum adjustment vector when using a space-frame NAC from an electronic structure program is a projected NAC where the projection removes the translational and rotational components of the NAC. If one is using a transformed NAC computed from transformation of a fitted diabatic representation, then (analogously to the discussion in Section 2.1), there is no angular-momentum-nonconservation or center-of-mass-motion nonconservation problem because the transformed NAC is a functional of internal coordinates only.

When a hop is frustrated, one can either ignore the frustrated hop and continue forward, or one can ignore it and reflect backward. The latter is motivated by thinking of the increase in potential energy at a called-for upward hop as a repulsive wall that bounces the trajectory backward. Reflecting the velocity leads to

$$\dot{\mathbf{R}}_a(t)|_{\text{postreflect}} = \dot{\mathbf{R}}_a(t)|_{\text{prereflect}} - g_{KL} \mathbf{h}_{KL,a} \quad (71)$$

where $\mathbf{h}_{KL,a}$ is the velocity reflection vector of atom a , and g_{KL} is a factor determined by satisfying energy conservation, which requires

$$\sum_a^{N_{\text{atoms}}} \frac{1}{2} M_a (\dot{\mathbf{R}}_a(t)|_{\text{postreflect}})^2 = \sum_a^{N_{\text{atoms}}} \frac{1}{2} M_a (\dot{\mathbf{R}}_a(t)|_{\text{prereflect}})^2 \quad (72)$$

This gives

$$g_{KL} = 2 \frac{\dot{\mathbf{R}}_a(t)|_{\text{prereflect}} \cdot \mathbf{h}_{KL,a}}{\mathbf{h}_{KL,a} \cdot \mathbf{h}_{KL,a}} \quad (73)$$

where K and L are respectively the active and frustrated states. There are many possible choices for the velocity reflection vector. For any of these choices, eq 73 conserves total energy because the kinetic energy is not changed by the reflection.

Another possible action at a frustrated hop is a conditional reflection.¹⁰¹ The first conditional reflection method is called the ∇V scheme,¹⁰¹ in which one reflects the velocity along the direction $\mathbf{h}_{KL,a}$ if

$$(-\nabla H_{LL}^{\text{elec[MCH]}} \cdot \mathbf{h}_{KL})(\mathbf{P}(t) \cdot \mathbf{h}_{KL}) < 0 \quad (74)$$

where $\mathbf{P}(t)$ is the nuclear momentum at the time t at which a frustrated hop occurs. Otherwise, i.e., if eq 74 is not satisfied, one ignores the frustrated hop. Later, an additional condition was suggested,^{102,103}

$$(-\nabla H_{KK}^{\text{elec[MCH]}} \cdot \mathbf{h}_{KL})(-\nabla H_{LL}^{\text{elec[MCH]}} \cdot \mathbf{h}_{KL}) < 0 \quad (75)$$

In this scheme, the trajectory is reflected only when both conditions eqs 74 and (75) are satisfied.

The following conditions need to be satisfied to conserve total nuclear angular momentum and center of mass motion after a velocity reflection

$$\begin{aligned} \sum_a^{N_{\text{atoms}}} \mathbf{R}_a(t) \times M_a \dot{\mathbf{R}}_a(t)|_{\text{postreflect}} \\ = \sum_a^{N_{\text{atoms}}} \mathbf{R}_a(t) \times M_a \dot{\mathbf{R}}_a(t)|_{\text{prereflect}} \end{aligned} \quad (76)$$

$$\sum_a^{N_{\text{atoms}}} M_a \dot{\mathbf{R}}_a(t)|_{\text{postreflect}} = \sum_a^{N_{\text{atoms}}} M_a \dot{\mathbf{R}}_a(t)|_{\text{prereflect}} \quad (77)$$

These conditions lead to

$$\sum_a^{N_{\text{atoms}}} \mathbf{R}_a(t) \times M_a \left(-2 \frac{\dot{\mathbf{R}}_a(t)|_{\text{prereflect}} \cdot \mathbf{h}_{KL,a}}{\mathbf{h}_{KL,a} \cdot \mathbf{h}_{KL,a}} \mathbf{h}_{KL,a} \right) = 0 \quad (78)$$

$$\sum_a^{N_{\text{atoms}}} M_a \left(-2 \frac{\dot{\mathbf{R}}_a(t)|_{\text{prereflect}} \cdot \mathbf{h}_{KL,a}}{\mathbf{h}_{KL,a} \cdot \mathbf{h}_{KL,a}} \mathbf{h}_{KL,a} \right) = 0 \quad (79)$$

One can use the same remedy as we have used above, namely, projecting out the translational and rotational components of a preprojected velocity reflection vector,

$$\mathbf{h}_{KL} = (\mathbf{1} - \mathbf{Q})\mathbf{h}_{KL}^{\text{preprojected}} \quad (80)$$

Our recommended procedure is conditional reflection with the ∇V scheme and the projected NAC as the velocity reflection vector.

2.3. More Discussion of Conservation of Angular Momentum and Center-of-Mass Momentum. From both Sections 2.1 and 2.2, to conserve total nuclear angular momentum and center-of-mass momentum, we have stressed the importance of using a force direction (nonadiabatic force direction in GSE, momentum adjustment vector or velocity reflection vector in FS-TSH) that does not have nonzero translational and rotational components. In contrast, the early literature considered only conservation of total energy. However, for a closed system, when electronic angular momentum is neglected (as is the case in mixed quantum-classical methods), the system's total nuclear angular momentum and center-of-mass linear momentum are required to be conserved because of the isotropy and translational symmetry of space.

Nuclear angular momentum nonconservation can be more severe in SCP methods based on GSE than in TSH methods. This is because one uses the nonadiabatic force direction at every time step in GSE, and therefore, the nonconservation is accumulated along a trajectory, while for TSH, nonconservation only happens at places where there is a hop. For example, our previous studies of ethylene nonadiabatic dynamics in 200 fs simulations with unprojected space-frame nonadiabatic

Table 1. Summary of Working Equations for GSE, SE, and TSH Methods in a General Basis, in the MCH Basis, and in the Diagonal Basis

Method	Basis	Formula	Equation
GSE	GB	Elec EOM	$[c_i^{\text{GB}}(t)]_{\text{GSE}} = - \sum_j^{N_{\text{states}}} \left(\frac{i}{\hbar} H_{ij}^{\text{elec[GB]}} + T_{ij}^{\text{GB}} \right) c_j^{\text{GB}}(t)$
		Nuc EOM	$[\dot{\mathbf{P}}^{\text{GB}}]_{\text{GSE}} = - \sum_{ij}^{N_{\text{states}}} \rho_{ij}^{\text{GB}} \nabla H_{ij}^{\text{elec[GB]}} + \sum_{ijl}^{N_{\text{states}}} \left(\frac{T_{il}^{\text{GB}} \rho_{lj}^{\text{GB}} H_{ij}^{\text{elec[GB]}} \mathbf{B}_{il}^{\text{GB}}}{\mathbf{B}_{il}^{\text{GB}} \cdot \mathbf{R}} - \frac{T_{lj}^{\text{GB}} \rho_{il}^{\text{GB}} H_{ij}^{\text{elec[GB]}} \mathbf{B}_{lj}^{\text{GB}}}{\mathbf{B}_{lj}^{\text{GB}} \cdot \mathbf{R}} \right)$
	diag	Elec EOM	$[c_i^{\text{diag}}(t)]_{\text{GSE}} = - \frac{i}{\hbar} H_{ii}^{\text{elec[diag]}} c_i^{\text{diag}}(t) - \sum_j^{N_{\text{states}}} (T_{ij}^{\text{diag}}) c_j^{\text{diag}}(t)$
		Nuc EOM	$[\dot{\mathbf{P}}^{\text{diag}}]_{\text{GSE}} = - \sum_i^{N_{\text{states}}} \rho_{ii}^{\text{diag}} \nabla H_{ii}^{\text{elec[diag]}} + 2 \sum_{ij}^{N_{\text{states}}} \text{Re} \left(\frac{T_{ij}^{\text{diag}} \rho_{ij}^{\text{diag}} \mathbf{B}_{ij}^{\text{diag}}}{\mathbf{B}_{ij}^{\text{diag}} \cdot \mathbf{R}} \right) H_{ii}^{\text{elec[diag]}}$
	MCH	Elec EOM	$[c_i^{\text{MCH}}(t)]_{\text{GSE}} = - \sum_j^{N_{\text{states}}} \left(\frac{i}{\hbar} H_{ij}^{\text{elec[MCH]}} + T_{ij}^{\text{MCH}} \right) c_j^{\text{MCH}}(t)$
		Nuc EOM	$[\dot{\mathbf{P}}^{\text{MCH}}]_{\text{GSE}} = - \sum_{ij}^{N_{\text{states}}} \rho_{ij}^{\text{MCH}} \nabla H_{ij}^{\text{elec[MCH]}} + \sum_{ijl}^{N_{\text{states}}} \left(\frac{T_{il}^{\text{MCH}} \rho_{lj}^{\text{MCH}} H_{ij}^{\text{elec[MCH]}} \mathbf{B}_{il}^{\text{MCH}}}{\mathbf{B}_{il}^{\text{MCH}} \cdot \mathbf{R}} - \frac{T_{lj}^{\text{MCH}} \rho_{il}^{\text{MCH}} H_{ij}^{\text{elec[MCH]}} \mathbf{B}_{lj}^{\text{MCH}}}{\mathbf{B}_{lj}^{\text{MCH}} \cdot \mathbf{R}} \right)$
SE	GB	Elec EOM	$[c_i^{\text{GB}}(t)]_{\text{SE}} = - \sum_j^{N_{\text{states}}} \left(\frac{i}{\hbar} H_{ij}^{\text{elec[GB]}} + T_{ij}^{\text{GB}} \right) c_j^{\text{GB}}(t)$
		Nuc EOM	$[\dot{\mathbf{P}}^{\text{GB}}]_{\text{SE}} = - \sum_{ij}^{N_{\text{states}}} \rho_{ij}^{\text{GB}} \nabla H_{ij}^{\text{elec[GB]}} + \sum_{ijl}^{N_{\text{states}}} (\rho_{lj}^{\text{GB}} H_{ij}^{\text{elec[GB]}} \mathbf{d}_{il}^{\text{GB}} - \rho_{il}^{\text{GB}} H_{ij}^{\text{elec[GB]}} \mathbf{d}_{lj}^{\text{GB}})$
	diag	Elec EOM	$[c_i^{\text{diag}}(t)]_{\text{SE}} = - \frac{i}{\hbar} H_{ii}^{\text{elec[diag]}} c_i^{\text{diag}}(t) - \sum_j^{N_{\text{states}}} (T_{ij}^{\text{diag}}) c_j^{\text{diag}}(t)$
		Nuc EOM	$[\dot{\mathbf{P}}^{\text{diag}}]_{\text{GSE}} = - \sum_i^{N_{\text{states}}} \rho_{ii}^{\text{diag}} \nabla H_{ii}^{\text{elec[diag]}} + 2 \sum_{ij}^{N_{\text{states}}} \text{Re}(\rho_{ij}^{\text{diag}} \mathbf{d}_{ij}^{\text{diag}}) H_{ii}^{\text{elec[diag]}}$
	MCH	Elec EOM	$[c_i^{\text{MCH}}(t)]_{\text{SE}} = - \sum_j^{N_{\text{states}}} \left(\frac{i}{\hbar} H_{ij}^{\text{elec[MCH]}} + T_{ij}^{\text{MCH}} \right) c_j^{\text{MCH}}(t)$
		Nuc EOM	$[\dot{\mathbf{P}}^{\text{MCH}}]_{\text{SE}} = - \sum_{ij}^{N_{\text{states}}} \rho_{ij}^{\text{MCH}} \nabla H_{ij}^{\text{elec[MCH]}} + \sum_{ijl}^{N_{\text{states}}} (\rho_{lj}^{\text{MCH}} H_{ij}^{\text{elec[MCH]}} \mathbf{d}_{il}^{\text{MCH}} - \rho_{il}^{\text{MCH}} H_{ij}^{\text{elec[MCH]}} \mathbf{d}_{lj}^{\text{MCH}})$
FS-TSH	GB	Elec EOM	$[c_i^{\text{GB}}(t)]_{\text{TSH}} = - \sum_j^{N_{\text{states}}} \left(\frac{i}{\hbar} H_{ij}^{\text{elec[GB]}} + T_{ij}^{\text{GB}} \right) c_j^{\text{GB}}(t)$
		Nuc EOM	$b_{kl}^{\text{GB}}(t) = 2 \left(\frac{1}{\hbar} \text{Im}(H_{kl}^{\text{elec[GB]}} \rho_{lk}^{\text{GB}}) - \text{Re}(T_{kl}^{\text{GB}} \rho_{lk}^{\text{GB}}) \right)$ $[\dot{\mathbf{P}}^{\text{GB}}]_{\text{TSH}} = - \nabla H_{kk}^{\text{elec[GB]}}$
	diag	Elec EOM	$[c_i^{\text{diag}}(t)]_{\text{TSH}} = - \frac{i}{\hbar} H_{ii}^{\text{elec[diag]}} c_i^{\text{diag}}(t) - \sum_j^{N_{\text{states}}} (T_{ij}^{\text{diag}}) c_j^{\text{diag}}(t)$
		Nuc EOM	$b_{kl}^{\text{diag}}(t) = -2 \text{Re}(T_{il}^{\text{diag}} \rho_{li}^{\text{diag}})$ $[\dot{\mathbf{P}}^{\text{diag}}]_{\text{TSH}} = - \nabla H_{kk}^{\text{elec[diag]}}$
	MCH	Elec EOM	$[c_i^{\text{MCH}}(t)]_{\text{TSH}} = - \sum_j^{N_{\text{states}}} \left(\frac{i}{\hbar} H_{ij}^{\text{elec[MCH]}} + T_{ij}^{\text{MCH}} \right) c_j^{\text{MCH}}(t)$

Table 1. continued

Method	Basis	Formula	Equation
		b_{kl}^{MCH}	$b_{kl}^{\text{MCH}}(t) = 2\left(\frac{1}{\hbar}\text{Im}(H_{ll}^{\text{elec[MCH]}}\rho_{ll}^{\text{MCH}}) - \text{Re}(T_{ll}^{\text{MCH}}\rho_{ll}^{\text{MCH}})\right)$
	Nuc EOM		$[\dot{\mathbf{P}}^{\text{MCH}}]_{\text{TSH}} = -\nabla H_{kk}^{\text{elec[MCH]}}$

coupling vectors showed that the SCP and TSH methods had nuclear angular momentum nonconservation by more than $10\hbar$ and $1\hbar$ respectively. (In both cases, though, angular momentum would be conserved if one used a NAC calculated in internal coordinates or a projected NAC that eliminates the overall translation and rotation.)

The original decay-of-mixing methods (decay-of-mixing methods will be motivated in Section 2.6 and discussed in detail in Section 5) did consider conservation of energy, angular momentum, and center of mass motion in the nuclear EOM.^{104,105} However, those methods were only applied to analytic coupled potential energy surfaces. Using a space-frame NAC in direct dynamics destroys conservation of angular momentum and center of mass momentum, as first discussed in ref 69. in 2020. Recently, this problem has been further discussed and elaborated.^{106,107}

Our suggested remedy to angular momentum and center of mass momentum nonconservation problems may be summarized as follows: All terms in the nuclear EOM should have a force direction for which the translational and rotational components are zero.

2.4. Choice of Basis for the Electronic Wave Function.

When SOC is included, the electronic Hamiltonian is usually split into two contributions,

$$H^{\text{elec}} = H^{\text{SOF}} + H^{\text{SOC}} \quad (81)$$

where H^{SOF} is the spin-orbit-free Hamiltonian that includes electronic kinetic energy and all Coulomb interactions between electrons and nuclei, and H^{SOC} is the SOC. As discussed in Section 2.1, one may then distinguish the MCH and the diagonal representations. To distinguish various matrix representations of the various Hamiltonians, we use the following notation,

$$H_{IJ}^{\text{A[GB]}} = \langle \phi_I^{\text{GB}} | H^{\text{A}} | \phi_J^{\text{GB}} \rangle \quad (82)$$

where A can be “elec”, “SOF”, or “SOC” as defined in eq 81.

The MCH basis diagonalizes H^{SOF} ,

$$H_{IJ}^{\text{SOF[MCH]}} = \langle \phi_I^{\text{MCH}} | H^{\text{SOF}} | \phi_J^{\text{MCH}} \rangle = V_I^{\text{SOF}} \delta_{IJ} \quad (83)$$

where V_I^{SOF} is the spin-free potential energy surface of MCH state I . And the diag basis diagonalizes H^{elec} (the diag basis functions are eigenvectors of H^{elec}):

$$H_{IJ}^{\text{elec[diag]}} = \langle \phi_I^{\text{diag}} | H^{\text{elec}} | \phi_J^{\text{diag}} \rangle = V_I^{\text{diag}} \delta_{IJ} \quad (84)$$

where V_I^{diag} is the fully adiabatic potential energy surface of diagonal state I .

When SOC is included, $\mathbf{H}^{\text{elec[MCH]}}$ has nonzero off-diagonal elements of the SOC operator in the MCH basis. However, one should not confuse the MCH basis with a diabatic basis, which also has a nondiagonal Hamiltonian. As mentioned above, a diabatic representation is one for which the nonadiabatic coupling vectors \mathbf{d}_{IJ} can be neglected anywhere on the potential energy surface,⁴³ but \mathbf{d}_{IJ} is not negligible in the MCH basis when SOC is included. Obtaining a diabatic

representation is useful when constructing analytic representations of potential energy surfaces because the diabatic potential energies and couplings are smooth functions of nuclear coordinates, but global diabatic representations are not useful in direct dynamics, because they are not straightforwardly available from electronic structure codes.

The difficulty of including SOC is that the trajectories may require gradients of V_I^{diag} , but electronic structure packages only produce gradients of V_I^{SOF} . One can diagonalize the total Hamiltonian in the MCH representation to obtain the Hamiltonian in the diagonal representation:

$$\mathbf{H}^{\text{elec[diag]}} = \mathbf{U}^\dagger \mathbf{H}^{\text{elec[MCH]}} \mathbf{U} \quad (85)$$

And therefore, one can transform from the MCH basis to the diagonal basis by

$$\mathbf{c}^{\text{diag}} = \mathbf{U}^\dagger \mathbf{c}^{\text{MCH}} \quad (86)$$

When the electronic structure software only provides potential energy surfaces and gradients in the MCH basis, all the required terms in the diagonal basis can nevertheless be obtained by the above transformations.^{67,108}

2.5. Summary of EOMs for GSE, SE, and FS-TSH in Various Bases. The GSE (or its special case the SE) provides the starting point for all SCP methods; in a later section we will recommend coherent switching with decay-of-mixing method (CSDM) and its extensions as the preferred SCP methods. The FS-TSH method provides the starting point for all TSH methods that are considered here; in a later section we will recommend fewest switches time-uncertainty trajectory-surface-hopping method (FSTU) and its extensions as the preferred TSH methods.

The EOMs for the GSE, SE, and TSH methods in the GB, diagonal, and MCH representations are summarized in Table 1. Notice that in Table 1, we do not summarize the \mathbf{B}^{MCH} force tensor in GSE or the momentum adjustment and velocity reflection vectors in FS-TSH because there is additional flexibility in choosing these ingredients.

2.6. Addition of Decoherence to the Electronic Density Matrix. A deficiency of the original FS-TSH method and of the pure SE and GSE methods is that they do not include decoherence. Decoherence is the tendency of the density matrix of a subsystem to assume a diagonal form corresponding to a classical mixture of populations, where the populations are the diagonal elements of the subsystem density matrix. The basis in which the density matrix becomes diagonal is called the pointer basis; it is selected by the environment, i.e., by the “measurement” being made.¹⁰⁹ In much of the literature on decoherence, the subsystem is considered to be a molecule in an environment such as a solvent or a solid surface. However, we now realize that the decoherence of the electronic subsystem of a molecule is often dominated by interaction of the electronic subsystem with the nuclei of the molecule rather than by interaction with an extramolecular environment.¹⁰⁴

The wave function for an entire system does not usually factor into a product of wave functions of its subsystems. Then a subsystem is not described by a wave function that evolves by a time-dependent Schrödinger equation.¹¹⁰ The most complete possible description of such a subsystem is by a reduced density matrix that evolves by a generalized master equation. The reduced density matrix of a subsystem does not usually correspond to a pure state described by a Schrödinger equation; rather it corresponds to a mixed state. A generalized master equation may also be called a nonunitary Liouville-von Neumann equation. The original Liouville-von Neumann equation (sometimes called the quantum Liouville equation) corresponds to unitary time evolution of a pure state and is equivalent to the time-dependent Schrödinger equation.^{111,112}

To describe the time evolution of a mixed state, one must add additional terms to the unitary Liouville-von Neumann equation;^{113–117} this yields a generalized master equation for the evolution of the mixed-state density matrix.

The electronic density matrix is a reduced density matrix of the molecular density matrix, given by⁵⁴

$$\rho^{\text{elec}} = \text{Tr}_{\text{nuc}}(\rho^{\text{mol}}) \quad (87)$$

where ρ^{elec} is defined in eq 23, and ρ^{mol} is the molecular density matrix. The reduced density matrix of the electronic subsystem, starting in a pure state, evolves to a mixed-state density matrix over time; this involves the off-diagonal elements of ρ^{elec} relaxing to zero. Since the off-diagonal elements of a density matrix are called coherences, this process is called decoherence. The reciprocal of the first-order decay rate constant of the coherence is called the decoherence time.

We consider the reduced density matrix ρ^{elec} of an isolated molecular system (either the temporary complex formed by a bimolecular collision or the whole molecule involved in a unimolecular process). The unitary propagation of ρ^{elec} is given by eq 24, which is equivalent to

$$i\hbar \frac{\partial}{\partial t} \rho^{\text{elec}} = [(T^{\text{elec}} + V^{\text{elec}} + H^{\text{nuc-elec}}), \rho^{\text{elec}}] \quad (88)$$

where T^{elec} , V^{elec} , $H^{\text{nuc-elec}}$ are respectively the electronic kinetic energy, the electron–electron Coulomb interactions, and the nuclear–electron interaction operators. The nonunitary propagation is given by

$$i\hbar \frac{\partial}{\partial t} \rho^{\text{elec}} = [(T^{\text{elec}} + V^{\text{elec}}), \rho^{\text{elec}}] + \text{Tr}_{\text{B}}([H^{\text{nuc-elec}}, \rho]) \quad (89)$$

The direct solution of eq 89 is not easy, and many approximations have been put forward.^{84,118–133} Phenomenologically, decoherence causes the off-diagonal matrix elements of ρ^{elec} to decay to zero exponentially (or like a Gaussian) with a time scale called the decoherence time. Therefore, one way to approach the problem is to treat the decoherence phenomenologically by replacing the physical decoherence with algorithmic decoherence, which we also call decay of mixing.^{80,83,104,105,134–138} Our preferred methods, called decay-of-mixing methods, start with the decoherence-free SE or GSE equations and add algorithmic decoherence by adding non-Markovian decay of the electronic coefficients of nonpointer states. The method can equivalently be recast as decay of the off-diagonal elements of the electronic density matrix.¹³⁹ This decay is due to the nuclear wave packets associated with different electronic states getting out of overlap.^{135,140} Therefore, between strong-interaction regions, the electronic

density matrix tends to become diagonal (in a basis called the pointer basis) on the decoherence time scale. Note that it is called pointer basis because it denotes the pointer on a measuring apparatus. On the same time scale, the decay of mixing drives the population of one state, called the pointer state K , to unity (and the others to zero). The identity of the pointer state is switched stochastically so that the final populations of an ensemble of trajectories provide a semi-classical approximation to the quantum mechanical distribution of final states. More details of the decay of mixing are given in the next paragraph.

In decay-of-mixing methods, one exponentially decays the coherence to zero:

$$\rho_{IK}^{\text{elec}}(t + dt) = \rho_{IK}^{\text{elec}}(t) e^{-dt/\tau_{IK}(\mathbf{R}(t))} \quad (90)$$

where I is a general state that is not the current pointer state K , and τ_{IK} is the position-dependent decay-of-mixing time. This means that coherence has a half-life of $\tau_{IK} \ln 2$, and it is equivalent to decaying the coefficients of all states except the pointer state to zero in eq 14. After the decay is complete, the electronic density matrix of a given trajectory is again pure, but only a single diagonal element survives and becomes unity; the rest of the elements are all zero. Note though that another strong interaction region may be encountered before the decay is complete, or the pointer state may change before the decay is complete. If one averages the final density matrices over an ensemble of mixed quantum-classical trajectories (with different initial conditions), the ensemble-averaged density matrix represents a mixed-state density matrix, diagonal but with more than one nonzero diagonal element. Only the ensemble-averaged electronic density matrix is physically meaningful.

There are many approaches to include decoherence,^{83,102,104,105,134,135,138,141–143} and it is beyond the present scope to provide a complete review; we refer interested readers to a recent review.⁵⁴

3. INTRODUCTION TO NONADIABATIC DYNAMICS WITHOUT WAVE FUNCTIONS

Section 3.1 summarizes the required electronic structure information for GSE, SE, and FS-TSH and shows where one requires electronic wave functions. Wave function-free mixed quantum-classical nonadiabatic dynamics involves two levels, namely, NAC-free mixed quantum-classical nonadiabatic dynamics, and overlap-free (TDC-free) mixed quantum-classical nonadiabatic dynamics. In the following text, we will simply call the mixed quantum-classical nonadiabatic dynamics as nonadiabatic dynamics for simplicity. Sections 3.2 and 3.3 consider the NAC-free level, which results in overlap-based algorithms, and Section 3.4 motivates the overlap-free approach, which results in curvature-driven algorithms. At the NAC-free level, one still needs wave functions because one needs the TDC; but the NAC-free level, in addition to its interest for practical calculations, is also of interest in providing a step-by-step route to the overlap-free level, which is wave function-free.

The NAC-free nonadiabatic dynamics methods are also called overlap-based nonadiabatic dynamics because one needs overlaps to compute TDCs. And the wave function-free nonadiabatic dynamics methods are also called overlap-free nonadiabatic dynamics or TDC-free nonadiabatic dynamics. We show below how we approximate TDCs with curvatures of potential energies. Then the wave function-free nonadiabatic

Table 2. Electronic Structure Information Required by Direct Dynamics Calculations for a Hamiltonian Without SOC^a

Method	Dynamics basis ^{a,b}	Required Information in Dynamics Basis			Required Information in MCH Basis		
		Energy	Gradient	Coupling	Energy	Gradient	Coupling
GSE	diag/MCH ^a	$\mathbf{H}^{\text{elec[MCH]}}$	$\nabla\mathbf{H}^{\text{elec[MCH]}}$	\mathbf{T}^{MCH}	$\mathbf{H}^{\text{elec[MCH]}}$	$\nabla\mathbf{H}^{\text{elec[MCH]}}$	\mathbf{T}^{MCH}
SE	diag/MCH	$\mathbf{H}^{\text{elec[MCH]}}$	$\nabla\mathbf{H}^{\text{elec[MCH]}}$	\mathbf{d}^{MCH}	$\mathbf{H}^{\text{elec[MCH]}}$	$\nabla\mathbf{H}^{\text{elec[MCH]}}$	\mathbf{d}^{MCH}
FS-TSH	diag/MCH	$\mathbf{H}^{\text{elec[MCH]}}$	$\nabla\mathbf{H}_{KK}^{\text{elec[diag]}}$	\mathbf{T}^{MCH}	$\mathbf{H}^{\text{elec[MCH]}}$	$\nabla\mathbf{H}_{KK}^{\text{elec[diag]}}$	\mathbf{T}^{MCH}

^aWhen there is no spin-orbit coupling in the Hamiltonian, the diagonal and MCH representations are identical. ^bWe denote the basis used to propagate the dynamics as the dynamics basis.

Table 3. Electronic Structure Information Required by Direct Dynamics Calculations for a Hamiltonian that Includes SOC

Method	Dynamics basis	Required Information in Dynamics Basis			Required Information in MCH Basis		
		Energy	Gradient	Coupling	Energy	Gradient	Coupling
Use nuclear gradient tensor scheme (NGT) for transformation							
GSE	diag	$\mathbf{H}^{\text{elec[diag]}}$	$\nabla\mathbf{H}^{\text{elec[diag]}}$	$\mathbf{T}^{\text{diag}} = \dot{\mathbf{R}} \cdot \mathbf{d}^{\text{diag}}$	$\mathbf{H}^{\text{elec[MCH]}}$	$\nabla\mathbf{H}^{\text{elec[MCH]}}$	$\nabla\mathbf{H}^{\text{elec[MCH]}}$ and \mathbf{d}^{MCH}
GSE	MCH	$\mathbf{H}^{\text{elec[MCH]}}$	$\nabla\mathbf{H}^{\text{elec[MCH]}}$	\mathbf{T}^{MCH}	$\mathbf{H}^{\text{elec[MCH]}}$	$\nabla\mathbf{H}^{\text{elec[MCH]}}$	\mathbf{T}^{MCH}
SE	diag	$\mathbf{H}^{\text{elec[diag]}}$	$\nabla\mathbf{H}^{\text{elec[diag]}}$	\mathbf{d}^{diag}	$\mathbf{H}^{\text{elec[MCH]}}$	$\nabla\mathbf{H}^{\text{elec[MCH]}}$	\mathbf{d}^{MCH}
SE	MCH	$\mathbf{H}^{\text{elec[MCH]}}$	$\nabla\mathbf{H}^{\text{elec[MCH]}}$	\mathbf{d}^{MCH}	$\mathbf{H}^{\text{elec[MCH]}}$	$\nabla\mathbf{H}^{\text{elec[MCH]}}$	\mathbf{d}^{MCH}
FS-TSH	diag	$\mathbf{H}^{\text{elec[diag]}}$	$\nabla\mathbf{H}_{KK}^{\text{elec[diag]}}$	$\mathbf{T}^{\text{diag}} = \dot{\mathbf{R}} \cdot \mathbf{d}^{\text{diag}}$	$\mathbf{H}^{\text{elec[MCH]}}$	$\nabla\mathbf{H}^{\text{elec[MCH]}}$ and \mathbf{d}^{MCH}	$\nabla\mathbf{H}^{\text{elec[MCH]}}$ and \mathbf{d}^{MCH}
FS-TSH	MCH	$\mathbf{H}^{\text{elec[MCH]}}$	$\nabla\mathbf{H}_{KK}^{\text{elec[MCH]}}$	\mathbf{T}^{MCH}	$\mathbf{H}^{\text{elec[MCH]}}$	$\nabla\mathbf{H}_{KK}^{\text{elec[MCH]}}$	\mathbf{T}^{MCH}
Use time-derivative matrix (TDM) scheme for transformation							
GSE	diag	$\mathbf{H}^{\text{elec[diag]}}$	$\nabla\mathbf{H}^{\text{elec[diag]}}$	\mathbf{T}^{diag}	$\mathbf{H}^{\text{elec[MCH]}}$	$\nabla\mathbf{H}^{\text{elec[MCH]}}$	\mathbf{T}^{MCH}
GSE	MCH	$\mathbf{H}^{\text{elec[MCH]}}$	$\nabla\mathbf{H}^{\text{elec[MCH]}}$	\mathbf{T}^{MCH}	$\mathbf{H}^{\text{elec[MCH]}}$	$\nabla\mathbf{H}^{\text{elec[MCH]}}$	\mathbf{T}^{MCH}
SE	diag	$\mathbf{H}^{\text{elec[diag]}}$	$\nabla\mathbf{H}^{\text{elec[diag]}}$	\mathbf{d}^{diag}	$\mathbf{H}^{\text{elec[MCH]}}$	$\nabla\mathbf{H}^{\text{elec[MCH]}}$	\mathbf{d}^{MCH}
SE	MCH	$\mathbf{H}^{\text{elec[MCH]}}$	$\nabla\mathbf{H}^{\text{elec[MCH]}}$	\mathbf{d}^{MCH}	$\mathbf{H}^{\text{elec[MCH]}}$	$\nabla\mathbf{H}^{\text{elec[MCH]}}$	\mathbf{d}^{MCH}
FS-TSH	diag	$\mathbf{H}^{\text{elec[diag]}}$	$\nabla\mathbf{H}_{KK}^{\text{elec[diag]}}$	\mathbf{T}^{diag}	$\mathbf{H}^{\text{elec[MCH]}}$	$\nabla\mathbf{H}^{\text{elec[MCH]}}$ and \mathbf{T}^{MCH}	\mathbf{T}^{MCH}
FS-TSH	MCH	$\mathbf{H}^{\text{elec[MCH]}}$	$\nabla\mathbf{H}_{KK}^{\text{elec[MCH]}}$	\mathbf{T}^{MCH}	$\mathbf{H}^{\text{elec[MCH]}}$	$\nabla\mathbf{H}_{KK}^{\text{elec[MCH]}}$	\mathbf{T}^{MCH}
GSE	diag/MCH	$\mathbf{H}^{\text{elec[MCH]}}$	$\nabla\mathbf{H}^{\text{elec[MCH]}}$	\mathbf{T}^{MCH}	$\mathbf{H}^{\text{elec[MCH]}}$	$\nabla\mathbf{H}^{\text{elec[MCH]}}$	\mathbf{T}^{MCH}
SE	diag/MCH	$\mathbf{H}^{\text{elec[MCH]}}$	$\nabla\mathbf{H}^{\text{elec[MCH]}}$	\mathbf{d}^{MCH}	$\mathbf{H}^{\text{elec[MCH]}}$	$\nabla\mathbf{H}^{\text{elec[MCH]}}$	\mathbf{d}^{MCH}
FS-TSH	diag/MCH	$\mathbf{H}^{\text{elec[MCH]}}$	$\nabla\mathbf{H}_{KK}^{\text{elec[MCH]}}$	\mathbf{T}^{MCH}	$\mathbf{H}^{\text{elec[MCH]}}$	$\nabla\mathbf{H}_{KK}^{\text{elec[MCH]}}$	\mathbf{T}^{MCH}

dynamics methods are ultimately called curvature-driven nonadiabatic dynamics.

We sometimes use the prefix “t” to denote that a dynamics method is an overlap-based algorithm; and the prefix “κ” to denote that such a method is a curvature-driven method. For example, tGSE denotes an overlap-based algorithm that starts from GSE, and κGSE denotes a curvature-driven algorithm that starts from GSE. Similarly, one can have tFS-TSH and κFS-TSH.

3.1. Electronic Structure Information Needed for GSE, SE, and FS-TSH. One can perform dynamics in any electronic basis (any electronic representation), for example, the diagonal basis or the MCH basis. However, calculations are more convenient in some bases than in others. For example, an FS-TSH simulation in the diagonal basis requires $\mathbf{H}^{\text{elec[diag]}}$, $\nabla\mathbf{H}_{KK}^{\text{elec[diag]}}$ and \mathbf{T}^{diag} , but the required data is not directly available, with the most significant lack being that electronic structure programs only provide analytic gradients in the MCH representation. We will address this kind of issue below.

We distinguish three types of information that can be obtained from electronic structure calculations, namely, energy information ($\mathbf{H}^{\text{elec[MCH]}}$), gradient information ($\nabla\mathbf{H}^{\text{elec[MCH]}}$), and coupling information (\mathbf{d}^{MCH} or \mathbf{T}^{MCH}).

\mathbf{T}^{MCH} is not directly available in any representation in most electronic structure packages; however, it can either be analytically computed from \mathbf{d}^{MCH} by using eq 18, or it can be approximated from overlap integrals of MCH electronic wave functions at successive time steps,^{52,144–146}

$$S_{ij}^{\text{MCH}}(t, t + \Delta t) = \langle \phi_i^{\text{MCH}}(t) | \phi_j^{\text{MCH}}(t + \Delta t) \rangle \quad (91)$$

where Δt is the time step to propagate the nuclear EOM. Employing overlap integrals to approximate TDCs is preferable to using eq 18 because it alleviates the trivial crossing problem.^{147–150} The simplest approximation to the TDC from an overlap integral is the Hammes-Schiffer–Tully scheme:³⁷

$$T_{ij}^{\text{MCH}}\left(t + \frac{1}{2}\Delta t\right) = \frac{S_{ij}^{\text{MCH}}(t, t + \Delta t) - S_{ji}^{\text{MCH}}(t, t + \Delta t)}{2\Delta t} \quad (92)$$

More accurate schemes are also available, for example, the norm-preserving interpolation scheme of Meek and Levine.¹⁴⁶ We refer the interested reader to ref 151 for a summary of available schemes.

Computing coupling information (\mathbf{d}^{MCH} or \mathbf{T}^{MCH}) requires using the electronic wave functions. The curvature-driven approximations discussed below are motivated by the goal of approximating \mathbf{d}^{MCH} or \mathbf{T}^{MCH} from MCH energy and gradient information without needing electronic wave functions.

Table 2 summarizes the information needed for GSE, SE, and FS-TSH in the MCH basis for Hamiltonians without SOC. Notice that when there is no SOC in the Hamiltonian, the MCH and diagonal bases are identical. The case of Hamiltonians without SOC is important because internal conversion among singlet electronic states can often be treated with useful accuracy without including SOC. We denote the basis used to propagate the dynamics as the dynamics basis. For Hamiltonians without SOC, the dynamics basis is MCH basis. Because the MCH and diagonal bases are identical in this case, the basis is often just called the adiabatic basis. When

SOC is not included, the dynamics basis is the same as the basis used in the electronic structure software; and dynamics algorithms can directly use the energy, gradient, and coupling information (if and when available) from electronic structure software.

Table 3 summarizes the information needed for GSE, SE, and FS-TSH in the diagonal or MCH basis for Hamiltonians with SOC. When SOC is present, the diagonal basis and the MCH basis differ from one another. Important considerations in choosing between them for use as the dynamics basis are that TSH methods are usually more accurate when dynamics is carried out in a fully adiabatic basis (which is the diagonal basis when SOC is present), but electronic structure software usually provides information most conveniently in the MCH basis. When the dynamics basis is different from the basis used in the electronic structure software, one needs to perform a transformation from the MCH basis to the basis used in the dynamics calculation.

To achieve wave function-free nonadiabatic dynamic, we first need to have a NAC-free nonadiabatic dynamics method so that we can propagate nonadiabatic dynamics with only potential energies, gradients, and TDCs. Second, we need to have a way to approximate TDCs from potential energies and gradients. In Sections 3.2 and 3.3 we will achieve NAC-free nonadiabatic dynamics; and in Section 3.4 we will motivate our ultimate goal, namely, wave function-free nonadiabatic dynamics with only potential energies and gradients.

3.2. NAC-Free Mixed Quantum-Classical Nonadiabatic Dynamics for Hamiltonians without SOC. For Hamiltonian without SOC, as summarized in Table 2, one can achieve NAC-free nonadiabatic dynamics by using either GSE or FS-TSH; however, the original SE requires computation of full NACs. For Hamiltonians without SOC, our starting point for NAC-free nonadiabatic dynamics is GSE for SCP methods and FS-TSH for TSH methods. When \mathbf{d}^{MCH} is not used in computing \mathbf{T}^{MCH} in the EOMs and nonadiabatic force tensors for GSE, the resulting algorithm is NAC-free, and is called tGSE; When \mathbf{d}^{MCH} is not used in computing \mathbf{T}^{MCH} in the EOMs and momentum adjustment vector and velocity reflection vector for FS-TSH, the resulting algorithm is called tFS-TSH. The same notation is adapted for Hamiltonians with SOC, which will be discussed in next section.

3.3. NAC-Free Mixed Quantum-Classical Nonadiabatic Dynamics for Hamiltonians with SOC. For Hamiltonian with SOC, one may use either the diagonal basis or the MCH basis as the dynamics basis.

When the dynamics basis is the MCH basis, the dynamics algorithm can directly use the energy, gradient, and coupling information from electronic structure software, and Table 3 shows that one can readily perform NAC-free nonadiabatic dynamics with GSE and FS-TSH. However, the preferred dynamics basis is the diagonal basis, especially for TSH methods. In that situation, the dynamics basis is different from the basis used by the electronic structure software, and one needs to perform a transformation from the MCH basis to diagonal basis for energy, gradient, and coupling information. Energy information in the diagonal basis can be obtained from information available in the MCH basis by the transformation of eq 85, but gradient and coupling information is more complicated as discussed below.

We distinguish two approaches to achieve a transformation or approximation to compute gradient and coupling information in the diagonal basis from information in the

MCH basis, namely, the nuclear gradient tensor (NGT) scheme developed by Mai, Marquetand, and González,¹⁰⁸ and the time-derivative matrix (TDM) scheme developed by us.⁶⁷ We will first discuss the NGT and TDM transformation approaches, and then—to illustrate the advantage of the TDM scheme—we will show how NAC-free nonadiabatic dynamics can be achieved by the TDM scheme.

3.3.1. Nuclear Gradient Tensor (NGT) Scheme. The NGT scheme works by defining a nuclear gradient tensor \mathcal{G}^{GB} ,

$$\mathcal{G}_{IJ}^{\text{GB}} \equiv \langle \phi_I^{\text{GB}} | \nabla H^{\text{elec}} | \phi_J^{\text{GB}} \rangle = \mathbf{g}_{IJ}^{\text{MCH}} + \langle \phi_I^{\text{GB}} | \nabla H^{\text{SOC}} | \phi_J^{\text{GB}} \rangle \quad (93)$$

where

$$\mathbf{g}_{IJ}^{\text{GB}} \equiv \langle \phi_I^{\text{GB}} | \nabla H^{\text{SOF}} | \phi_J^{\text{GB}} \rangle \quad (94)$$

Recall that H^{SOF} and H^{SOC} are defined in eq 81. Notice that both \mathcal{G}^{GB} and \mathbf{g}^{GB} are $N_{\text{states}} \times N_{\text{states}} \times 3N_{\text{atoms}}$ tensors. Similarly to the way we treat NACs, we treat \mathcal{G}^{GB} and \mathbf{g}^{GB} as $N_{\text{states}} \times N_{\text{states}}$ matrices in which the matrix elements are $(3N_{\text{atoms}})$ -dimensional vectors. One can show that,^{67,108}

$$\mathcal{G}_{IJ}^{\text{diag}} = \nabla H_{II}^{\text{elec[diag]}} \delta_{IJ} - (H_{II}^{\text{elec[diag]}} - H_{JJ}^{\text{elec[diag]}}) \mathbf{d}_{IJ}^{\text{diag}} \quad (95)$$

$$\mathbf{g}_{IJ}^{\text{MCH}} = \nabla H_{II}^{\text{SOF[MCH]}} \delta_{IJ} - (H_{II}^{\text{SOF[MCH]}} - H_{JJ}^{\text{SOF[MCH]}}) \mathbf{d}_{IJ}^{\text{MCH}} \quad (96)$$

The key approximation of the NGT scheme is to assume that

$$\left\langle \phi_I^{\text{GB}} \left| \frac{\partial H^{\text{SOC}}}{\partial \mathbf{R}} \right| \phi_J^{\text{GB}} \right\rangle = 0, \text{ and therefore,} \\ \mathcal{G}^{\eta, \text{diag}} \approx \mathcal{G}^{\eta, \text{diag, NGT}} \equiv \mathbf{U}^\dagger \mathbf{g}^{\eta, \text{MCH}} \mathbf{U} \quad (97)$$

where the superscript NGT denotes that this is an NGT approximation, and where the transformation matrix \mathbf{U} is defined in eq 85, and $\mathcal{G}^{\eta, \text{diag}} \approx \mathcal{G}^{\eta, \text{diag, NGT}}$ and $\mathbf{g}^{\eta, \text{MCH}}$ are $N_{\text{states}} \times N_{\text{states}}$ matrices with elements $\mathcal{G}_{IJ}^{\eta, \text{diag, NGT}}$ and $\mathbf{g}_{IJ}^{\eta, \text{MCH}}$ respectively, and $\eta = 1, 2, \dots, 3N_{\text{atoms}}$. With this notation, the matrix elements $\mathcal{G}^{\eta, \text{diag, NGT}}$ and $\mathbf{g}^{\eta, \text{MCH}}$ are components of the vectors that are the matrix elements of \mathcal{G}^{GB} and \mathbf{g}^{GB} . Therefore,

$$\frac{\partial H_{II}^{\text{elec[diag]}}}{\partial \mathbf{R}} \approx -\mathcal{G}_{II}^{\text{diag, NGT}} \quad (98)$$

$$\mathbf{d}_{IJ}^{\text{diag}} \approx (H_{JJ}^{\text{elec[diag]}} - H_{II}^{\text{elec[diag]}})^{-1} \mathcal{G}_{IJ}^{\text{diag, NGT}} \quad (99)$$

In summary, the NGT scheme first forms a \mathbf{g}^{MCH} tensor by using gradients and NACs in the MCH representation, and then it forms to $\mathcal{G}^{\text{diag}}$ according to eq 97. The gradients and NACs in the diagonal representations are obtained according to eqs 98 and 99 respectively. That is why we show in Table 3 that one needs NACs in MCH basis to propagate the nuclear EOM for FS-TSH calculations in the diagonal basis if one uses the NGT scheme.

3.3.2. Time-Derivative Matrix (TDM) Scheme. The TDM scheme starts by defining a time-derivative matrix \mathcal{K}^{GB} ,

$$\mathcal{K}_{IJ}^{\text{GB}} \equiv \left\langle \phi_I^{\text{GB}} \left| \frac{d}{dt} H^{\text{elec}} \right| \phi_J^{\text{GB}} \right\rangle = k_{IJ}^{\text{GB}} + \left\langle \phi_I^{\text{GB}} \left| \frac{dH^{\text{SOC}}}{dt} \right| \phi_J^{\text{GB}} \right\rangle \quad (100)$$

where

$$k_{ij}^{\text{GB}} \equiv \left\langle \phi_i^{\text{GB}} \left| \frac{dH^{\text{SO}}}{dt} \right| \phi_j^{\text{GB}} \right\rangle \quad (101)$$

and where that H^{SO} and H^{SOC} are defined in eq 81. Notice that \mathcal{K}^{GB} is an $N_{\text{states}} \times N_{\text{states}}$ matrix. One can show that⁶⁷

$$\mathcal{K}_{IJ}^{\text{diag}} = \frac{dH_{II}^{\text{elec[diag]}}}{dt} \delta_{IJ} - (H_{II}^{\text{elec[diag]}} - H_{JJ}^{\text{elec[diag]}}) T_{IJ}^{\text{diag}} \quad (102)$$

$$k_{ij}^{\text{MCH}} = \frac{dH_{II}^{\text{SO[MCH]}}}{dt} \delta_{ij} - (H_{II}^{\text{SO[MCH]}} - H_{JJ}^{\text{SO[MCH]}}) T_{ij}^{\text{MCH}} \quad (103)$$

The key approximation of the TDM scheme is to assume

$$\left\langle \phi_i^{\text{GB}} \left| \frac{dH^{\text{SOC}}}{dt} \right| \phi_j^{\text{GB}} \right\rangle = 0; \text{ and this leads to} \\ \mathcal{K}^{\text{diag, TDM}} \approx \mathbf{U}^\dagger \mathbf{k}^{\text{MCH}} \mathbf{U} \quad (104)$$

where the TDM superscript denotes that this is from the TDM approximation. The “approximately equal” sign in eqs 97 and 104 comes from the observation that SOC is more system-dependent than nuclear-geometry-dependent.^{152,153} Therefore,

$$\frac{dH_{II}^{\text{elec[diag]}}}{dt} \approx \mathcal{K}_{II}^{\text{diag, TDM}} \quad (105)$$

$$T_{IJ}^{\text{diag}} \approx (H_{JJ}^{\text{elec[diag]}} - H_{II}^{\text{elec[diag]}})^{-1} \mathcal{K}_{IJ}^{\text{diag, TDM}} \quad (106)$$

Eq 105 is useful because one can use the chain rule to rewrite it as

$$\nabla H_{II}^{\text{elec[diag]}} \cdot \dot{\mathbf{R}} \approx \mathcal{K}_{II}^{\text{diag, TDM}} \quad (107)$$

In a similar way to the derivation that we used above to derive the GSE nuclear EOMs, one can obtain a general solution for the gradient as

$$\nabla H_{II}^{\text{elec[diag]}} = \frac{\mathcal{K}_{II}^{\text{diag, TDM}}}{\dot{\mathbf{R}} \cdot \mathbf{F}_{II}} \mathbf{F}_{II} \quad (108)$$

where we require that \mathbf{F}_{II} is real and not normal to $\dot{\mathbf{R}}$. One physically motivated choice for \mathbf{F}_{II} is

$$\mathbf{F}_{II} = \nabla H_{LL}^{\text{SO[MCH]}} \equiv \mathbf{F}^{\text{MCH}} \quad (109)$$

where the state L is the state in the MCH representation that corresponds to state I in the diagonal representation (L and I can be different because the state index in the MCH and diagonal representations may be different). Combining eqs 108 and 109 yields

$$\nabla H_{II}^{\text{elec[diag]}} = \frac{\mathcal{K}_{II}^{\text{diag, TDM}}}{\dot{\mathbf{R}} \cdot \nabla H_{LL}^{\text{SO[MCH]}}} \nabla H_{LL}^{\text{SO[MCH]}} \quad (110)$$

In summary, the TDM scheme first forms a \mathbf{k}^{MCH} matrix by using time derivatives of potential energies (which can be computed either by the chain rule or by finite differences⁶⁷) and TDCs in the MCH representation, and then it transforms to \mathbf{k}^{MCH} according to eq 104. The gradients and TDCs in the diagonal representation are obtained according to eqs 110 and 106 respectively.

3.3.3. Further Discussion of the SOC-Inclusive Case. As discussed above, when SOC is present in the Hamiltonian, the dynamics basis can be different from MCH basis. We are especially interested in the case where the dynamics basis is the fully adiabatic basis, i.e., the diagonal basis. In that case, a transformation from the MCH basis to the dynamics basis is

required. The NGT scheme¹⁰⁸ needs NACs in MCH basis to transform the gradient and NAC of the MCH basis to the diagonal basis, whereas the TDM scheme⁶⁷ achieves the transformation without the NACs of the MCH basis.

When using the NGT scheme, one can see from Table 3 that FS-TSH dynamics in the diagonal basis requires the NACs of the MCH basis. They are needed both for computing a single-state gradient $\nabla H_{KK}^{\text{elec[diag]}}$ and for computing \mathbf{T}^{diag} . In contrast, using GSE dynamics in the diagonal basis requires NACs in MCH basis only for computing \mathbf{T}^{diag} . This is because GSE uses a mean-field potential (V^{SCP}) instead of a single-state potential energy surface, and one can show that it is equivalent for MCH and diagonal representations.

$$\dot{\mathbf{P}}_{\text{GSE}}^{\text{diag}} = -\nabla V^{\text{SCP}} = -\nabla \text{tr}(\rho^{\text{diag}} \mathbf{H}^{\text{elec[diag]}}) \\ = -\nabla \text{tr}(\rho^{\text{MCH}} \mathbf{H}^{\text{elec[MCH]}}) \quad (111)$$

When SOC is not present, FS-TSH is more efficient than GSE or SE because only a single state gradient $\nabla H_{KK}^{\text{elec[MCH]}}$ needs to be computed in FS-TSH, while GSE or SE requires computing gradients of all states. However, when SOC is included, to compute $\nabla H_{KK}^{\text{elec[diag]}}$ requires derivative of all states i.e., $\nabla \mathbf{H}^{\text{elec[MCH]}}$, if one is using the NGT scheme. Therefore, the computational advantage of FS-TSH over GSE (or SE) is lost when SOC is present in the Hamiltonian and when one uses the NGT scheme.

The TDM scheme gives a NAC-free nonadiabatic dynamics method for both SCP and TSH methods, even when SOC is present in the Hamiltonian. It enables tGSE and tFS-TSH methods for Hamiltonians with SOC.

We have seen that development of GSE and the TDM scheme provide a computational framework that can propagate nonadiabatic trajectories without computing full NACs, not only when SOC is not present in the Hamiltonian, but also when it is. In general, one prefers algorithms based on overlap integrals to algorithms based on full NACs because overlap integrals are computationally more efficient. But an even stronger reason to prefer overlap-based algorithms is that they can be a starting point for the development of wave function-free methods, and that is discussed next.

3.4. From Overlap-Free (TDC-Free) Methods to Wave-Function-Free Methods. Our final goal in this work is to achieve methods that do not use electronic wave functions at all, in particular, methods that use only energies and gradients in MCH basis. This requires eliminating the calculation not only of full NACs but also of overlap integrals. Furthermore, we want the method to be wave function-free not only when SOC is neglected but also when it is included.

Computing overlap integrals not only involves computational cost, but also it prohibits the use of direct dynamics with electronic structure methods for which the electronic wave function is not available, or not defined, or defined but requires extra computational cost. For examples, multistate pair density functional theory^{154,155} has no definition of electronic wave functions, perturbation theory requires extra step to compute electronic wave functions,^{156–158} and machine learning potentials may even be devoid of electronic wave functions.^{159,160} Another reason to avoid overlap integrals (or NACs) is that the number of NACs or overlap integrals scales quadratically with the number of electronic states considered.

Our route to performing nonadiabatic dynamics with only energies and gradients is to approximate TDCs by energies and

gradients. The physical picture was anticipated in Section 1, namely that the coupling of electronic states is strong only near locally avoided crossings, where the potential energy surfaces evaluated along a path have second derivatives (curvatures) with opposite signs. We illustrate this in Figure 1 for a

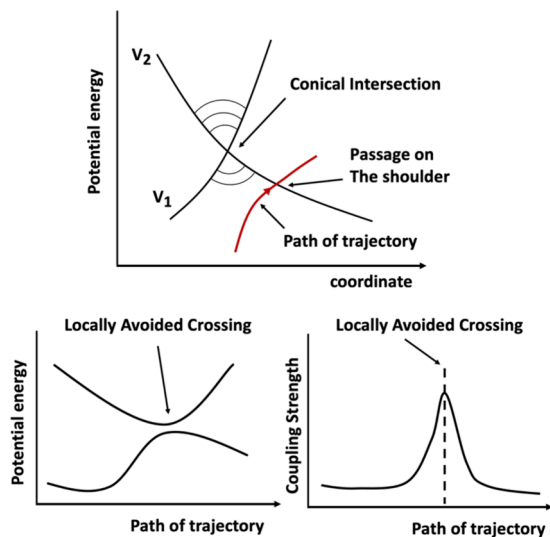


Figure 1. Top panel: schematic of the potential energy surface near a conical intersection and path of a trajectory passing near a conical intersection. Bottom left panel: the potential energy surfaces of the two electronic states showing a locally avoided crossing along the path. Lower right panel: magnitude of the TDC or NAC along the same path.

trajectory passing near to a conical intersection. Along the path of the trajectory, one observes a locally avoided crossing. The coupling strength (for example the magnitude of the NAC or the TDC) should have a peak close to the location where the difference in the signed curvatures of the two surfaces peaks. And the coupling strength should increase if one passes closer to the locally avoided crossing. (It eventually becomes infinite on the conical intersection seam.^{21,23–25}) This motivates evaluating the coupling strength in terms of the difference of the two curvatures.

Early attempts to approximate couplings with energies were based on model Hamiltonians. Our goal, however, is to develop methods based on the actual potential surfaces computed by direct dynamics. The first TSH paper by Tully and Preston³⁴ used the parametrized Landau–Zener (LZ) formula^{161,162} for the hopping probability. In that work, they first fit a LZ model Hamiltonian, and the parameters are used in the LZ formula for the hopping probability. Similar approaches are used in later work,^{163–166} including the more sophisticated Zhu–Nakamura theory.¹⁶⁷ All these methods require nonlocal knowledge of potential energy surfaces, and therefore are not useful or practical in direct dynamics. In the next section we present the curvature-driven methods that require only local information.

4. THEORY: CURVATURE-DRIVEN METHODS

Baek and An proposed a wave function-free approximation to the NACs for 1-dimensional systems¹⁶⁸ by considering the relationship between the Lorentzian dependence of NACs along a diabaticization coordinate and the linear vibronic coupling scheme; they obtained

$$d_{IJ}^{\text{Baek-An}} \equiv \left\langle \phi_I^{\text{MCH}} \left| \frac{d}{dq} \right| \phi_J^{\text{MCH}} \right\rangle = \frac{1}{2} \left[\frac{d^2 \Delta H_{IJ}^{\text{elec[MCH]}}}{dq^2} \frac{1}{\Delta H_{IJ}^{\text{elec[MCH]}}} \right]^{1/2} \quad (112)$$

where q is the one-dimensional nuclear coordinate, and

$$\Delta H_{IJ}^{\text{elec[MCH]}} = H_{II}^{\text{elec[MCH]}} - H_{JJ}^{\text{elec[MCH]}} \quad (113)$$

where $H_{II}^{\text{elec[MCH]}}$ and $H_{JJ}^{\text{elec[MCH]}}$ are MCH (spin-free adiabatic) potential energies for states I and J respectively. Notice that we have adopted our notation in eq 112.

Later, two groups of researchers independently recognized that the one-dimensional result may be applied to multidimensional trajectories by replacing the one-dimensional coordinate by time.^{169,170} This yields

$$T_{IJ}^{\text{Baek-An}} \equiv \left\langle \phi_I^{\text{MCH}} \left| \frac{d}{dt} \right| \phi_J^{\text{MCH}} \right\rangle = \frac{1}{2} \left[\frac{d^2 \Delta H_{IJ}^{\text{elec[MCH]}}}{dt^2} \frac{1}{\Delta H_{IJ}^{\text{elec[MCH]}}} \right]^{1/2} \quad (114)$$

Therefore, one can approximate the TDC in terms of the curvature of the spin-free adiabatic potential energy surfaces as functions of propagation time. For this reason, we have called this approximation the curvature-driven approximation. We denote quantities obtained using this approximation by a superscript κ . The approximation yields

$$T_{IJ}^{\text{MCH},\kappa} \equiv \left\langle \phi_I^{\text{MCH}} \left| \frac{d}{dt} \right| \phi_J^{\text{MCH},\kappa} \right\rangle = \begin{cases} \frac{1}{2} \left[\frac{d^2 \Delta H_{IJ}^{\text{elec[MCH]}}}{dt^2} \frac{1}{\Delta H_{IJ}^{\text{elec[MCH]}}} \right]^{1/2} & \text{for radicand} \geq 0, I > J \\ -T_{JI}^{\text{MCH},\kappa} & \text{for radicand} \geq 0, I < J \\ 0 & \text{for radicand} < 0 \end{cases} \quad (115)$$

We label the TDC computed using the curvature-driven approximation shown in eq 115 as κ TDC, and in general we will use a prefix κ for methods that use κ TDC.

The key quantity to be computed is $d^2 \Delta H_{IJ}^{\text{elec[MCH]}}/dt^2$, and there are two approaches to compute it. The energy formula^{169,170} computes the second derivative of energy with respect to time using a backward finite-difference formula, which can start at the third step of trajectory integration with

$$\left. \frac{d^2 \Delta H_{IJ}^{\text{elec[MCH]}}}{dt^2} \right|_e \approx \frac{1}{\Delta t^2} [\Delta H_{IJ}^{\text{elec[MCH]}}(t) - 2\Delta H_{IJ}^{\text{elec[MCH]}}(t - \Delta t) + \Delta H_{IJ}^{\text{elec[MCH]}}(t - 2\Delta t)] \quad (116)$$

where $|_e$ denotes that the quantity is computed using the energy formula, and Δt is the step size used to integrate nuclear EOM. Start from fourth step, one can use a higher-order backward finite-difference formula,

Table 4. Working Equations for κ GSE and κ FS-TSH for a General Basis

Method	Basis	Formula	Equation Form
κ GSE	GB	Elec EOM	$[\dot{c}_I^{\text{GB}}(t)]_{\kappa\text{GSE}} = - \sum_J^{N_{\text{states}}} \left(\frac{i}{\hbar} H_{IJ}^{\text{elec[GB]}} + T_{IJ}^{\text{GB},\kappa} \right) c_J^{\text{GB}}(t)$
		Nuc EOM	$[\dot{\mathbf{P}}^{\text{GB}}]_{\kappa\text{GSE}} = - \sum_{IJ}^{N_{\text{states}}} \rho_{IJ}^{\text{GB}} \nabla H_{IJ}^{\text{elec[GB]}} + \sum_{IJL}^{N_{\text{states}}} \left(\frac{T_{IL}^{\text{GB},\kappa} \rho_{LJ}^{\text{GB}} H_{IJ}^{\text{elec[GB]}} \mathbf{D}_{IL}^{\text{GB}}}{\mathbf{B}_{IL}^{\text{GB}} \cdot \dot{\mathbf{R}}} - \frac{T_{LJ}^{\text{GB},\kappa} \rho_{IL}^{\text{GB}} H_{IJ}^{\text{elec[GB]}} \mathbf{D}_{LJ}^{\text{GB}}}{\mathbf{B}_{LJ}^{\text{GB}} \cdot \dot{\mathbf{R}}} \right)$
κ FS-TSH	GB	Elec EOM	$[\dot{c}_I^{\text{GB}}(t)]_{\kappa\text{TSH}} = - \sum_J^{N_{\text{states}}} \left(\frac{i}{\hbar} H_{IJ}^{\text{elec[GB]}} + T_{IJ}^{\text{GB},\kappa} \right) c_J^{\text{GB}}(t)$
		Nuc EOM	$b_{KI}^{\text{GB},\kappa}(t) = 2 \left(\frac{1}{\hbar} \text{Im}(H_{KI}^{\text{elec[GB]}}) \rho_{IK}^{\text{GB}} - \text{Re}(T_{KI}^{\text{GB},\kappa} \rho_{IK}^{\text{GB}}) \right)$ $[\dot{\mathbf{P}}^{\text{GB}}]_{\kappa\text{TSH}} = - \nabla H_{KK}^{\text{elec[GB]}}$

$$\left. \frac{d^2 \Delta H_{IJ}^{\text{elec[MCH]}}}{dt^2} \right|_{\mathbf{e}} \approx \frac{1}{\Delta t^2} [2 \Delta H_{IJ}^{\text{elec[MCH]}}(t) - 5 \Delta H_{IJ}^{\text{elec[MCH]}}(t - \Delta t) + 4 \Delta H_{IJ}^{\text{elec[MCH]}}(t - 2\Delta t) - \Delta H_{IJ}^{\text{elec[MCH]}}(t - 3\Delta t)] \quad (117)$$

Alternatively, we prefer to use a formula based on analytic gradients:

$$\left. \frac{d^2 \Delta H_{IJ}^{\text{elec[MCH]}}}{dt^2} \right|_{\mathbf{g}} \approx \frac{\Delta \dot{H}_{IJ}^{\text{elec[MCH]}}(t) - \Delta \dot{H}_{IJ}^{\text{elec[MCH]}}(t - \Delta t)}{\Delta t} \quad (118)$$

where $\left. \cdot \right|_{\mathbf{g}}$ denotes that the quantity is computed using the gradient formula, and where $\dot{\cdot}$ (as introduced in section 2.1) an overdot indicates a time derivative. The gradient formula uses the information on gradients,

$$\Delta \dot{H}_{IJ}^{\text{elec[MCH]}}(t) = \nabla(\Delta H_{IJ}^{\text{elec[MCH]}}(t)) \cdot \dot{\mathbf{R}} \quad (119)$$

For small enough Δt , the energy formula and the gradient formula should give identical results, but for practical finite Δt , the gradient formula should be more numerically stable.

Although the SE method requires more than the TDC (it requires the full NAC), Section 3 shows that when using the TDM scheme, the tGSE and tFS-TSH are overlap-based algorithms that can be propagated by computing only potential energies, gradients, and TDCs in the MCH basis even when the dynamics basis is the diagonal basis. Therefore, our starting point for using κ TDC in nonadiabatic dynamics is tGSE or tFS-TSH. One can simply replace \mathbf{T}^{MCH} by $\mathbf{T}^{\text{MCH},\kappa}$ in the working equations of Table 1 (electronic and nuclear EOMs in GSE and electronic and nuclear EOMs and hopping probability in FS-TSH). Furthermore, $\mathbf{T}^{\text{MCH},\kappa}$ can be computed using eqs 115–119. The resulting methods are called κ GSE and κ FS-TSH.

In summary, the TDM scheme and curvature-driven approximation provide a path to compute $\mathbf{H}^{\text{elec[diag]}}$, $\nabla \mathbf{H}^{\text{elec[diag]}}$, and $\mathbf{T}^{\text{diag},\kappa}$ from $\mathbf{H}^{\text{elec[MCH]}}$, $\nabla \mathbf{H}^{\text{elec[MCH]}}$ and $\mathbf{T}^{\text{MCH},\kappa}$. This satisfies our goal of performing direct nonadiabatic dynamics with only MCH potential energies and

MCH gradients, i.e., without quantities (full NACs or overlap integrals) that require electronic wave functions. The use of curvature-driven methods not only improves the computational efficiency (recall that the number of NACs or overlap integrals scales quadratically with the number of electronic states considered), but also provides the possibility of using electronic structure theories for which the electronic wave functions are not made available to the user or are too expensive to compute.

Tables 2 and 3 show that if one does not use the GSE method and TDM scheme, use of the curvature-approximated TDC is possible only for TSH methods, and even for TSH methods it is possible only when SOC is not present in the Hamiltonian. The development the GSE method and the TDM scheme has enabled broader use the curvature-driven methods, in particular they can be used with both SCP and TSH methods even when SOC is included. Table 4 summarizes the working equations for κ GSE and κ TSH in a general basis. The next section gives more details of the specific κ GSE and κ TSH methods that we recommend.

5. THEORY: ACCURATE CURVATURE-DRIVEN MIXED QUANTUM-CLASSICAL NONADIABATIC DYNAMICS METHODS

In Section 2, we introduced the foundational mixed quantum-classical nonadiabatic dynamics methods, namely, GSE, SE, and FS-TSH; in Section 3, we moved a step forward to show how to achieve NAC-free mixed quantum-classical nonadiabatic dynamics methods, resulting in tGSE and tFS-TSH methods; and in Section 4, we introduced the curvature-driven approximation in the context of GSE and FS-TSH, resulting in the κ GSE and κ FS-TSH methods. With the curvature-driven approximation, one is able to perform mixed quantum-classical nonadiabatic dynamics with only potential energies and gradients.

Next we introduce practical mixed quantum-classical nonadiabatic dynamics methods that build on the foundational methods of the previous sections. Section 5.1 introduces coherent switching with decay-of-mixing (CSDM)^{50,83} which is an SCP method whose starting point is SE Section 5.2 introduces generalized coherent switching with decay-of-mixing (GCSDM)^{52,83} which is an SCP method whose starting point is GSE. Section 5.3 introduces fewest-switches with time

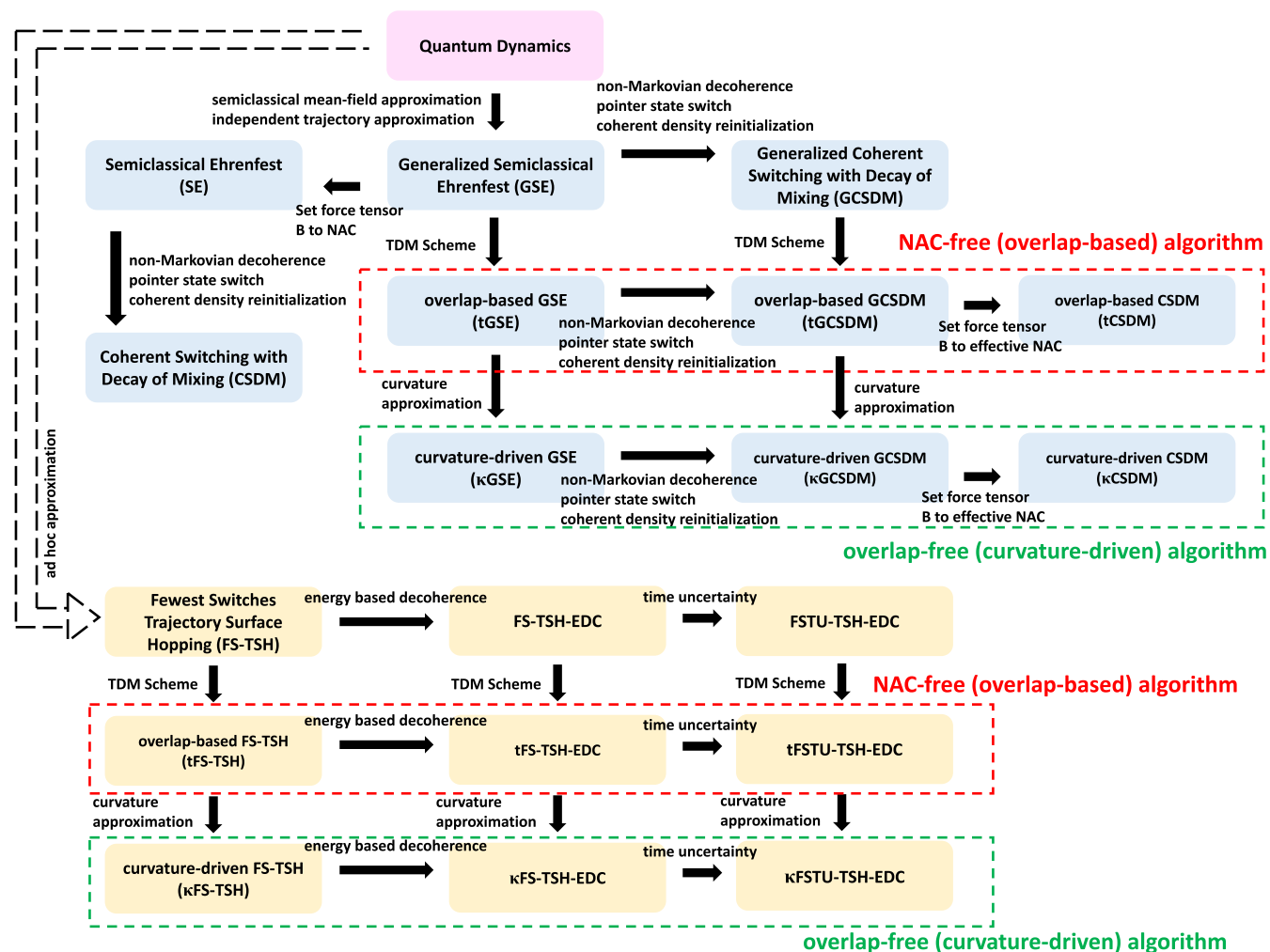


Figure 2. Relations between discussed mixed quantum-classical nonadiabatic dynamics methods.

uncertainty and energy-based decoherence time uncertainty (FSTU-EDC),^{54,94} which adds energy-based decoherence¹³⁸ to FSTU,¹⁷¹ which adds time uncertainty¹⁷¹ to FS-TSH. Section 5.4 shows how the curvature-driven scheme is added to GCSDM, yielding κ GCSDM, and to FSTU-EDC, yielding κ FSTU-EDC. The κ GCSDM and κ FSTU-EDC methods are our recommended practical curvature-driven mixed quantum-classical nonadiabatic dynamics methods.

We summarize the relations between foundational methods and advanced methods in Figure 2.

5.1. Coherent Switching with Decay of Mixing (CSDM). Complete details of the CSDM method are presented elsewhere;¹³⁹ hence the present section is just a brief summary.

The CSDM method adds non-Markovian decoherence to SE by using the decay-of-mixing formalism.^{50,105} The electronic and nuclear EOMs of CSDM involve adding decay-of-mixing terms to the EOMs of SE:

$$\dot{c}_I^{\text{GB}}(t)|_{\text{CSDM}} = \dot{c}_I^{\text{GB}}(t)|_{\text{SE}} + \dot{c}_I^{\text{GB}}(t)|_{\text{D/CSDM}} \quad (120)$$

$$\dot{\mathbf{p}}^{\text{GB}}|_{\text{CSDM}} = \dot{\mathbf{p}}^{\text{GB}}|_{\text{SE}} + \dot{\mathbf{p}}^{\text{GB}}|_{\text{D/CSDM}} \quad (121)$$

where $\blacksquare|_{\text{CSDM}}$ denotes a CSDM variable, and $\blacksquare|_{\text{D/CSDM}}$ denotes a decay-of-mixing term added to the nuclear EOM of CSDM.

In a similar way to the above derivation of the GSE nuclear EOM from conservation of total energy, one is able to derive the CSDM decay-of-mixing force $[\dot{\mathbf{p}}^{\text{GB}}]_{\text{D/CSDM}}$. The electronic and nuclear decay-of-mixing terms in CSDM become

$$\dot{c}_I^{\text{GB}}(t)|_{\text{D/CSDM}} = \begin{cases} -\frac{1}{2\tau_{IK}^{\text{GB}}} c_I^{\text{GB}}(t), & I \neq K \\ \sum_{J \neq K} \frac{1}{2\tau_{JK}^{\text{GB}}} \frac{\rho_{JJ}^{\text{GB}}}{\rho_{KK}^{\text{GB}}} c_I^{\text{GB}}(t), & I = K \end{cases} \quad (122)$$

$$\dot{\mathbf{p}}^{\text{GB}}|_{\text{D/CSDM}} = \sum_{I \neq K} \frac{\rho_{II}^{\text{GB}}}{\tau_{IK}^{\text{GB}}} \frac{(H_{II}^{\text{elec[GB]}} - H_{KK}^{\text{elec[GB]})}{(\mathbf{s}_{IK}^{\text{GB}} \cdot \dot{\mathbf{R}})} \mathbf{s}_{IK}^{\text{GB}} \quad (123)$$

where K is the pointer state in the general basis, τ_{IK}^{GB} is the decay-of-mixing time between GB states I and K , and $\mathbf{s}_{IK}^{\text{GB}}$ is the $3N_{\text{atoms}}$ -dimensional decay-of-mixing vector in the general basis. The physical meaning of $[\dot{c}_I^{\text{GB}}(t)]_{\text{D/CSDM}}$ is that the density of pointer state K is increased from contributions of all the nonpointer states. Correspondingly, the density of nonpointer state I is exponentially decreased to zero during the decay-of-mixing time τ_{IK}^{GB} . The decay-of-mixing vector in the general basis is,

$$\mathbf{s}_{IK}^{\text{GB}} = \text{Re} \left(\frac{a_0 \mathbf{P}_{\text{vib}} \cdot \mathbf{d}_{IK}^{\text{GB}}}{|\mathbf{d}_{IK}^{\text{GB}}|} \mathbf{d}_{IK}^{\text{GB}} \right) + \mathbf{P}_{\text{vib}} \quad (124)$$

where $a_0 \equiv 1$ bohr, $\mathbf{d}_{IK}^{\text{GB}}$ is the NAC in the general basis, and \mathbf{P}_{vib} is the vibrational momentum, which is computed by removing the translational and rotational components of the nuclear momentum \mathbf{P} ,

$$\mathbf{P}_{\text{vib}} = (\mathbf{1} - \mathbf{Q})\mathbf{P} \quad (125)$$

where $\mathbf{1}$ is the identity operator, and \mathbf{Q} is a projection operator that projects onto translational and rotational motions;⁶⁹ both $\mathbf{1}$ and \mathbf{Q} are $3N_{\text{atoms}} \times 3N_{\text{atoms}}$ matrices. The CSDM decay-of-mixing time uses the following energy-based decoherence time:

$$\tau_{IK}^{\text{GB}} = \frac{\hbar}{|H_{II}^{\text{elec[GB]}} - H_{KK}^{\text{elec[GB]}}|} \left(1 + \frac{2E_0}{\sum_{\eta} \frac{(\mathbf{P}_{\eta} \cdot \hat{\mathbf{s}}_{IK,\eta}^{\text{GB}})^2}{2M_{\eta}}} \right) \quad (126)$$

where E_0 is a parameter set to 0.1 hartree, \mathbf{P}_{η} , $\hat{\mathbf{s}}_{IK,\eta}^{\text{GB}}$, and M_{η} are the nuclear momentum, decay-of-mixing direction (a normalized decay-of-mixing vector), and the atomic mass respectively of the atom associated with coordinate η , and $\eta = 1, 2, \dots, 3N_{\text{atoms}}$. The pointer state K is stochastically switched according to the FS-TSH hopping probability, which we label as the switching probability:

$$P_{K \rightarrow I}^{\text{GB}}(t, t + \Delta t) = \max \left(\frac{\tilde{b}_{KI}^{\text{GB}}(t) \Delta t}{\tilde{\rho}_{KK}^{\text{GB}}(t)}, 0 \right) \quad (127)$$

where

$$\tilde{b}_{KI}^{\text{GB}}(t) = 2 \left(\frac{1}{\hbar} \text{Im}(H_{KI}^{\text{elec[GB]}} \tilde{\rho}_{IK}^{\text{GB}}) - \text{Re}(T_{KI}^{\text{GB}} \tilde{\rho}_{IK}^{\text{GB}}) \right) \quad (128)$$

and where $\tilde{\rho}^{\text{GB}}$ is the coherent density matrix in the general basis, which is computed from the coherent coefficient,

$$\tilde{\rho}_{IJ}^{\text{GB}} = \tilde{c}_I^{\text{GB}}(\tilde{c}_J^{\text{GB}})^* \quad (129)$$

The coherent electronic EOM of CSDM is same as the electronic EOM of SE,

$$\dot{\tilde{c}}_I^{\text{GB}}(t)|_{\text{CSDM}} = \dot{\tilde{c}}_I^{\text{GB}}(t)|_{\text{SE}} \quad (130)$$

and the coherent coefficient \tilde{c}_I^{GB} is reinitialized to the true CSDM coefficient c_I^{GB} at each local minimum of the NAC strength,

$$D_K^{\text{GB}}(t) = \sum_{I \neq K} |\mathbf{d}_{IK}^{\text{GB}}| \quad (131)$$

Therefore, $\tilde{\rho}^{\text{GB}}$ does not maintain coherence completely along the trajectory, it is "decay of mixed" at every local minimum of $D_K^{\text{GB}}(t)$.

In summary, CSDM is an advanced SCP mixed quantum-classical nonadiabatic dynamics method that is based on SE. The CSDM method includes algorithmic decoherence by decay of mixing and pointer-state switching by the fewest-switches criterion using the coherent density. One propagates two sets of coefficients in the CSDM method, namely, the true CSDM coefficients (which involve the decay-of-mixing term), and the coherent CSDM coefficients (which do not). The true CSDM coefficients govern the propagation of the electronic and nuclear EOMs of the system, whereas the coherent CSDM coefficients control the pointer-state switching. Probably most

importantly, CSDM involves a self-consistent description of electronic and nuclear EOM that results in a continuous trajectory (as compared to FS-TSH, which is an *ad hoc* theory that involves discontinuities when hops occur).

It is shown elsewhere that CSDM agrees well with accurate quantum dynamics for realistic full-dimensional electronically inelastic collisions when the CSDM and accurate dynamics calculations are carried out with the same coupled potential surfaces.^{53,83,84,172–174}

5.2. Generalized Coherent Switching with Decay of Mixing (GCSDM). Just as CSDM EOMs are based on SE, GCSDM EOMs are based on GSE:

$$\dot{c}_I^{\text{GB}}(t)|_{\text{GCSDM}} = \dot{c}_I^{\text{GB}}(t)|_{\text{GSE}} + \dot{c}_I^{\text{GB}}(t)|_{\text{D/GCSDM}} \quad (132)$$

$$\dot{\mathbf{P}}^{\text{GB}}|_{\text{GCSDM}} = \dot{\mathbf{P}}^{\text{GB}}|_{\text{GSE}} + \dot{\mathbf{P}}^{\text{GB}}|_{\text{D/GCSDM}} \quad (133)$$

The decay-of-mixing terms are the same as for CSDM,

$$\dot{c}_I^{\text{GB}}(t)|_{\text{D/GCSDM}} = \begin{cases} -\frac{1}{2\tau_{IK}^{\text{GB}}} c_I^{\text{GB}}(t), & I \neq K \\ \sum_{J \neq K} \frac{1}{2\tau_{JK}^{\text{GB}}} \frac{\rho_{JJ}^{\text{GB}}}{\rho_{KK}^{\text{GB}}} c_I^{\text{GB}}(t), & I = K \end{cases} \quad (134)$$

$$\dot{\mathbf{P}}^{\text{GB}}|_{\text{D/GCSDM}} = \sum_{I \neq K} \frac{\rho_{II}^{\text{GB}}}{\tau_{IK}^{\text{GB}}} \frac{(H_{II}^{\text{elec[GB]}} - H_{KK}^{\text{elec[GB]}})}{(\mathbf{s}_{IK}^{\text{GB}} \cdot \dot{\mathbf{R}})} \mathbf{s}_{IK}^{\text{GB}} \quad (135)$$

The GCSDM decay-of-mixing vector differs from that of CSDM; instead of using \mathbf{d}^{GB} , it uses the force tensor \mathbf{B}^{GB} :

$$\mathbf{s}_{IK}^{\text{GB}} = \text{Re} \left(\frac{a_0 \mathbf{P}_{\text{vib}} \cdot \mathbf{B}_{IK}^{\text{GB}}}{|\mathbf{B}_{IK}^{\text{GB}}|} \mathbf{B}_{IK}^{\text{GB}} \right) + \mathbf{P}_{\text{vib}} \quad (136)$$

The decay-of-mixing time and pointer-state switching probability are the same as for CSDM as shown in eqs 126 and 127. The coherent electronic EOM of GCSDM is same as the electronic EOM of GSE (which is the same as that of SE),

$$\dot{\tilde{c}}_I^{\text{GB}}(t)|_{\text{GCSDM}} = \dot{\tilde{c}}_I^{\text{GB}}(t)|_{\text{GSE}} \quad (137)$$

The coherent coefficient $\tilde{c}_I^{\text{GB}}(t)|_{\text{GCSDM}}$ is reinitialized to the true GCSDM coefficient $c_I^{\text{GB}}(t)|_{\text{GCSDM}}$ at each local minimum of the TDC strength,

$$D_K^{\text{GB}}(t) = \sum_{I \neq K} |T_{IK}^{\text{GB}}| \quad (138)$$

Eq 138 has been called the CSDM-C criterion.⁸³

In summary, the EOMs of CSDM start from those of SE, and the EOMs of GCSDM start from those of GSE. Just as GSE differs from SE in not using full NACs, GCSDM differs from CSDM in not using full NACs.

One can develop overlap-based GCSDM algorithm by computing TDCs with overlap integrals, and the resulting algorithm is called tGCSDM. Furthermore, one can develop a curvature-driven GCSDM algorithm that is based on tGCSDM, and the resulting algorithm is called κ GCSDM. The two most widely studied versions of GCSDM are tCSDM and κ CSDM; tCSDM sets the force vector \mathbf{B}^{GB} to the effective NAC defined in eqs 52–54, and κ CSDM is explained in detail below in Section 5.4.

5.3. Trajectory Surface Hopping by Fewest Switches with Time Uncertainty with Energy-Based Decoherence

(FSTU-EDC). The new ingredients in FSTU-EDC⁹³ are the addition to FS-TSH of energy-based decoherence^{83,84,138} by means of the decay-of-mixing formalism and of time uncertainty,¹⁷¹ which reduces the number of frustrated hops.

The decay-of-mixing term added to the electronic EOM is in principle the same as that of CSDM; and the nuclear EOM of FSTU-EDC is identical to that of FS-TSH:

$$\dot{c}_I^{\text{GB}}(t)|_{\text{FSTU-TSH-EDC}} = \dot{c}_I^{\text{GB}}(t)|_{\text{TSH}} + \dot{c}_I^{\text{GB}}(t)|_{\text{D/EDC}} \quad (139)$$

$$\dot{\mathbf{P}}^{\text{GB}}|_{\text{FSTU-TSH-EDC}} = \dot{\mathbf{P}}^{\text{GB}}|_{\text{TSH}} \quad (140)$$

where in principle $\dot{c}_I^{\text{GB}}(t)|_{\text{D/EDC}} = \dot{c}_I^{\text{GB}}(t)|_{\text{D/CSDM}}$. The decoherence time is similar to that of CSDM^{83,84} but slightly different,¹³⁸

$$\tau_{IK}^{\text{GB}} = \frac{\hbar}{|H_{II}^{\text{elec[GB]}} - H_{KK}^{\text{elec[GB]}}|} \left(1 + \frac{E_0}{E_{\text{kin}}} \right) \quad (141)$$

where K is the FSTU active state in the general basis, E_0 is a parameter set to 0.1 hartree, and E_{kin} is the nuclear kinetic energy.

The physical picture of the time-uncertainty formalism to allow the possibility of nonlocal hops by using the energy-time uncertainty relation,

$$\Delta t^{\text{KL}} = \frac{\hbar}{2|\Delta E^{\text{KL}}(t_0)|} \quad (142)$$

where $\Delta E^{\text{KL}}(t_0)$ is defined in eq 65, and time t_0 is when a frustrated hop from state K to state L happens. The trajectory is searched backward and forward for a time of Δt^{KL} to check if a $K \rightarrow L$ hop is possible (not frustrated). If it is possible, one performs a $K \rightarrow L$ hop; otherwise, one treats the frustrated hop at time t_0 in the same way that one treats a frustrated hop in FS-TSH. The actual algorithm is described into detail in refs 93, 94. Therefore, the time-uncertainty formalism reduces the number of frustrated hops.

5.4. Curvature-Driven SCP Method: κ CSDM. The κ CSDM method is based on tCSDM. For simplicity and for consistency with previous papers, we have used the terminology of κ CSDM and tCSDM, but a more systematic way of naming these two methods should be κ GCSDM and tGCSDM. In the following discussion, we will use κ CSDM and κ GCSDM as synonyms, and tCSDM and tGCSDM as synonyms. The difference between κ CSDM and tCSDM is similar as the difference between κ GSE and tGSE:

$$\dot{c}_I^{\text{GB}}(t)|_{\kappa\text{GCSDM}} = \dot{c}_I^{\text{GB}}(t)|_{\kappa\text{GSE}} + \dot{c}_I^{\text{GB}}(t)|_{\text{D}/\kappa\text{GCSDM}} \quad (143)$$

$$\dot{\mathbf{P}}^{\text{GB}}|_{\kappa\text{GCSDM}} = \dot{\mathbf{P}}^{\text{GB}}|_{\kappa\text{GSE}} + \dot{\mathbf{P}}^{\text{GB}}|_{\text{D}/\kappa\text{GCSDM}} \quad (144)$$

The electronic decay-of-mixing term $\dot{c}_I^{\text{GB}}(t)|_{\text{D}/\kappa\text{GCSDM}}$ and the nuclear decay-of-mixing term $\dot{\mathbf{P}}^{\text{GB}}(t)|_{\text{D}/\kappa\text{GCSDM}}$ are similar to those of CSDM,

$$\dot{c}_I^{\text{GB}}(t)|_{\text{D}/\kappa\text{GCSDM}} = \begin{cases} -\frac{1}{2\tau_{IK}^{\text{GB},\kappa}} c_I^{\text{GB}}(t), & I \neq K \\ \sum_{J \neq K} \frac{1}{2\tau_{JK}^{\text{GB},\kappa}} \frac{\rho_{JJ}^{\text{GB}}}{\rho_{KK}^{\text{GB}}} c_I^{\text{GB}}(t), & I = K \end{cases} \quad (145)$$

$$\dot{\mathbf{P}}^{\text{GB}}|_{\text{D}/\kappa\text{GCSDM}} = \sum_{I \neq K} \frac{\rho_{II}^{\text{GB}}}{\tau_{IK}^{\text{GB},\kappa}} \frac{(H_{II}^{\text{elec[GB]}} - H_{KK}^{\text{elec[GB]}})}{(\mathbf{s}_{IK}^{\text{GB},\kappa} \cdot \dot{\mathbf{R}})} \mathbf{s}_{IK}^{\text{GB},\kappa} \quad (146)$$

The curvature-driven decay-of-mixing vector is

$$\mathbf{s}_{IK}^{\text{GB},\kappa} = \text{Re} \left(\frac{a_0 \mathbf{P}_{\text{vib}} \cdot \mathbf{B}_{IK}^{\text{GB}}}{|\mathbf{B}_{IK}^{\text{GB}}|} \mathbf{B}_{IK}^{\text{GB}} \right) + \mathbf{P}_{\text{vib}} \quad (147)$$

where \mathbf{B}^{GB} is defined in eq 37. The curvature-driven decay-of-mixing time is

$$\tau_{IK}^{\text{GB}} = \frac{\hbar}{|H_{II}^{\text{elec[GB]}} - H_{KK}^{\text{elec[GB]}}|} \left(1 + \frac{2E_0}{\sum_{\eta} \frac{(\mathbf{P}_{\eta} \cdot \mathbf{s}_{IK,\eta}^{\text{GB},\kappa})^2}{2M_{\eta}}} \right) \quad (148)$$

where $\hat{\mathbf{s}}_{IK}^{\text{GB},\kappa}$ is curvature-driven decay-of-mixing direction, which is the normalized $\mathbf{s}_{IK}^{\text{GB},\kappa}$ vector. The pointer-state switching probability is

$$P_{K \rightarrow I}^{\text{GB},\kappa}(t, t + \Delta t) = \max \left(\frac{\tilde{b}_{KI}^{\text{GB},\kappa}(t) \Delta t}{\tilde{\rho}_{KK}^{\text{GB}}(t)}, 0 \right) \quad (149)$$

where

$$\tilde{b}_{KI}^{\text{GB},\kappa}(t) = 2 \left(\frac{1}{\hbar} \text{Im}(H_{KI}^{\text{elec[GB]}} \tilde{\rho}_{IK}^{\text{GB}}) - \text{Re}(T_{KI}^{\text{GB},\kappa} \tilde{\rho}_{IK}^{\text{GB}}) \right) \quad (150)$$

and where $\tilde{\rho}^{\text{GB}}$ is the coherent density matrix of κ CSDM. The coherent electronic EOM of κ CSDM is same as the electronic EOM of κ GSE:

$$\dot{c}_I^{\text{GB}}(t)|_{\kappa\text{GCSDM}} = \dot{c}_I^{\text{GB}}(t)|_{\kappa\text{GSE}} \quad (151)$$

The coherent density reinitialized at local minima of the TDC strength,

$$D_K^{\text{GB}}(t) = \sum_{I \neq K} |T_{IK}^{\text{GB},\kappa}| \quad (152)$$

In summary, κ CSDM is similar to GCSDM except that it is based on κ GSE; it uses the \mathbf{B}^{GB} tensor for the decay-of-mixing vector, and it uses the TDC strength for reinitialization.

5.5. Curvature-Driven TSH Method: κ FSTU-EDC. The κ FSTU-EDC method adds electronic decoherence and time uncertainty to κ FS-TSH. The working equations are the same as those of FSTU-EDC except that one is using κ TDC instead of an overlap integral and that the NAC or projected NAC is not used as the momentum adjustment vector or velocity reflection vector. Avoidance of using the NAC for these steps raises the question of what the best choice is. A recent investigation by Barbatti,¹⁰⁰ studying ethylene, found that among choices available when the NAC is not available, using the direction of the momentum vector worked best, although it was only slightly better than the difference gradient vector. However, a later study on pyrene found poor results when the momentum vector was used.¹⁷⁵ To resolve this, Toldo et al.¹⁷⁶ made a detailed study of fulvene and a protonated Schiff base and concluded that the difference gradient vector is a better choice than the momentum vector when the NAC is not available and that the effective NAC of eqs 52–54 should be as good as using the difference gradient vector. We recommend using the effective NAC when using the κ FS-TSH method, and

Table 5. Excited-State Lifetimes of Ethylene from Nonadiabatic Dynamics Simulations and Experiment

Dynamics Method	Potential Energy Surface	Reference (s)	Excited-State Lifetime (fs)
FS-TSH	FOMO-AM1-CASCI(2,2) ^a	178	105, 139 ^b
AIMS ^c	SA3-CASSCF(2,2)/6-31G* ^c	180	110
AIMS ^c	SA3-CASSCF(2,2)/MS-CASPT2/6-31G* ^{d,e}	180	89
FS-TSH-EDC ^f	SA3-CASSCF(2,2)/6-31G** ^d	50	100
tFS-TSH-EDC ^g	SA3-CASSCF(2,2)/6-31G** ^d	170	50
κ FS-TSH-EDC ^h	SA3-CASSCF(2,2)/6-31G** ^d	70	84
CSDM	SA3-CASSCF(2,2)/6-31G** ^d	50	57
tCSDM	SA3-CASSCF(2,2)/6-31G** ^d	170	48
κ CSDM	SA3-CASSCF(2,2)/6-31G** ^d	170	78
Experiment		183–186	50

^aAustin Model 1¹⁸⁷ floating occupation semiempirical molecular orbital¹⁸⁸ method followed by complete active space configuration interaction of 2 electrons in 2 orbitals; ^bdepending on initial conditions; ^cab initio multiple spawning;¹⁹⁰ ^dstate-averaged complete active state self-consistent field theory;¹⁸⁹ ^emultistate second order perturbation theory;¹⁵⁶ ^fFS-TSH with energy-based decoherence;¹³⁸ ^goverlap-based FS-TSH algorithm with energy-based decoherence, specifically, use local diabaticization algorithm to propagate electronic coefficients; ^hcurvature-driven FS-TSH-EDC.¹⁷⁰

this is the choice that was made in the applications of κ FS-TSH discussed in Section 6.

6. EXAMPLES OF SUCCESSFUL APPLICATIONS

6.1. Ethylene. We start by considering ethylene isomerization^{177–182} Ethylene has two S_0/S_1 minimum-energy conical intersections (MECIs), namely, a twisted-pyramidalized MECI and an ethylidene-like MECI. The major feature of the nonadiabatic dynamical behavior of ethylene is the twisting of the C=C double bond followed by pyramidalizing a CH₂ group or a 1,2 shift of H. Time-resolved measurements showed that the excited-state lifetime of ethylene is approximately 50 fs.^{183–186}

Several direct dynamics calculations of the excited-state lifetimes have been performed, and they are summarized with references^{170,50,178,180} in Table 5. The κ CSDM and κ FS-TSH-EDC simulations involve ensembles of 300 and 200 trajectories, respectively, with initial conditions sampled by vertical excited to the first electronically excited state from the ground-vibrational-state Wigner distribution of the ground electronic state. The CSDM, tCSDM, FS-TSH-ED, and tFS-TSH-EDC simulations are for the same kind of initial conditions, although with different sizes of the ensemble. The table shows that the curvature-driven nonadiabatic dynamics methods¹⁷⁰ κ CSDM and κ FS-TSH-EDC predict the excited-state lifetime of ethylene to be 78 and 84 fs respectively, which are not very different from the respective CSDM and FS-TSH-EDC predictions. This demonstrates the accuracy of curvature-driven approximation.

It was demonstrated in ab initial multiple spawning (AIMS)¹⁹⁰ simulations that the Rydberg states do not have a big effect on the excited-state lifetime,¹⁸² and this validates the simulations in Table 5 that did not consider Rydberg states.

The first excited state population of ethylene as a function of time for CSDM, tCSDM, κ CSDM, FS-TSH-EDC, tFS-TSH-EDC, and κ FS-TSH-EDC is shown Figure 3. This shows good agreement of all the methods.

6.2. Ammonia. We next consider ammonia photo-dissociation.^{191–196} Electronically excited ammonia dissociates H atom(s) from NH₃. The S_0/S_1 MECI is planar with stretched NH bonds and distorted HNH angles.^{192,197} We sampled trajectories starting with the ground-state Wigner distribution and vertically excited them to S_1 . The resulting photodissociation is ultrafast; about 60% of the excited-state population decays within 30 fs.⁹³ And the dissociation of the H

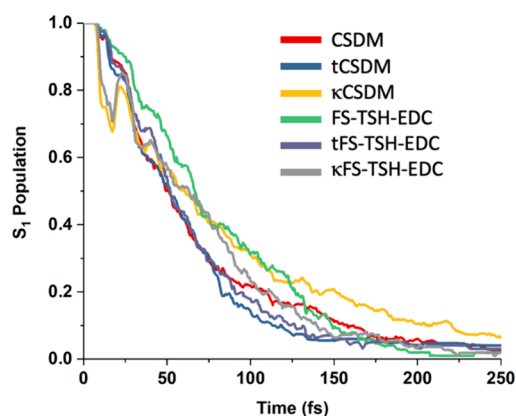


Figure 3. First excited-state population as a function of time for ethylene.

atom from NH₃ is almost finished for all trajectories within the first 30 fs; the averaged N–H distance is about 5 Å at 30 fs. If one propagates the FS-TSH trajectories beyond 30 fs, the ensuing dynamics is dominated by NH₂ vibration and relative translation of the fragments. After 30 fs, there are two contributions to population decay, namely, physical decay—which exists in all dynamics methods; and population leaking—which only exists in TSH methods. The physical decay is caused by the trajectory passing through locally avoided crossings, and the population leaking is caused by the frustrated hops in TSH methods. Although there is a relatively large energy gap between the states, the transition probability of excited-state trajectories to the ground electronic state is not zero. Therefore, if one carries out the FS-TSH simulation to long enough times, there will be some hopping to the ground state. The trajectories arriving in the ground state will undergo intramolecular vibrational energy redistribution, and attempted hops back to the excited state will be frustrated. This causes unphysical excited-state population leaking in TSH calculations.⁹³ FSTU alleviates population leaking, although it does not eliminate it, but CSDM and κ CSDM do not suffer population leaking. The first excited state population of ammonia as a function of time for CSDM, tCSDM, κ CSDM, tFS-TSH-EDC, and tFSTU-EDC is shown in Figure 4 for the same ensemble as discussed above. This figure also zooms in on the range from 20 to 500 fs is shown to illustrate the population leaking. The agreement between CSDM, tCSDM, and κ CSDM is very good over the whole time interval. The

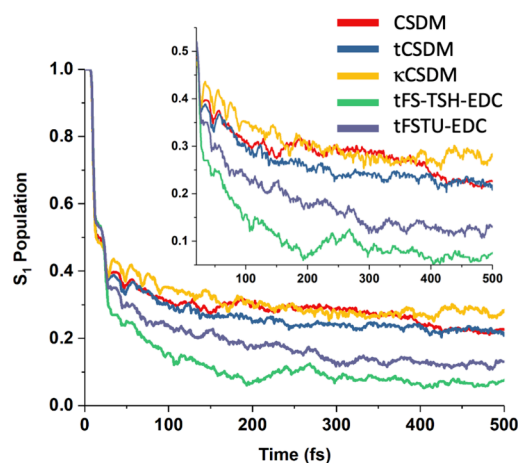


Figure 4. First excited state population as a function of time for ammonia.

average number of frustrated hops per trajectory is 1.49 and 0.99 for tFS-TSH-EDC and tFSTU-EDC respectively. As can be seen in Figure 4, the first excited state population of tFS-TSH-EDC has almost decayed to zero in 500 fs, resulting a close to 0 branching ratio between \tilde{A} state/ \tilde{X} state. Table 6

Table 6. Branching Ratios^a between \tilde{A} and \tilde{X} States of NH₂

Dynamics algorithm	Branching ratio	
	at 30 fs ^b	at 500 fs
tFS-TSH-EDC ^c	0.41	0.08
tFSTU-EDC ^c	0.54	0.15
CSDM	0.64	0.29
tCSDM	0.61	0.27
κCSDM	0.67	0.39
Quantum	0.35	

^aThe branching ratio is the ratio of population in the excited state (\tilde{A}) to population in the ground state (\tilde{X}). ^bThe results at 30 fs are not final results but are shown to illustrate the time dependence of the results at short times. ^cElectronic EOM is propagated with local diabatization algorithm.

shows the \tilde{A} state/ \tilde{X} state branching ratio for various methods. Clearly, the κCSDM results are very close to those of CSDM, which again demonstrates the accuracy of curvature-driven approximation. In addition, the final branching ratios (0.30 and 0.39) from the CSDM and κCSDM methods are much closer than the final FS-TSH-EDC and FSTU-EDC results (0.08 and 0.15) to the results (0.35)¹⁹³ from a quantum simulation.

6.3. 1,3-Cyclohexadiene. We have also demonstrated the accuracy of curvature-driven nonadiabatic dynamics methods for more complex photochemical reactions. For example, we have used 42-dimensional, 3-state κCSDM dynamics interfaced with extended multistate complete active space second-order perturbation theory¹⁵⁸ (XMS-CASPT2) to study the ring-opening nonadiabatic dynamics of 1,3-cyclohexadiene.¹⁹⁸ There are two products, namely hexatriene and 1,3-cyclohexadiene. The predicted hexatriene quantum yield is 40%, and the calculated lifetime of the excited state is 117 fs (including the induction period). These are comparable to experimental observations which gave quantum yield of 0.3–0.5 and an excited-state lifetime 130–142 fs.^{199–203} Table 7 shows the hexatriene quantum yield and excited-state lifetime from

selected nonadiabatic dynamics simulations (this is not a complete review of this classic problem).

Table 7. Hexatriene Product Ratios and Excited-State Lifetimes

Dynamics algorithm	Potential energy surfaces	Hexatriene quantum yield	Excited state lifetime ^a (fs)
ZN-TSH ^{b,204}	MS-CASPT2	0.40	68
FS-TSH ²⁰⁵	XMS-CASPT2	N/A	68
ZN-TSH ^{b,206}	SA-CASSCF	0.47	120
FS-TSH-EDC ²⁰⁷	XMS-CASPT2	0.47	89
EF-TSH ^{c,208}	REKS ^d	0.36	277
FS-TSH ²⁰⁹	XMS-CASPT2	<0.5	<125
FS-TSH ²¹⁰	TDA-TDDFT ^e	0.65	81
AIMS ²¹¹	α-SA-CASSCF ²¹²	~0.5	139
κCSDM ¹⁹⁸	XMS-CASPT2	0.40	117
Quantum (2D) ²¹³	MRCI ^f	0.5	130
Experiment		0.3–0.5	130–142

^aThe excited-state lifetime here includes the induction period. ^bTrajectory surface hopping with the Zhu-Nakamura theory to predict the hopping probability.¹⁶⁷ ^cTrajectory surface hopping with based on the exact factorization formalism.²¹⁴ ^dRestricted ensemble-referenced Kohn–Sham theory.²¹⁵ ^eTamm-Dancoff-approximation time-dependent density functional theory with the PBE0 density functional.²¹⁶ ^fMultireference configuration interaction. The dynamics simulation employs a reduced dimensional surface (2-dimensional).

6.4. Isomerization and Ring-Opening Reactions with 4–24 Atoms. A recent survey of six photochemical reactions compared results between κFS-TSH-EDC and FS-TSH-EDC.^{151,217} (Notice that the apparently inaccurate curvature-driven dynamics results in ref 217 were due to a programming error—not to deficiencies in the method; this was corrected in ref 151.) Table 8 summarizes the final ground-state and excited-state populations at the end of the simulation for κFS-TSH-EDC and FS-TSH-EDC. The mean unsigned deviation (MUD) of κFS-TSH-EDC state populations as compared to FS-TSH-EDC state populations—averaged over 6 molecules and 18 states—is only 0.06.

The 0.06 mean unsigned deviation is almost within the statistical error for different methods to propagate the electronic EOM using NACs and overlap integrals. For example, in ref 151, the MUD of state population between tFS-TSH-EDC (specifically, uses the local diabatization algorithm¹⁴⁵ to propagate the electronic EOM) and FS-TSH-EDC averaged over the 6 molecules and the 18 states—is 0.03. The tFS-TSH-EDC final state population is included in Table 8 as well.

If we omit the only especially bad case, namely, *trans*-AZB, the resulting MUDs over 14 states between κFS-TSH-EDC and FS-TSH-EDC, and tFS-TSH-EDC and FS-TSH-EDC are both 0.04, which is shown in the parenthesis in the last row of Table 8—so that one cannot distinguish between the NAC-based algorithm, the overlap-based algorithm, and the curvature-driven algorithm. If one also omits from consideration the small final-state populations of the S₂ and S₃ states of *cis*-AZB, the resulting mean unsigned percentage deviation between κFS-TSH-EDC and FS-TSH-EDC is 13%, and the mean unsigned percentage deviation between tFS-TSH-EDC and FS-TSH-EDC is 14%.

Figure 5 shows the population difference between κFS-TSH-EDC and tFS-TSH-EDC for the first excited state as a function

Table 8. Final Electronic Populations

System ^a	Δt^b (fs)	FS-TSH-EDC				tFS-TSH-EDC ^c				κ FS-TSH-EDC			
		S ₀	S ₁	S ₂	S ₃	S ₀	S ₁	S ₂	S ₃	S ₀	S ₁	S ₂	S ₃
<i>cis</i> -AZM	150	0.72	0.28			0.81	0.19			0.81	0.19		
<i>trans</i> -AZM	350	0.95	0.05			0.95	0.05			0.94	0.06		
<i>cis</i> -AZB	100	0.86	0.12	0.01	0.01	0.91	0.09	0.00	0.00	0.78	0.12	0.05	0.05
<i>trans</i> -AZB	100	0.02	0.96	0.02	0.00	0.02	0.97	0.00	0.01	0.19	0.73	0.07	0.01
butyrolactone	100	0.52	0.27	0.21		0.42	0.31	0.27		0.46	0.34	0.20	
furanone	150	0.43	0.31	0.26		0.46	0.27	0.27		0.38	0.37	0.25	
MUD							0.03 (0.04)				0.06 (0.04)		

^aAZM = azomethane; AZB = azobenzene. ^bSimulation time. ^cElectronic EOM is propagated with local diabaticization algorithm.

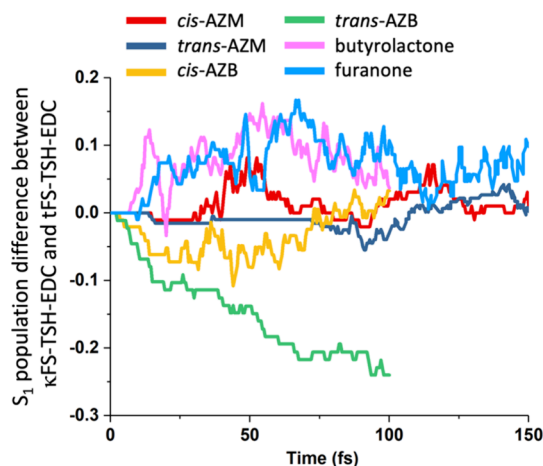


Figure 5. First excited state population difference between κ FS-TSH-EDC and tFS-TSH-EDC as a function of time for the six systems considered.

of time. Except for *trans*-AZB, the excited-state populations by the two methods are very close over the whole simulation time.

In practice, one sometimes approximates the overlap integral. Reference¹⁵¹ also provides a direct comparison between κ TDCs, analytic TDCs computed from eq 18, and overlap-based TDCs computed in three different ways approximated from eq 91. The comparison shows that dynamics calculations based on the curvature-driven approximation can actually agree better with dynamics calculations based on the full NAC than do dynamics calculations based on a TDC computed from an overlap integral.

6.5. O + O₂ Collisions. The curvature-driven methods have also been applied to bimolecular collisions to calculate cross sections for $O(^3P) + O_2(^3\Sigma_g^-) \rightarrow O(^3P) + O_2(^3\Delta_u)$ including six coupled ⁵A' adiabatic potential energy surfaces obtained from diabatic fits to XMS-CASPT2 energies. We compared CSDM using a NAC in the electronic EOM to κ CSDM for 35 combinations of initial collision energy and initial diatomic vibrational state. The results are shown in Figure 6, which shows that the electronically nonadiabatic collision cross sections are very close.²¹⁸ The mean unsigned deviation of electronically nonadiabatic collision cross sections over 35 initial conditions is 0.09 Å². This is only 5% of the average cross section of 1.89 Å².

7. OUTLOOK

Simulations including electronic nonadiabaticity are important in many areas of chemistry including photochemistry,

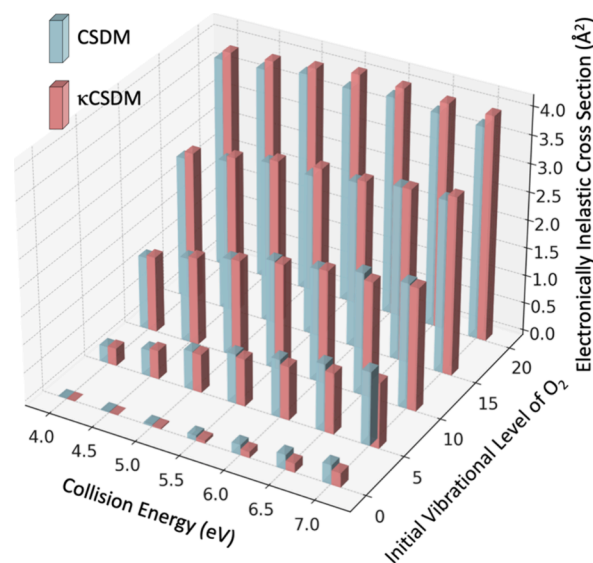


Figure 6. Electronically nonadiabatic collision cross sections for 35 initial conditions.

photocatalysis, collisions of electronically excited species, chemiluminescent reactions, and two-state reactivity. It is particularly convenient if this kind of calculation is carried out using methods where the nuclei follow mixed quantum-classical trajectories and using direct dynamics where one avoids prior fitting of potential energy surfaces and couplings by carrying out electronic structure calculations along the trajectory wherever the dynamics algorithm needs energies, gradients, or couplings. With most electronic structure packages, energies and gradients are more straightforward than couplings (NACs or TDCs). In this perspective, we have reviewed recent success in the development of wave function-free electronically nonadiabatic dynamics methods. In the process we also explained a generalized version of the semiclassical Ehrenfest method and used it as a way to see the relation between various approximations that have been proposed.

There are two steps to achieve wave function-free methods, namely, the NAC-free methods in which the trajectory needs energies, gradients, and TDCs; and the wave function-free methods in which the trajectory needs only energies and gradients.

Achieving the NAC-free methods itself is already a useful step forward. This is so for two reasons. First, the NACs are computationally inconvenient. For example, one needs to ensure NACs have consistent phases along a trajectory, the

number of NACs scales quadratically with the number of electronic states considered, and the NACs are singular at conical intersections. Second, using NACs from electronic structure software causes theoretical difficulties. For example, these NACs depend on the origin of the coordinate system, they do not account for the momentum of electrons moving with nuclei, they often have spurious long-range coupling, and they do not conserve total nuclear angular momentum and center of mass momentum.

The first attempt remove NACs was to recognize that only one component of the NAC appears in the TDC in the electronic EOM, and this component (the scalar product of the nuclear velocity vector and the NAC) can be computed as an overlap integral of the electronic wave functions at successive time steps. However, this only enables NAC-free trajectory surface hopping methods for systems whose Hamiltonian does not include SOC, and even in the absence of SOC, it does not enable NAC-free computations employing SCP methods like SE or CSDM.

Further work was required to achieve wider applicability of NAC-free methods, and for this purpose we developed generalized semiclassical Ehrenfest (GSE) dynamics method and a new gradient correction scheme called the time-derivative matrix (TDM) scheme. Although we have used GSE in previous papers,^{52,94,151,170,198,218} the full details are presented here for the first time. These two developments (GSE and TDM) have enabled a complete computational framework for simulating nonadiabatic processes—both when SOC is present and when it is not—without NACs by both surface hopping methods and SCP methods.

We often label methods that are NAC-free as overlap-based algorithms, with a prefix “t,” for example, tGSE and tFS-TSH. The only information required from electronic structure packages for propagating mixed quantum-classical nonadiabatic trajectories using time-derivative methods consists of energies, gradients, and TDCs (approximated, for example, from overlap integrals of adiabatic electronic wave functions at successive time steps).

The overlap-based algorithms are the starting point for our ultimate goal, namely, wave function-free mixed quantum-classical nonadiabatic dynamics. One key development in achieving this is the curvature-driven approximation to the TDC, in which we approximate the TDC by local information about the curvatures of the potential energy surfaces along a path; the curvature information can be obtained from energy gradients without using electronic wave functions. The curvature-driven approximation to the TDC is called κ TDC. Using the κ TDC in the equations of motion results in dynamics algorithms, for example, κ GSE and κ FS-TSH, that require energies and gradients only. Therefore, these algorithms are not only NAC-free, but they are also wave function-free.

Therefore, with the development of the GSE, the TDM scheme, and the curvature-driven approximation to the TDC, we have provided a complete computational framework for simulations of nonadiabatic processes with only potential energies and gradients.

The κ GSE and κ FS-TSH methods form the basic two classes of curvature-driven mixed quantum-classical nonadiabatic dynamics methods, and each class contains variations within the general framework. In the SCP class (whose starting point is κ GSE), we especially recommend curvature-driven coherent switching with decay of mixing (κ CSDM), and in the TSH

class (whose starting point is κ FS-TSH), we especially recommend curvature-driven fewest switches with time uncertainty trajectory surface hopping with energy-based decoherence (κ FSTU-EDC). The present article also reviews both of these methods.

There have already been several successful applications to realistic multidimensional nonadiabatic dynamics simulations for both unimolecular processes and collision dynamics, showing encouragingly high accuracy, and we review these in the Section 6 of the paper. We expect that the new methods are applicable to most or even all nonradiative transitions in large organic molecules. The applicability may be even wider though, for example the methods may be applicable to defect-induced nonradiative recombination on semiconductor nanocrystals.²¹⁹ Such broader applicability would be interesting for further study.

The curvature-driven methods are available for both SCP and TSH calculations in SHARC²²⁰ (since version 3.0) and SHARC-MN²²¹ (since version 1.1) and for TSH calculations in Newton-X²²² (since version 2.4). In SHARC and SHARC-MN, the curvature-driven methods are denoted by a prefix κ , for examples, κ CSDM, κ TSH; in Newton-X, the curvature-driven approximation is called Baeck-An coupling.

The methods discussed here, like all mixed-quantum classical nonadiabatic dynamics algorithms that employ classical trajectories, have the drawback that quantum effects on nuclear motion are not included even when propagation proceeds on a single surface. For example, nuclear-motion tunneling is neglected in the standard versions of the method, although some quantum mechanical tunneling effects can be and have been added to CSDM calculations as an extension.^{223–225} Constructive and destructive nuclear-motion interference effects are lost because of the independent trajectory approximation and the neglect of WKB-like phases. Maintenance of zero-point vibrational energy is not enforced. Intramolecular vibrational relaxation is different in classical and quantal systems. Nevertheless, tests of CSDM against accurate quantum dynamics for realistic multisurface systems show errors that are of the same order as the errors in single-surface classical trajectories.^{53,83,84,172–174}

8. SUMMARY

This paper is a perspective on semiclassical methods for nonadiabatic dynamics and how their requirement for electronic-structure quantities can be altered to make them ‘wave function-free.’ It contains a combination of selective background review and new material, with the objective that it provides an outlook on the encouraging future prospects for wave function-free electronically nonadiabatic dynamics, i. e., dynamics calculations that require only potential energy surfaces and their gradients, not needing time derivatives of wave functions or coupling matrix elements that need to be computed from electronic wave functions.

We provide background on Ehrenfest and surface-hopping dynamics, using a general notation for the electronic basis (adiabatic/diabatic or spin-adiabatic/spin-diabatic). We also treat decoherence. After introducing the required electronic-structure quantities for nonadiabatic dynamics, we discuss different strategies for wave function-free semiclassical dynamics. We summarize the working equations for each specific method in tables and provide a scheme (Figure 2) organizing the connections between the different methods presented.

Table A1. Acronyms and Abbreviations

Abbreviation	Complete terminology	Explanation
Dynamics		
A	adiabatic	not involving a change in adiabatic electronic state
AIMS	ab initio multiple spawning	an approximate method based on Gaussian wave packets centered on classical trajectories
CSDM	coherent switching with decay-of-mixing	an SCP method for molecular dynamics with electronic transitions and decoherence
diag	diagonal	the fully adiabatic electronic basis, i.e., the basis that diagonalizes the electronic Hamiltonian, including (when present) SOC
EDC	energy-based decoherence	decoherence scheme based on potential and kinetic energies
elec	electronic	referring to the electronic degrees of freedom
EOM	equation of motion	The nuclear EOM governs time evolution of atomic coordinates; the electronic EOM governs time evolution of the electronic state.
FS-TSH	fewest switches trajectory-surface-hopping	the basic surface-hopping method for molecular dynamics with electronic transitions
FSTU	fewest switches time-uncertainty	an improvement of FS-TSH incorporating quantum uncertainty into the hopping times of classically forbidden hops
GB	general basis	an electronic basis that may be adiabatic, diabatic, partially adiabatic, or any other
GCSDM	generalized coherent switching with decay of mixing	a variant of CSDM that is based on GSE
GSE	generalized semiclassical Ehrenfest	a variant of SE that does not require electronic wave functions, TDCs, or NACs
κ	curvature-driven	calculating electronic-state couplings from the curvatures of adiabatic potential energy surfaces without requiring electronic wave functions, TDCs, or NACs
κ CSDM	curvature-driven coherent switching with decay of mixing	curvature-driven CSDM
κ FS-TSH	curvature-driven fewest switches trajectory-surface-hopping	curvature-driven FS-TSH
κ FSTU	curvature-driven fewest switches with time uncertainty	curvature-driven FSTU
κ GSE	curvature-driven generalized semiclassical Ehrenfest	curvature-driven GSE
κ TDC	curvature-driven time derivative coupling	an approximated TDC that is computed from potential energies and time derivatives of potential energies
κ TSH	curvature-driven trajectory surface hopping	curvature-driven TSH
MCH	molecular-Coulomb-Hamiltonian	an electronic basis that diagonalizes the SOC-free electronic Hamiltonian
NA	nonadiabatic	involving a transition among adiabatic electronic states
NAC	nonadiabatic coupling	vector electronic-state coupling matrix element in the electronically adiabatic basis
NGT	nuclear gradient tensor	a tensor used for a gradient correction scheme in the diagonal basis
nuc	nuclear	referring to the coordinates of the nuclei
SCP	self-consistent potential	the mean-field potential energy (based on the expectation value of the electronic energy even when the electronic state is a not a Born–Oppenheimer eigenstate) that governs nuclear motion in an Ehrenfest-type algorithm for electronically nonadiabatic dynamics.
SE	semiclassical Ehrenfest	“Semiclassical” in this context denotes mixed quantum-classical where the electronic structure is treated quantum mechanically and the nuclear motion is treated by trajectories. “Ehrenfest” denotes that the potential energy governing nuclear motion is based on an SCP.
SOC	spin–orbit coupling	a relativistic effect coupling electronic states with different spin multiplicities. We use the usual shorthand by which SOC refers to the sum of all magnetic terms in the electronic Hamiltonian.
SOF	spin–orbit-free	neglecting SOC
tCSDM	time derivative coherent switching with decay of mixing	a variant of CSDM that is NAC-free but requires the TDC
TDC	time-derivative coupling	scalar electronic-state coupling matrix element equal to the scalar product of the NAC and the nuclear velocity
TDM	time-derivative matrix	matrix representation of the TDC
tFS-TSH	time derivative fewest-switches trajectory-surface-hopping	a variant of FS-TSH that is NAC-free but requires the TDC
tGSE	time-derivative generalized semiclassical Ehrenfest	a variant of GSE that is NAC-free but requires the TDC
TSH	trajectory surface hopping	any version of trajectory surface hopping
ZN-TSH	Zhu–Nakamura trajectory surface hopping	trajectory surface hopping method based on the Zhu–Nakamura theory of a nonadiabatic transition
2D	two-dimensional	referring to a model with two nuclear degrees of freedom
Electronic Structure		
α -SA-CASSCF	α state-averaged complete active space self-consistent field	a semiempirical configuration interaction method
FOMO-AM1-CASSCI	floating occupation molecular orbital Austin model 1 complete active space configuration interaction	a semiempirical configuration interaction method
SA n -CASSCF	state-averaged n -states complete active space self-consistent field	a first-principles configuration interaction method

Table A1. continued

Abbreviation	Complete terminology	Explanation
Electronic Structure		
MRCI	multireference configuration interaction	a first-principles configuration interaction method
MS-CASPT2	multistate complete-active-space second-order perturbation theory	a first-principles perturbation theory method
REKS	spin-restricted ensemble-referenced Kohn–Sham	a density functional method
TDA-TDDFT	Tamm–Dancoff approximation time-dependent density functional theory	a density functional method
XMS-CASPT2	extended multistate complete-active-space second-order perturbation theory	a first-principles perturbation theory method
Molecules		
AZB	azobenzene	(C ₆ H ₅) ₂ N ₂
AZM	azomethane	(CH ₃) ₂ N ₂

At the end, we briefly review several successful applications from our own work providing examples highlighting comparisons between mixed quantum–classical trajectory methods for nonadiabatic dynamics when carried out with and without wave function input. We present evidence that the wave function-free methods produce results quite comparable to methods based on calculated nonadiabatic couplings for systems with conical intersections.

■ APPENDIX A. EXPLANATION OF ACRONYMS AND ABBREVIATIONS

Table A1 explains acronyms and abbreviations used in this Perspective.

■ AUTHOR INFORMATION

Corresponding Author

Donald G. Truhlar – Department of Chemistry, Chemical Theory Center, and Minnesota Supercomputing Institute, University of Minnesota, Minneapolis, Minnesota 55455-0431, United States; orcid.org/0000-0002-7742-7294; Email: truhlar@umn.edu

Author

Yinan Shu – Department of Chemistry, Chemical Theory Center, and Minnesota Supercomputing Institute, University of Minnesota, Minneapolis, Minnesota 55455-0431, United States; orcid.org/0000-0002-8371-0221

Complete contact information is available at: <https://pubs.acs.org/10.1021/acs.jctc.4c00424>

Notes

The authors declare no competing financial interest.

■ ACKNOWLEDGMENTS

This work was supported in part by the U.S. Department of Energy, Office of Science, Office of Basic Energy Sciences under Award DE-SC0015997.

■ REFERENCES

- (1) Born, M.; Oppenheimer, J. R. Zur Quantentheorie der Molekeln. *Ann. Phys.* **1927**, *389*, 457–484.
- (2) Mead, C. A. The Born–Oppenheimer Approximation in Molecular Quantum Mechanics. In *Mathematical Frontiers in Computational Chemical Physics*, Truhlar, D. G., Ed.; The IMA Vols in Mathematics and its Applications, Vol. 15, Springer-Verlag, 1988; pp 1–17.

- (3) Mead, C. A. Born–Oppenheimer Expansion at Constant Energy. *J. Chem. Phys.* **2006**, *125*, 204109.
- (4) Mott, N. F. On the Theory of Excitation by Collision with Heavy Particles. *Proc. Cambridge Philos. Soc.* **1931**, *27*, 553–560.
- (5) Lichten, W. Resonant Charge Exchange in Atomic Collisions. *Phys. Rev.* **1963**, *131*, 229–238.
- (6) Berry, R. S.; Nielsen, S. E. Dynamic Coupling Phenomena in Molecular Excited States. I. General Formulation and Vibronic Coupling H₂. *Phys. Rev. A* **1970**, *1*, 383–394.
- (7) Delos, J. B.; Thorson, W. R.; Knudson, S. K. Semiclassical Theory of Inelastic Collisions. I. Classical Picture and Semiclassical Formulation. *Phys. Rev. A* **1972**, *6*, 709–720.
- (8) Tully, J. C. Nonadiabatic Processes in Molecular Collisions. In *Dynamics of Molecular Collisions*, Part B, Miller, W. H., Ed.; Plenum Press, New York, 1976; pp 217–268.
- (9) Child, M. S. Electronic Excitation: Nonadiabatic Transitions. In *Atom–Molecule Collision Theory*, Bernstein, R. B., Ed.; Plenum: New York, 1979; pp 427–465.
- (10) Chapman, S. The Classical Trajectory–Surface Hopping Approach to Charge-Transfer Processes. *Adv. Chem. Phys.* **1992**, *82*, 423–483.
- (11) Tully, J. C. Mixed Quantum–Classical Dynamics. *Faraday Discuss.* **1998**, *110*, 407–419.
- (12) London, F. Zur Theorie Nicht Adiabatisch Verlaufender Chemischer Prozesse. *Z. Phys.* **1932**, *74*, 143–174.
- (13) Hush, N. S. A Glimpse of the Evolution of Adiabaticity. In *Personal and Scientific Reminiscences: Tributes to Ahmed Zewail*; Chergui, M., Marcus, R. A., Thomas, J. M., Zhong, D., Eds.; World Scientific: Singapore, 2017; pp 141–151.
- (14) Wigner, E. The Transition State Method. *Trans. Faraday Soc.* **1938**, *34*, 29–41.
- (15) Teller, E. The Crossing of Potential Surfaces. *J. Phys. Chem.* **1937**, *41*, 109–116.
- (16) Teller, E. Internal Conversion in Polyatomic Molecules. *Israel J. Chem.* **1969**, *7*, 227–235.
- (17) Truhlar, D. G.; Mead, C. A. The Relative Likelihood of Encountering Conical Intersections and Avoided Intersections on the Potential Energy Surfaces of Polyatomic Molecules. *Phys. Rev. A* **2003**, *68*, 32501.
- (18) Born, M. Kopplung Der Elektronen- und Kernbewegung in Molekeln und Kristallen. *Nachr. Akad. Wiss. Göttingen, Math.-Phys.* **1951**, *6*, 1–3.
- (19) Born, M.; Huang, K. *The Dynamical Theory of Crystal Lattices*; Oxford University Press: London, 1954.
- (20) Hirschfelder, J. O.; Meath, W. J. The Nature of Intermolecular Forces. *Adv. Chem. Phys.* **1967**, *12*, 3–106.
- (21) Thompson, T. C.; Truhlar, D. G.; Mead, C. A. On the Form of the Adiabatic and Diabatic Representations and the Validity of the Adiabatic Approximation for X₃ Jahn–Teller Systems. *J. Chem. Phys.* **1985**, *82*, 2392–2407.

- (22) Tawa, G. J.; Mielke, S. L.; Truhlar, D. G.; Schwenke, D. W. Algebraic Variational and Propagation Formalisms for Quantal Dynamics Calculations of Electronic-to-Vibrational, Rotational Energy Transfer and Application to the Quenching of the 3p State of Sodium by Hydrogen Molecules. *J. Chem. Phys.* **1994**, *100*, 5751–5777.
- (23) Mead, C. A. Electronic Hamiltonian, Wave Functions, and Energies, and Derivative Coupling Between Born–Oppenheimer States in the Vicinity of a Conical Intersection. *J. Chem. Phys.* **1983**, *78*, 807–814.
- (24) Thompson, T. C.; Mead, C. A. Adiabatic Electronic Energies and Nonadiabatic Couplings to All Orders for System of Three Identical Nuclei with Conical Intersection. *J. Chem. Phys.* **1985**, *82*, 2408–2417.
- (25) Varandas, A. J. C.; Brown, F. B.; Mead, C. A.; Truhlar, D. G.; Blais, N. C. A Double Many-Body Expansion of the Two Lowest-Energy Potential Surfaces and Nonadiabatic Coupling for H₃. *J. Chem. Phys.* **1987**, *86*, 6258–6269.
- (26) Wang, L.; Akimov, A.; Prezhdo, O. V. Recent Progress in Surface Hopping: 2011–2015. *J. Phys. Chem. Lett.* **2016**, *7*, 2100–2112.
- (27) Crespo-Otero, R.; Barbatti, M. Recent Advances and Perspectives on Nonadiabatic Mixed Quantum-Classical Dynamics. *Chem. Rev.* **2018**, *118*, 7026–7068.
- (28) Mai, S.; González, L. Molecular Photochemistry: Recent Developments in Theory. *Angew. Chem., Int. Ed.* **2020**, *59*, 16832–16846.
- (29) *Quantum Chemistry and Dynamics of Excited States: Methods and Applications*; González, L.; Lindh, R., Eds.; Wiley: Hoboken, 2021.
- (30) Nelson, T. R.; White, A. J.; Bjorgaard, J. A.; Sifain, A. E.; Zhang, Y.; Nebgen, B.; Fernandez-Alberti, S.; Mozysky, D.; Roitberg, A. E.; Tretiak, S. Non-adiabatic Excited-State Molecular Dynamics: Theory and Applications for Modeling Photophysics in Extended Molecular Materials. *Chem. Rev.* **2020**, *120*, 2215–2287.
- (31) Santoro, F.; Green, J. A.; Martinez-Fernandez, L.; Cerezo, J.; Improta, R. Quantum and Semiclassical Dynamical Studies of Nonadiabatic Processes in Solution: Achievements and Perspectives. *Phys. Chem. Chem. Phys.* **2021**, *23*, 8181–8199.
- (32) Han, S.; Xie, C.; Hu, X.; Yarkony, D. R.; Guo, H.; Xie, D. Quantum Dynamics of Photodissociation: Recent Advances and Challenges. *J. Phys. Chem. Lett.* **2023**, *14*, 10517–10530.
- (33) Wu, B.; He, X.; Liu, J. Nonadiabatic Field on Quantum Phase Space: A Century after Ehrenfest. *J. Phys. Chem. Lett.* **2024**, *15*, 644–658.
- (34) Tully, J. C.; Preston, R. K. Trajectory Surface Hopping Approach to Nonadiabatic Collisions: The Reaction of H⁺ with D₂. *J. Chem. Phys.* **1971**, *55*, 562–572.
- (35) Blais, N. C.; Truhlar, D. G. Trajectory-Surface-Hopping Study of Na(3p ²P) + H₂ → Na(3s ²S) + H₂(*v*, *j*, *θ*). *J. Chem. Phys.* **1983**, *79*, 1334–1342.
- (36) Tully, J. C. Molecular Dynamics with Electronic Transitions. *J. Chem. Phys.* **1990**, *93*, 1061–1071.
- (37) Hammes-Schiffer, S.; Tully, J. C. Proton Transfer in Solution: Molecular Dynamics with Quantum Transitions. *J. Chem. Phys.* **1994**, *101*, 4657–4667.
- (38) Meyer, H.-D.; Miller, W. H. A Classical Analog for Electronic Degrees of Freedom in Nonadiabatic Collision Processes. *J. Chem. Phys.* **1979**, *70*, 3214–3223.
- (39) Gerber, R. B.; Buch, V.; Ratner, M. A. Time-Dependent Self-Consistent Field Approximation for Intramolecular Energy Transfer. I. Formulation and Application to Dissociation of van der Waals Molecules. *J. Chem. Phys.* **1982**, *77*, 3022–3030.
- (40) Micha, D. A. A Self-Consistent Eikonal Treatment of Electronic Transitions in Molecular Collisions. *J. Chem. Phys.* **1983**, *78*, 7138–7145.
- (41) Volobuev, Y. L.; Hack, M. D.; Topaler, M. S.; Truhlar, D. G. Continuous Surface Switching: An Improved Time-Dependent Self-Consistent-Field Method for Nonadiabatic Dynamics. *J. Chem. Phys.* **2000**, *112*, 9716–9726.
- (42) Hack, M. D.; Truhlar, D. G. Electronically Nonadiabatic Trajectories: Continuous Surface Switching II. *J. Chem. Phys.* **2001**, *114*, 2894–2902.
- (43) Shu, Y.; Varga, Z.; Kanchanakungwankul, S.; Zhang, L.; Truhlar, D. G. Diabatic States of Molecules. *J. Phys. Chem. A* **2022**, *126*, 992–1018.
- (44) Mead, C. A.; Truhlar, D. G. Conditions for the Definition of a Strictly Diabatic Electronic Basis for Molecular Systems. *J. Chem. Phys.* **1982**, *77*, 6090–6098.
- (45) Richter, M.; Marquetand, P.; González-Vázquez, J.; Sola, I.; González, L. SHARC: Ab Initio Molecular Dynamics with Surface Hopping in the Adiabatic Representation Including Arbitrary Couplings. *J. Chem. Theory Comput.* **2011**, *7*, 1253–1258.
- (46) Granucci, G.; Persico, M.; Spighi, G. Surface Hopping Trajectory Simulations with Spin-Orbit and Dynamical Couplings. *J. Chem. Phys.* **2012**, *137*, 22A501.
- (47) Cui, G.; Thiel, W. Generalized Trajectory Surface-Hopping Method for Internal Conversion and Intersystem Crossing. *J. Chem. Phys.* **2014**, *141*, 124101.
- (48) Curchod, B. F. E.; Rauer, C.; Marquetand, P.; González, L.; Martínez, T. J. Communication: GAIMS – Generalized Ab Initio Multiple Spawning for Both Internal Conversion and Intersystem Crossing Processes. *J. Chem. Phys.* **2016**, *144*, 101102.
- (49) Mai, S.; Marquetand, P.; González, L. Nonadiabatic Dynamics: The SHARC Approach. *WIREs Comput. Mol. Sci.* **2018**, *8*, No. e1370.
- (50) Shu, Y.; Zhang, L.; Mai, S.; Sun, S.; González, L.; Truhlar, D. G. Implementation of Coherent Switching with Decay of Mixing into the SHARC Program. *J. Chem. Theory Comput.* **2020**, *16*, 3464–3475.
- (51) Xie, B.; Jia, P.; Wang, K.; Chen, W.; Liu, X.; Cui, G. Generalized Ab Initio Nonadiabatic Dynamics Simulation Methods from Molecular to Extended Systems. *J. Phys. Chem. A* **2022**, *126*, 1789–1804.
- (52) Shu, Y.; Zhang, L.; Sun, S.; Truhlar, D. G. Time-Derivative Couplings for Self-Consistent Electronically Nonadiabatic Dynamics. *J. Chem. Theory Comput.* **2020**, *16*, 4098–4106.
- (53) Truhlar, D. G. Decoherence in Combined Quantum Mechanical and Classical Mechanical Methods for Dynamics as Illustrated for Non-Born-Oppenheimer Trajectories. In *Quantum Dynamics of Complex Molecular Systems*, Micha, D. A.; Burghardt, I., Eds.; Springer Series in Chemical Physics, Vol. 83; Springer: Berlin, 2007; pp 227–243.
- (54) Shu, Y.; Truhlar, D. G. Decoherence and Its Role in Electronically Nonadiabatic Dynamics. *J. Chem. Theory Comput.* **2023**, *19*, 380–395.
- (55) Agostini, F.; Gross, E. K. U.; Curchod, B. F. E. Electron-Nuclear Entanglement in the Time-Dependent Molecular Wavefunction. *Comput. Theor. Chem.* **2019**, *1151*, 99–106.
- (56) Bohm, D. A Suggested Interpretation of the Quantum Theory in Terms of “Hidden” Variables. I. *Phys. Rev.* **1952**, *85*, 166–179.
- (57) Messiah, A. *Quantum Mechanics*, Wiley: New York, 1962; Vol. 2, pp 222–228.
- (58) Tully, J. C. Nonadiabatic Dynamics. In *Modern Methods for Multidimensional Dynamics Calculations in Chemistry*, Thompson, D. L., Ed., World Scientific: Singapore, 1998; pp 34–72.
- (59) Marx, D.; Hutter, J. *Ab Initio Molecular Dynamics: Basic Theory and Advanced Methods*; Cambridge University Press: Cambridge, 2009; pp 14–16.
- (60) Curchod, B. F. E.; Rothlisberger, U.; Tavernelli, I. Trajectory-Based Nonadiabatic Dynamics with Time-Dependent Density Functional Theory. *ChemPhysChem* **2013**, *14*, 1314–1340.
- (61) Ballentine, L. E. *Quantum Mechanics: A Modern Development*. 2nd ed.; World Scientific: Singapore, 2014; Chap. 14.
- (62) Giordano, D.; Amodio, P. Considerations about the Incompleteness of the Ehrenfest’s Theorem in Quantum Mechanics. *Eur. J. Phys.* **2021**, *42*, 065405.
- (63) Hunter, G. Conditional Probability Amplitudes in Wave Mechanics. *Int. J. Quantum Chem.* **1975**, *9*, 237–242.

- (64) Abedi, A.; Maitra, N. T.; Gross, E. K. U. Exact Factorization of the Time-Dependent Electron-Nuclear Wave Function. *Phys. Rev. Lett.* **2010**, *105*, 123002.
- (65) Skodje, R.; Truhlar, D. G. Localized Gaussian Wavepacket Methods for Inelastic Collisions Involving Anharmonic Oscillators. *J. Chem. Phys.* **1984**, *80*, 3123–3136.
- (66) Hack, M. D.; Wensmann, A. M.; Truhlar, D. G.; Ben-Nun, M.; Martínez, T. J. Comparison of Full Multiple Spawning, Trajectory Surface Hopping, and Converged Quantum Mechanics for Electronically Nonadiabatic Dynamics. *J. Chem. Phys.* **2001**, *115*, 1172–1186.
- (67) Shu, Y.; Zhang, L.; Wu, D.; Chen, X.; Sun, S.; Truhlar, D. G. New Gradient Correction Scheme for Electronically Nonadiabatic Dynamics Involving Multiple Spin States. *J. Chem. Theory Comput.* **2023**, *19*, 2419–2429.
- (68) Truhlar, D. G.; Duff, J. W.; Blais, N. C.; Tully, J. C.; Garrett, B. C. The Quenching of Na (3^2P) by H₂: Interactions and Dynamics. *J. Chem. Phys.* **1982**, *77*, 764–776.
- (69) Shu, Y.; Zhang, L.; Varga, Z.; Parker, K. A.; Kanchanakungwankul, S.; Sun, S.; Truhlar, D. G. Conservation of Angular Momentum in Direct Nonadiabatic Dynamics. *J. Phys. Chem. Lett.* **2020**, *11*, 1135–1140.
- (70) Braams, B. L.; Bowman, J. M. Permutationally Invariant Potential Energy Surfaces in High Dimensionality. *Int. Rev. Phys. Chem.* **2009**, *28*, 577–606.
- (71) Jiang, B.; Guo, H. Permutation Invariant Polynomial Neural Network Approach to Fitting Potential Energy Surfaces. *J. Chem. Phys.* **2013**, *139*, 054112.
- (72) Shu, Y.; Truhlar, D. G. Diabatization by Machine Intelligence. *J. Chem. Theory Comput.* **2020**, *16*, 6456–6464.
- (73) Li, C.; Hou, S.; Xie, C. Constructing Diabatic Potential Energy Matrices with Neural Networks Based on Adiabatic Energies and Physical Considerations: Toward Quantum Dynamic Accuracy. *J. Chem. Theory Comput.* **2023**, *19*, 3063–3079.
- (74) Han, S.; Xie, C.; Hu, X.; Yarkony, D. R.; Guo, H.; Xie, D. Quantum Dynamics of Photodissociation: Recent Advances and Challenges. *J. Phys. Chem. Lett.* **2023**, *14*, 10517–10530.
- (75) Batzner, S.; Musaelian, A.; Sun, L.; Geiger, M.; Mailoa, J. P.; Kornbluth, M.; Molinari, N.; Smidt, T. E.; Kozinsky, B. E(3)-Equivariant Graph Neural Networks for Data-Efficient and Accurate Interatomic Potentials. *Nat. Commun.* **2022**, *13*, 2453.
- (76) Bayatya, I.; Kovács, D. P.; Simm, G. N. C.; Ortner, C.; Csányi, G. MACE: Higher Order Equivariant Message Passing Neural Networks for Fast and Accurate Force Fields. *Advances in Neural Information Processing Systems*, 2022.
- (77) Liu, Y.; Wang, L.; Liu, M.; Lin, Y.; Zhang, X.; Oztekin, B.; Ji, S. Spherical Message Passing for 3D Molecular Graphs. *International Conference on Learning Representations (ICLR)*, 2022.
- (78) Musaelian, A.; Batzner, S.; Johansson, A.; Sun, L.; Owen, C. J.; Kornbluth, M.; Kozinsky, B. Learning Local Equivariant Representations for Large-Scale Atomistic Dynamics. *Nat. Commun.* **2023**, *14*, 579.
- (79) Hack, M. D.; Truhlar, D. G. Nonadiabatic Trajectories at an Exhibition. *J. Phys. Chem. A* **2000**, *104*, 7917–7926.
- (80) Jasper, A. W.; Hack, M. D.; Chakraborty, A.; Truhlar, D. G.; Piecuch, P. Photodissociation of LiFH and NaFH van der Waals Complexes: A Semiclassical Trajectory Study. *J. Chem. Phys.* **2001**, *115*, 7945–7952.
- (81) Müller, U.; Stock, G. Surface-Hopping Modeling of Photoinduced Relaxation Dynamics on Coupled Potential-Energy Surface. *J. Chem. Phys.* **1997**, *107*, 6230–6245.
- (82) Jasper, A. W.; Zhu, C.; Nangia, S.; Truhlar, D. G. Introductory Lecture: Nonadiabatic Effects in Chemical Dynamics. *Faraday Discuss.* **2004**, *127*, 1–22.
- (83) Zhu, C.; Nangia, S.; Jasper, A. W.; Truhlar, D. G. Coherent Switching with Decay of Mixing: An Improved Treatment of Electronic Coherence for Non-Born-Oppenheimer Trajectories. *J. Chem. Phys.* **2004**, *121*, 7658–7670.
- (84) Zhu, C.; Jasper, A. W.; Truhlar, D. G. Non-Born-Oppenheimer Liouville-von Neumann Dynamics. Evolution of a Subsystem Controlled by Linear and Population-Driven Decay of Mixing with Decoherent and Coherent Switching. *J. Chem. Theory Comput.* **2005**, *1*, 527–540.
- (85) Hazra, A.; Soudackov, A. V.; Hammes-Schiffer, S. Role of Solvent Dynamics in Ultrafast Photoinduced Proton-Coupled Electron Transfer Reactions in Solution. *J. Phys. Chem. B* **2010**, *114*, 12319–12332.
- (86) Landry, B. R.; Subotnik, J. E. Standard Surface Hopping Predicts Incorrect Scaling for Marcus Golden-Rule Rate: The Decoherence Problem Cannot Be Ignored. *J. Chem. Phys.* **2011**, *135*, 191101.
- (87) Wang, L.; Sifain, A. E.; Prezhdo, O. V. Fewest Switches Surface Hopping in Liouville Space. *J. Phys. Chem. Lett.* **2015**, *6*, 3827–3833.
- (88) Parandekar, P. V.; Tully, J. C. Mixed Quantum-Classical Equilibrium. *J. Chem. Phys.* **2005**, *122*, 094102.
- (89) Schmidt, J. R.; Parandekar, P. V.; Tully, J. C. Mixed-Quantum Classical Equilibrium: Surface Hopping. *J. Chem. Phys.* **2008**, *129*, 044104.
- (90) Sifain, A.; Wang, L.; Prezhdo, O. V. Communication: Proper Treatment of Classically Forbidden Electronic Transitions Significantly Improves Detailed Balance in Surface Hopping. *J. Chem. Phys.* **2016**, *144*, 211102.
- (91) Menger, M. F. S. J.; Ou, Q.; Shao, Y.; Faraji, S.; Subotnik, J. E.; Cofer-Shabica, D. V. Nature of Hops, Coordinates, and Detailed Balance for Nonadiabatic Simulations in the Condensed Phase. *J. Phys. Chem. A* **2023**, *127*, 8427–8436.
- (92) Limbu, D. K.; Shakib, F. A. Real-Time Dynamics and Detailed Balance in Ring Polymer Surface Hopping: The Impact of Frustrated Hops. *J. Phys. Chem. Lett.* **2023**, *14*, 8658–8666.
- (93) Jasper, A. W.; Hack, M. D.; Truhlar, D. G. The Treatment of Classically Forbidden Electronic Transitions in Semiclassical Trajectory Surface Hopping. *J. Chem. Phys.* **2001**, *115*, 1804–1816.
- (94) Zhao, X.; Shu, Y.; Zhang, L.; Xu, X.; Truhlar, D. G. Direct Nonadiabatic Dynamics of Ammonia with Curvature-Driven Coherent Switching with Decay of Mixing and with Fewest Switches with Time Uncertainty: An Illustration of Population Leaking in Trajectory Surface Hopping Due to Frustrated Hops. *J. Chem. Theory Comput.* **2023**, *19*, 1672–1685.
- (95) Coker, D. F.; Xiao, L. Methods for Molecular Dynamics with Nonadiabatic Transitions. *J. Chem. Phys.* **1995**, *102*, 496–510.
- (96) Topaler, M. S.; Allison, T. C.; Schwenke, D. W.; Truhlar, D. G. Test of Trajectory Surface Hopping Against Accurate Quantum Dynamics for an Electronically Nonadiabatic Chemical Reaction. *J. Phys. Chem. A* **1998**, *102*, 1666–1673.
- (97) Hack, M. D.; Jasper, A. W.; Volobuev, Y. L.; Schwenke, D. W.; Truhlar, D. G. Quantum Mechanical and Quasiclassical Trajectory Surface Hopping Studies of the Electronically Nonadiabatic Predissociation of the \tilde{A} State of NaH₂. *J. Phys. Chem. A* **1999**, *103*, 6309–6326.
- (98) Shenai, P. M.; Fernandez-Alberti, S. F.; Bricker, W. P.; Tretiak, S.; Zhao, Y. Internal Conversion and Vibrational Energy Redistribution in Chlorophyll A. *J. Phys. Chem. B* **2016**, *120*, 49–58.
- (99) Alfonso-Hernandez, L.; Athanasopoulos, S.; Tretiak, S.; Miguel, B.; Bastida, A.; Fernandez-Alberti, S. Vibrational Energy Redistribution During Donor-Acceptor Electronic Energy Transfer: Criteria to Identity Subsets of Active Normal Modes. *Phys. Chem. Chem. Phys.* **2020**, *22*, 18454–18466.
- (100) Barbatti, M. Velocity Adjustment in Surface Hopping: Ethylene as a Case Study of the Maximum Error Caused by Direct Choice. *J. Chem. Theory Comput.* **2021**, *17*, 3010–3018.
- (101) Jasper, A. W.; Truhlar, D. G. Improved Treatment of Momentum at Classically Forbidden Electronic Transitions in Trajectory Surface Hopping Calculations. *Chem. Phys. Lett.* **2003**, *369*, 60–67.
- (102) Jain, A.; Alguire, E.; Subotnik, J. E. An Efficient, Augmented Surface Hopping Algorithm That Includes Decoherence for Use in Large-Scale Simulations. *J. Chem. Theory Comput.* **2016**, *12*, 5256–5268.

- (103) Plasser, F.; Mai, S.; Fumanal, M.; Gindensperger, E.; Daniel, C.; González, L. Strong Influence of Decoherence Corrections and Momentum Rescaling in Surface Hopping Dynamics of Transition Metal Complexes. *J. Chem. Theory Comput.* **2019**, *15*, 5031–5045.
- (104) Hack, M. D.; Truhlar, D. G. A Natural Decay of Mixing Algorithm for Non-Born-Oppenheimer Trajectories. *J. Chem. Phys.* **2001**, *114*, 9305–9314.
- (105) Zhu, C.; Jasper, A. W.; Truhlar, D. G. Non-Born-Oppenheimer Trajectories with Self-Consistent Decay of Mixing. *J. Chem. Phys.* **2004**, *120*, 5543–5557.
- (106) Athavale, V.; Bian, X.; Tao, Z.; Wu, Y.; Qiu, T.; Rawlinson, J.; Littlejohn, R. G.; Subotnik, J. E. Surface Hopping, Electron Translation Factors, Electron Rotation Factors, Momentum Conservation, and Size Consistency. *J. Chem. Phys.* **2023**, *159*, 114120.
- (107) Wu, Y.; Rawlinson, J.; Littlejohn, R. G.; Subotnik, J. E. Linear and Angular Momentum Conservation in Surface Hopping Methods. *J. Chem. Phys.* **2024**, *160*, 024119.
- (108) Mai, S.; Marquetand, P.; González, L. A General Method to Describe Intersystem Crossing Dynamics in Trajectory Surface Hopping. *Int. J. Quantum Chem.* **2015**, *115*, 1215–1231.
- (109) Zurek, W. H. Environment-Induced Superselection Rules. *Phys. Rev. D* **1982**, *26*, 1862.
- (110) Landau, L. D.; Lifshitz, E. M. *Quantum Mechanics: Non-relativistic Theory*; Pergamon Press: Oxford, 1977; pp 38–39.
- (111) Gottfried, K.; Yan, T.-M. *Quantum Mechanics: Fundamentals*, 2nd ed.; Springer: New York, 2003; p 64.
- (112) Sakurai, J. J.; Napolitano, J. *Modern Quantum Mechanics*, 3rd ed.; Cambridge University Press: Cambridge, 2021; p 175.
- (113) Zwanzig, R. Ensemble Method in the Theory of Irreversibility. *J. Chem. Phys.* **1960**, *33*, 1338–1341.
- (114) Basilevsky, M. V.; Voronin, A. I. Nonadiabatic Transitions in the Condensed Phase. *J. Chem. Soc. Faraday Trans.* **1997**, *93*, 989–996.
- (115) Micha, D. A.; Thorndyke, B. Dissipative Dynamics in Many-Atom Systems: A Density Matrix Treatment. *Int. J. Quantum Chem.* **2002**, *90*, 759–771.
- (116) May, V.; Kühn, O. *Charge and energy Transfer Dynamics in Molecular Systems*; Wiley-VCH, 2000; pp 104–105.
- (117) Schlosshauer, M. Quantum Decoherence. *Phys. Reports* **2019**, *831*, 1–57.
- (118) Redfield, A. G. On the Theory of Relaxation Processes. *IBM J. Res. Dev.* **1957**, *1*, 19–31.
- (119) Redfield, A. G. The Theory of Relaxation Processes. *Adv. Mag. Opt. Resonance* **1965**, *1*, 1–32.
- (120) Lindblad, G. On the Generators of Quantum Dynamical Semigroups. *Commun. Math. Phys.* **1976**, *48*, 119–130.
- (121) Berman, M.; Kosloff, R.; Tal-Ezer, H. Solution of the Time-Dependent Liouville-von Neumann Equation: Dissipative Evolution. *J. Phys. A* **1992**, *25*, 1283–1307.
- (122) Grigorescu, M. Decoherence and Dissipation in Quantum Two-State Systems. *Physica A: Statistical Mechanics and its Applications* **1998**, *256*, 149–162.
- (123) Kapral, R.; Ciccotti, G. Mixed Quantum-Classical Dynamics. *J. Chem. Phys.* **1999**, *110*, 8919–8929.
- (124) Rau, A. R. P.; Wendell, R. A. Embedding Dissipation and Decoherence in Unitary Evolution Schemes. *Phys. Rev. Lett.* **2002**, *89*, 220405.
- (125) Micha, D. A.; Thorndyke, B. The Quantum-Classical Density Operator for Electronically Excited Molecular Systems. *Adv. Quantum Chem.* **2004**, *47*, 293–314.
- (126) Breuer, H.-P.; Petruccione, F. *The Theory of Open Quantum Systems*; Oxford University Press, 2006; pp 105ff.
- (127) Burghardt, I. Non-Markovian Dynamics at a Conical Intersection: Ultrafast Excited-State Processes in the Presence of an Environment. In *Quantum Dynamics of Complex Molecular Systems*; Micha, D. A.; Burghardt, I., Eds.; Springer: Berlin, 2007; pp 135–163.
- (128) Micha, D. A.; Leathers, A.; Thorndyke, B. Density Matrix Treatment of Electronically Excited Molecular Systems: Applications to Gaseous and Adsorbate Dynamics. In *Quantum Dynamics of Complex Molecular Systems*; Micha, D. A.; Burghardt, I., Eds.; Springer: Berlin, 2007; pp 165–194.
- (129) Truhlar, D. G. Decoherence in Combined Quantum Mechanical and Classical Methods for Dynamics as Illustrated for Non-Born-Oppenheimer Dynamics. In *Quantum Dynamics of Complex Molecular Systems*; Micha, D. A., Burghardt, I., Eds.; Springer: Berlin, 2007; pp 227–243.
- (130) Cai, Z.; Barthel, T. Algebraic versus Exponential Decoherence in Dissipative Many-Particle Systems. *Phys. Rev. Lett.* **2013**, *111*, 150403.
- (131) Kapral, R. Quantum dynamics in Open Quantum-Classical Systems. *J. Phys.: Condens. Matter* **2015**, *27*, 073201.
- (132) de Vega, I.; Alonso, D. Dynamics of Non-Markovian Open Quantum Systems. *Rev. Mod. Phys.* **2017**, *89*, 015001.
- (133) Weimer, H.; Kshetrimayum, A.; Orús, R. Simulation Methods for Open Quantum Many-Body Systems. *Rev. Mod. Phys.* **2021**, *93*, 015008.
- (134) Bittner, E. R.; Rossky, P. J. Quantum Decoherence in Mixed Quantum-Classical Systems: Nonadiabatic Processes. *J. Chem. Phys.* **1995**, *103*, 8130–8143.
- (135) Schwartz, B. J.; Bittner, E. R.; Prezhdo, O. V.; Rossky, P. J. Quantum Decoherence and the Isotope Effect in Condensed Phase Nonadiabatic Molecular Dynamics Simulations. *J. Chem. Phys.* **1996**, *104*, 5942–5955.
- (136) Prezhdo, O. V.; Rossky, P. J. Evaluation of Quantum Transition Rates from Quantum-Classical Molecular Dynamics Simulations. *J. Chem. Phys.* **1997**, *107*, 5863–5878.
- (137) Prezhdo, O. V. Mean field Approximation for the Stochastic Schrödinger Equation. *J. Chem. Phys.* **1999**, *111*, 8366–8377.
- (138) Granucci, G.; Persico, M. Critical Appraisal of the Fewest Switches Algorithm for Surface Hopping. *J. Chem. Phys.* **2007**, *126*, 134114.
- (139) Jasper, A. W.; Truhlar, D. G. Non-Born-Oppenheimer Molecular Dynamics for Conical Intersections, Avoided Crossings, and Weak Interactions. In *Conical Intersections: Theory, Computation, and Experiment*, Domcke, W.; Yarkony, D. R.; Köppel, H., Eds.; World Scientific, 2011; pp 375–412.
- (140) Jasper, A. W.; Truhlar, D. G. Electronic Decoherence Time for Non-Born-Oppenheimer Trajectories. *J. Chem. Phys.* **2005**, *123*, 064103.
- (141) Jaeger, H. M.; Fischer, S.; Prezhdo, O. V. Decoherence-Induced Surface Hopping. *J. Chem. Phys.* **2012**, *137*, 22A545.
- (142) Esch, M. P.; Levine, B. G. State-Pairwise Decoherence Times for Nonadiabatic Dynamics on More Than Two Electronic States. *J. Chem. Phys.* **2020**, *152*, 234105.
- (143) Esch, M. P.; Levine, B. G. Decoherence-Corrected Ehrenfest Molecular Dynamics on Many Electronic States. *J. Chem. Phys.* **2020**, *153*, 114104.
- (144) Martínez, T. J. Ab Initio Molecular Dynamics around a Conical Intersection: Li(2p) + H₂. *Chem. Phys. Lett.* **1997**, *272*, 139–147.
- (145) Granucci, G.; Persico, M.; Toniolo, A. Direct Semiclassical Simulation of Photochemical Processes with Semiempirical Wave Functions. *J. Chem. Phys.* **2001**, *114*, 10608–10615.
- (146) Meek, G. A.; Levine, B. G. Evaluation of the Time-Derivative Coupling for Accurate Electronic State Transition Probabilities from Numerical Simulations. *J. Phys. Chem. Lett.* **2014**, *5*, 2351–2356.
- (147) Fernandez-Alberti, S.; Roitberg, A. E.; Nelson, T.; Tretiak, S. Identification of Unavoided Crossings in Nonadiabatic Photoexcited Dynamics Involving Multiple Electronic States in Polyatomic Conjugated Molecules. *J. Chem. Phys.* **2012**, *137*, 014512.
- (148) Nelson, T.; Fernandez-Alberti, S.; Roitberg, A. E.; Tretiak, S. Artifacts Due to Trivial Unavoided Crossings in the Modeling of Photoinduced Energy Transfer Dynamics in Extended Conjugated Molecules. *Chem. Phys. Lett.* **2013**, *590*, 208–213.
- (149) Wang, L.; Prezhdo, O. V. A Simple Solution to the Trivial Crossing Problem in Surface Hopping. *J. Phys. Chem. Lett.* **2014**, *5*, 713–719.

- (150) Meek, G. A.; Levine, B. G. Accurate and Efficient Evaluation of Transition Probabilities at Unavoided Crossings in Ab Initio Multiple Spawning. *Chem. Phys.* **2015**, *460*, 117–124.
- (151) Zhao, X.; Merritt, I. C. D.; Lei, R.; Shu, Y.; Jacquemin, D.; Zhang, L.; Xu, X.; Vacher, M.; Truhlar, D. G. Nonadiabatic Coupling in Trajectory Surface Hopping: Accurate Time Derivative Couplings by the Curvature-Driven Approximation. *J. Chem. Theory Comput.* **2023**, *19*, 6577–6588.
- (152) Cohen, J. S.; Schneider, B. Ground and Excited States of Ne₂ and Ne₂⁺. I. Potential Curves With and Without Spin-Orbit Coupling. *J. Chem. Phys.* **1974**, *61*, 3230–3239.
- (153) Hay, P. J.; Dunning, T. H., Jr The Electronic States of KrF. *J. Chem. Phys.* **1977**, *66*, 1306–1316.
- (154) Bao, J. J.; Zhou, C.; Varga, Z.; Kanchanakungwankul, S.; Gagliardi, L.; Truhlar, D. G. Multi-State Pair Density Functional Theory. *Faraday Discuss.* **2020**, *224*, 348–372.
- (155) Bao, J. J.; Zhou, C.; Truhlar, D. G. Compressed-State Multistate Pair-Density Functional Theory. *J. Chem. Theory Comput.* **2020**, *16*, 7444–7452.
- (156) Finley, J.; Malmqvist, P.-Å.; Roos, B. O.; Serrano-Andrés, L. The Multi-State CASPT2Method. *Chem. Phys. Lett.* **1998**, *288*, 299–306.
- (157) Granovsky, A. A. Extended Multi-Configuration Quasi-Degenerate Perturbation Theory: the New Approach to Multi-State Reference Perturbation Theory. *J. Chem. Phys.* **2011**, *134*, 214113.
- (158) Shiozaki, T.; Gyöffy, W.; Celani, P.; Werner, H.-J. Extended Multi-State Complete Active Space Second-Order Perturbation Theory: Energy and Nuclear Gradients. *J. Chem. Phys.* **2011**, *135*, 081106.
- (159) Montavon, G.; Rupp, M.; Gobre, V.; Vazquez-Mayagoitia, A.; Hansen, K.; Tkatchenko, A.; Müller, K.-R.; von Lilienfeld, O. A. Machine Learning of Molecular Electronic Properties in Chemical Compound Space. *New J. Phys.* **2013**, *15*, 095003.
- (160) Kulik, H. J.; Hammerschmidt, T.; Schmidt, J.; Botti, S.; Marques, M. A. L.; Boley, M.; Scheffler, M.; Todorovic, M.; Rinke, P.; Oses, C.; Smolyanyuk, A.; Curtarolo, S.; Tkatchenko, A.; Bartok, A. P.; Manzhos, S.; Ihara, M.; Carrington, T.; Behler, J.; Isayev, O.; Veit, M.; Grisafi, A.; Nigam, J.; Ceriotti, M.; Schutt, K. T.; Westermayr, J.; Gastegger, M.; Maurer, R. J.; Kalita, B.; Burke, K.; Nagai, R.; Akashi, R.; Sugino, O.; Hermann, J.; Noe, F.; Pilati, S.; Draxl, C.; Kuban, M.; Rigamonti, S.; Scheidgen, M.; Esters, M.; Hicks, D.; Toher, C.; Balachandran, P. V.; Tamblyn, I.; Whitelam, S.; Bellinger, C.; Ghiringhelli, L. M. Roadmap on Machine Learning in Electronic Structure. *Electron. Struct.* **2022**, *4*, 023004.
- (161) Landau, L. D. Zur Theorie der Energieübertragung II. *Phys. Z. Sowjetunion* **1932**, *2*, 46–51.
- (162) Zener, C. Non-adiabatic Crossing of Energy Levels. *Proc. R. Soc. London, Ser. A* **1932**, *137*, 696–702.
- (163) Voronin, A. I.; Marques, J. M. C.; Varandas, A. J. C. Trajectory Surface Hopping Study of the Li + Li²(X¹Σ_g⁺) Dissociation Reaction. *J. Phys. Chem. A* **1998**, *102*, 6057–6062.
- (164) Belyaev, A. K.; Lasser, C.; Trigila, G. Landau-Zener Type Surface Hopping Algorithms. *J. Chem. Phys.* **2014**, *140*, 224108.
- (165) Belyaev, A. K.; Domcke, W.; Lasser, C.; Trigila, G. Nonadiabatic Nuclear Dynamics of the Ammonia Cation Studied by Surface Hopping Classical Trajectory Calculations. *J. Chem. Phys.* **2015**, *142*, 104307.
- (166) Belyaev, A. K.; Lebedev, O. V. Nonadiabatic Nuclear Dynamics of Atomic Collisions Based on Branching Classical Trajectories. *Phys. Rev. A* **2011**, *84*, 014701.
- (167) Zhu, C.; Nobusada, K.; Nakamura, H. New Implementation of the Trajectory Surface Hopping Method with Use of the Zhu-Nakamura Theory. *J. Chem. Phys.* **2001**, *115*, 3031–3044.
- (168) Baeck, K. K.; An, H. Practical Approximation of the Non-Adiabatic Coupling Terms for Same-Symmetry Interstate Crossings by Using Adiabatic Potential Energies Only. *J. Chem. Phys.* **2017**, *146*, 064107.
- (169) do Casal, M. T.; Toldo, J. M.; Pinheiro, M., Jr; Barbatti, M. Fewest Switches Surface Hopping with Baeck-An Couplings. *Open Res. Europe* **2021**, *1*, 49.
- (170) Shu, Y.; Zhang, L.; Chen, X.; Sun, S.; Huang, Y.; Truhlar, D. G. Nonadiabatic Dynamics Algorithms with Only Potential Energies and Gradients: Curvature-Driven Coherent Switching with Decay of Mixing and Curvature-Driven Trajectory Surface Hopping. *J. Chem. Theory Comput.* **2022**, *18*, 1320–1328.
- (171) Jasper, A. W.; Stechmann, S. N.; Truhlar, D. G. Fewest-Switches with Time Uncertainty: A Modified Trajectory Surface-Hopping Algorithm with Better Accuracy for Classically Forbidden Electronic Transitions. *J. Chem. Phys.* **2002**, *116*, 5424–5431.
- (172) Jasper, A. W.; Nangia, S.; Zhu, C.; Truhlar, D. G. Non-Born-Oppenheimer Molecular Dynamics. *Acc. Chem. Res.* **2006**, *39*, 101–108.
- (173) Lu, D.; Guo, H. Quantum and Semiclassical Dynamics of Nonadiabatic Electronic Excitation of C(³P) to C(¹D) by Hyperthermal Collisions with N₂. *J. Phys. Chem. A* **2023**, *127*, 3190–3199.
- (174) Lu, D.; Galvão, B. R.; Varandas, A. J.; Guo, H. Quantum and semiclassical studies of nonadiabatic electronic transitions between N(⁴S) and N(²D) by collisions with N₂. *Phys. Chem. Chem. Phys.* **2023**, *25*, 15656.
- (175) Braun, G.; Borges, I., Jr; Aquino, A.; Lischka, H.; Plasser, F.; do Monte, S. A.; Ventura, E.; Mukherjee, S.; Barbatti, M. Non-Kasha Fluorescence of Pyrene Emerges from a Dynamic Equilibrium Between Excited States. *J. Chem. Phys.* **2022**, *157*, 154305.
- (176) Toldo, J. M.; Mattos, R. S.; Pinheiro, M., Jr; Mukherjee, S.; Barbatti, M. Recommendations for Velocity Adjustment in Surface Hopping. *J. Chem. Theory Comput.* **2024**, *20*, 614–624.
- (177) Ben-Nun, M.; Martínez, T. J. Ab Initio Molecular Dynamics Study of *cis-trans* Photoisomerization in Ethylene. *Chem. Phys. Lett.* **1998**, *298*, 57–65.
- (178) Barbatti, M.; Ruckebauer, M.; Lischka, H. The Photo-dynamics of Ethylene: A Surface-Hopping Study on Structural Aspects. *J. Chem. Phys.* **2005**, *122*, 174307.
- (179) Levine, B. G.; Martínez, T. J. Isomerization Through Conical Intersections. *Annu. Rev. Phys. Chem.* **2007**, *58*, 613–634.
- (180) Tao, H.; Levine, B. G.; Martínez, T. J. Ab Initio Multiple Spawning Dynamics Using Multi-State Second-Order Perturbation Theory. *J. Phys. Chem. A* **2009**, *113*, 13656–13662.
- (181) Tao, H.; Allison, T. K.; Wright, T. W.; Stooke, A. M.; Khurmi, C.; van Tilborg, J.; Liu, Y.; Falcone, R. W.; Belkacem, A.; Martínez, T. J. Ultrafast Internal Conversion in Ethylene. I. The Excited State Lifetime. *J. Chem. Phys.* **2011**, *134*, 244306.
- (182) Mori, T.; Glover, W. J.; Schuurman, M. S.; Martínez, T. J. Role of Rydberg States in the Photochemical Dynamics of Ethylene. *J. Phys. Chem. A* **2012**, *116*, 2808–2818.
- (183) Farmanara, P.; Stert, V.; Radloff, W. Ultrafast Internal Conversion and Fragmentation in Electronically Excited C₂H₄ and C₂H₃Cl Molecules. *Chem. Phys. Lett.* **1998**, *288*, 518–522.
- (184) Mestdagh, J. M.; Visticot, J. P.; Elhanine, M.; Soep, B. Preactive Evolution of Monoalkenes Excited in the 6 eV Region. *J. Chem. Phys.* **2000**, *113*, 237–248.
- (185) Stert, V.; Lippert, H.; Ritze, H.-H.; Radloff, W. Femtosecond Time-Resolved Dynamics of the Electronically Excited Ethylene Molecule. *Chem. Phys. Lett.* **2004**, *388*, 144–149.
- (186) Kosma, K.; Trushin, S. A.; Fuss, W.; Schmid, W. E. Ultrafast Dynamics and Coherent Oscillations in Ethylene and Ethylene-d₄ Excited at 162 nm. *J. Phys. Chem. A* **2008**, *112*, 7514–7529.
- (187) Dewar, M. J. S.; Zoebisch, E.; Healy, E. F.; Stewart, J. J. P. AM1: A New General Purpose Quantum Mechanical Molecular Model. *J. Am. Chem. Soc.* **1985**, *107*, 3902–3909.
- (188) Granucci, G.; Toniolo, A. Molecular Gradients for Semi-empirical CI Wave Functions. *Chem. Phys. Lett.* **2000**, *325*, 79–85.
- (189) Roos, B. O.; Taylor, P. R.; Sigbahn, P. E. M. A Complete Active Space SCF Method (CASSCF) using a Density-Matrix Formulated Super-CI Approach. *Chem. Phys.* **1980**, *48*, 157–173.

- (190) Ben-Nun, M.; Quenneville, J.; Martínez, T. J. Ab Initio Multiple Spawning: Photochemistry from First Principles Quantum Molecular Dynamics. *J. Phys. Chem. A* **2000**, *104*, 5161–5175.
- (191) Biesner, J.; Schnieder, L.; Schmeer, J.; Ahlers, G.; Xie, X.; Welge, K. H.; Ashfold, M. N. R.; Dixon, R. N. State Selective Photodissociation Dynamics of A State Ammonia. I. *J. Chem. Phys.* **1988**, *88*, 3607–3616.
- (192) Nangia, S.; Truhlar, D. G. Direct Calculation of Coupled Diabatic Potential-Energy Surfaces for Ammonia and Mapping of a Four-Dimensional Conical Intersection Seam. *J. Chem. Phys.* **2006**, *124*, 124309.
- (193) Lai, W.; Lin, S. Y.; Xie, D.; Guo, H. Nonadiabatic Dynamics of A-State Photodissociation of Ammonia: A Four-Dimensional Wave Packet Study. *J. Phys. Chem. A* **2010**, *114*, 3121–3126.
- (194) Ma, J.; Zhu, X.; Guo, H.; Yarkony, D. R. First Principles Determination of the NH₂/ND₂ (,) Branching Ratios for Photodissociation of NH₃/ND₃ via Full-Dimensional Quantum Dynamics Based on a New Quasi-Diabatic Representation of Coupled *Ab Initio* Potential Energy Surfaces. *J. Chem. Phys.* **2012**, *137*, 22A541.
- (195) Xie, C.; Ma, J.; Zhu, X.; Zhang, D. H.; Yarkony, D. R.; Xie, D.; Guo, H. Full-Dimensional Quantum State-to-State Nonadiabatic Dynamics for Photodissociation of Ammonia in its A-Band. *J. Phys. Chem. Lett.* **2014**, *5*, 1055–1060.
- (196) Xie, C.; Zhu, X.; Ma, J.; Yarkony, D. R.; Xie, D.; Guo, H. Communication: On the Competition Between Adiabatic and Nonadiabatic Dynamics in Vibrationally Mediated Ammonia Photodissociation in Its A Band. *J. Chem. Phys.* **2015**, *142*, 091101.
- (197) Shu, Y.; Parker, K. A.; Truhlar, D. G. Dual-Functional Tamm-Dancoff Approximation with Self-Interaction-Free Orbitals: Vertical Excitation Energies and Potential Energy Surfaces Near an Intersection Seam. *J. Phys. Chem. A* **2017**, *121*, 9728–9735.
- (198) Zhang, L.; Shu, Y.; Bhaumik, S.; Chen, X.; Sun, S.; Huang, Y.; Truhlar, D. G. Nonadiabatic Dynamics of 1,3-Cyclohexadiene by Curvature-Driven Coherent Switching with Decay of Mixing. *J. Chem. Theory Comput.* **2022**, *18*, 7073–7081.
- (199) Garavelli, M.; Page, C. S.; Celani, P.; Olivucci, M.; Schmid, W. E.; Trushin, S. A.; Fuss, W. Reaction Path of a Sub-200 fs Photochemical Electrocyclic Reaction. *J. Phys. Chem. A* **2001**, *105*, 4458–4469.
- (200) Adachi, S.; Sato, M.; Suzuki, T. Direct Observation of Ground-State Product Formation in a 1,3-Cyclohexadiene Ring-Opening Reaction. *J. Phys. Chem. Lett.* **2015**, *6*, 343–346.
- (201) Pemberton, C. C.; Zhang, Y.; Saita, K.; Kirrander, A.; Weber, P. M. From the (1B) Spectroscopic State to the Photochemical Product of the Ultrafast Ring-Opening of 1,3-Cyclohexadiene: A Spectral Observation of the Complete Reaction Path. *J. Phys. Chem. A* **2015**, *119*, 8832–8845.
- (202) Kosma, K.; Trushin, S. A.; Fuss, W.; Schmid, W. E. Cyclohexadiene Ring Opening Observed with 13 fs Resolution: Coherent Oscillations Confirm the Reaction Path. *Phys. Chem. Chem. Phys.* **2009**, *11*, 172–181.
- (203) Kuthirummal, N.; Rudakov, F. M.; Evans, C. L.; Weber, P. M. Spectroscopy and Femtosecond Dynamics of the Ring Opening Reaction of 1,3-Cyclohexadiene. *J. Chem. Phys.* **2006**, *125*, 133307.
- (204) Ohta, A.; Kobayashi, O.; Danielache, S. O.; Nanbu, S. Nonadiabatic Ab Initio Molecular Dynamics of Photoisomerization Reaction Between 1,3-Cyclohexadiene and 1,3,5-*cis*-Hexatriene. *Chem. Phys.* **2015**, *459*, 45–53.
- (205) Karashima, S.; Humeniuk, A.; Uenishi, R.; Horio, T.; Kanno, M.; Ohta, T.; Nishitani, J.; Mitric, R.; Suzuki, T. Ultrafast Ring-Opening Reaction of 1,3-Cyclohexadiene: Identification of Non-adiabatic Pathway via Doubly Excited State. *J. Am. Chem. Soc.* **2021**, *143*, 8034–8045.
- (206) Lei, Y.; Wu, H.; Zheng, X.; Zhai, G.; Zhu, C. Photo-Induced 1,3-Cyclohexadiene Ring Opening Reaction: Ab Initio On-the-Fly Nonadiabatic Molecular Dynamics Simulation. *J. Photochem. Photobiol., A* **2016**, *317*, 39–49.
- (207) Polyak, I.; Hutton, L.; Crespo-Otero, R.; Barbatti, M.; Knowles, P. J. Ultrafast Photoinduced Dynamics of 1,3-Cyclohexadiene Using XMS-CASPT2 Surface Hopping. *J. Chem. Theory Comput.* **2019**, *15*, 3929–3940.
- (208) Filatov, M.; Min, S. K.; Kim, K. S. Non-adiabatic Dynamics of Ring Opening in Cyclohexa-1,3-Diene Described by Ensemble Density-Functional Theory Method. *Mol. Phys.* **2019**, *117*, 1128–1141.
- (209) Travnikova, O.; Pitesa, T.; Ponzi, A.; Sapunar, M.; Squibb, R. J.; Richter, R.; Finetti, P.; Di Fraia, M.; De Fanis, A.; Mahne, N.; Manfreda, M.; Zhaunerchyk, V.; Marchenko, T.; Guillemin, R.; Journal, L.; Prince, K. C.; Callegari, C.; Simon, M.; Feifel, R.; Decleva, P.; Doslic, N.; Piancastelli, M. N. Photochemical Ring-Opening Reaction of 1,3-Cyclohexadiene: Identifying the True Reactive State. *J. Am. Chem. Soc.* **2022**, *144*, 21878–21886.
- (210) Schalk, O.; Geng, T.; Thompson, T.; Baluyot, N.; Thomas, R. D.; Tapavicza, E.; Hansson, T. Cyclohexadiene Revisited: A Time-Resolved Photoelectron Spectroscopy and Ab Initio Study. *J. Phys. Chem. A* **2016**, *120*, 2320–2329.
- (211) Wolf, T. J. A.; Sanchez, D. M.; Yang, J.; Parrish, R. M.; Nunes, J. P. F.; Centurion, M.; Coffee, R.; Cryan, J. P.; Guhr, M.; Hegazy, K.; Kirrander, A.; Li, R. K.; Ruddock, J.; Shen, X.; Vecchione, T.; Weathersby, S. P.; Weber, P. M.; Wilkin, K.; Yong, H.; Zheng, Q.; Wang, X. J.; Minitti, M. P.; Martinez, T. J. The Photochemical Ring-Opening of 1,3-Cyclohexadiene Imaged by Ultrafast Electron Diffraction. *Nat. Chem.* **2019**, *11*, 504–509.
- (212) Snyder, J. W.; Parrish, R. M.; Martinez, T. J. α -CASSCF: An Efficient, Empirical Correction for SA-CASSCF to Closely Approximate MS-CASPT2 Potential Energy Surface. *J. Phys. Chem. Lett.* **2017**, *8*, 2432–2437.
- (213) Tamura, H.; Nanbu, S.; Ishida, T.; Nakamura, H. Ab Initio Nonadiabatic Quantum Dynamics of Cyclohexadiene/Hexatriene Ultrafast Photomerization. *J. Chem. Phys.* **2006**, *124*, 084313.
- (214) Ha, J.-W.; Lee, I. S.; Min, S. K. Surface Hopping Dynamics beyond Nonadiabatic Couplings for Quantum Coherence. *J. Phys. Chem. Lett.* **2018**, *9*, 1097–1104.
- (215) Kazaryan, A.; Heuver, J.; Filatov, M. Excitation Energies from Spin-Restricted Ensemble-Referenced Kohn-Sham Method: A State-Averaged Approach. *J. Phys. Chem. A* **2008**, *112*, 12980–12988.
- (216) Adamo, C.; Barone, V. Toward Reliable Density Functional Methods without Adjustable Parameters: The PBE0Model. *J. Chem. Phys.* **1999**, *110*, 6158–6170.
- (217) Merritt, I. C. D.; Jacquemin, D.; Vacher, M. Nonadiabatic Coupling in Trajectory Surface Hopping: How Approximations Impact Excited-State Reaction Dynamics. *J. Chem. Theory Comput.* **2023**, *19*, 1827–1842.
- (218) Akher, F. B.; Shu, Y.; Varga, Z.; Truhlar, D. G. Semiclassical Multistate Dynamics for Six Coupled ⁵A' States of O + O₂. *J. Chem. Theory Comput.* **2023**, *19*, 4389–4401.
- (219) Shu, T.; Fales, S.; Levine, B. G. Defect-Induced Conical Intersections Promote Nonradiative Recombination. *Nano Lett.* **2015**, *15*, 6247–6253.
- (220) Mai, S.; Avagliano, D.; Heindl, M.; Marquetand, P.; Menger, F. S. J.; Oettel, M.; Plasser, F.; Polonius, S.; Ruckebauer, M.; Shu, Y.; Truhlar, D. G.; Zhang, L.; Zobel, P.; González, L. SHARC release 3.0.2; González Group: Wien, 2024. <https://sharc-md.org> (accessed May 13, 2024).
- (221) Shu, Y.; Zhang, L.; Truhlar, D. G. SHARC-MN v3.0; CERN, Zenodo, 2023. DOI: 10.5281/zenodo.10344984 (accessed May 13, 2024).
- (222) Barbatti, M.; Bondanza, M.; Crespo-Otero, R.; Demoulin, B.; Dral, P. O.; Granucci, G.; Kossoski, F.; Lischka, H.; Mennucci, B.; Mukherjee, S.; Pederzoli, M.; Persico, M.; Pinheiro, M., Jr; Pittner, J.; Plasser, F.; Sangiogo Gil, E.; Stojanovic, L. Newton-X Platform: New Software Developments for Surface Hopping and Nuclear Ensembles. *J. Chem. Theory Comput.* **2022**, *18*, 6851–6865.
- (223) Zheng, J.; Meana-Pañeda, R.; Truhlar, D. G. Including Tunneling in Non-Born-Oppenheimer Simulations. *J. Phys. Chem. Lett.* **2014**, *5*, 2039–2043.
- (224) Yang, K. R.; Xu, X.; Zheng, J.; Truhlar, D. G. Full-Dimensional Potential Energies and State Couplings and Multidimensional

Tunneling Calculations for the Photodissociation of Phenol. *Chem. Sci.* **2014**, *5*, 4661–4680.

(225) Xu, X.; Zheng, J.; Yang, K. R.; Truhlar, D. G. Photodissociation Dynamics of Phenol: Multistate Trajectory Simulations Including Tunneling. *J. Am. Chem. Soc.* **2014**, *136*, 16378–16386.